A Szilikátipari Tudományos Egyesület lapja

építőanyag

Journal of Silicate Based and Composite Materials

A TARTALOMBÓL:

2021/3

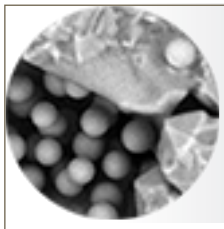

We are pleased to announce the organization of

ec-siliconf2

THE 2ND EUROPEAN CONFERENCE ON SILICON AND SILICA BASED MATERIALS

to be held in Hotel Palota in Miskolc-Lillafüred, Hungary, in October 4-8, 2021

The **ec-siliconf2** conference will be held in the wonderful palace of **Hotel Palota** in the exceptionally beautiful environment of **Beech Mountain** in **Miskolc-Lillafüred** in **Hungary**. In 2019 in the previous conference scientists had participated from **21** countries of **Asia, Europe, North- and South America** and **Africa**.

THE CONFERENCE SESSIONS

SESSION 1: Silicon and silica in inorganic and molecular chemistry
SESSION 2: Metallic silicon and silicon as an alloying agent
SESSION 3: Silicon (Si) and silica (SiO2) in medicine, therapy and health
SESSION 4: Silicon in micro and nanoelectronics and devices
SESSION 5: Silicon and silica in functional materials
SESSION 6: Silicon and silica in polymers
SESSION 7: Silicon and silica in ceramics and composites
SESSION 8: Silicon and silica in construction materials and glass
SESSION 9: Silicon and silica in biological systems and technologies
SESSION 10: Silicon and silica in smart materials and technologies
SESSION 11: Silicon and silica in minerals and rocks
SESSION 12: Testing and characterization methods, tools and errors
SESSION 13: Other results in research and development of silicon and silica and materials contain of them
SESSION 14: Other results in processing and application of silicon and silica and materials contain of them
SESSION 15: Miscellaneous in silicon and silica materials science

Registration abstract submission, and further information are available in:
www.ec-siliconf.eu

építőanyag

Journal of Silicate Based and Composite Materials

2021/3

TARTALOM

CONTENT

A finomkerámia-, üveg-, cement-, mész-, beton-, tégla- és cserép-, kő- és kavics-, tűzállóanyag-, szigetelőanyag-iparágak szakmai lapja
Scientific journal of ceramics, glass, cement, concrete, clay products, stone and gravel, insulating and fireproof materials and composites

A folyóiratot referálja · The journal is referred by:

A folyóiratban lektorált cikkek jelennek meg.
All published papers are peer-reviewed.
Kiadó · Publisher: Szilikátipari Tudományos Egyesület (SZTE)
Elnök · President: ASZTALOS István
1034 Budapest, Bécsi út 120.
Tel.: +36-1/201-9360 ▪ E-mail: epitoanyag@szte.org.hu
Tördelő szerkesztő · Layout editor: NÉMETH Hajnalka
Címlapfotó · Cover photo: GYURKÓ Zoltán

Hirdetési árak 2021 ▪ Advertising rates 2021:

B2 borító színes · cover colour	76 000 Ft	304 EUR
B3 borító színes · cover colour	70 000 Ft	280 EUR
B4 borító színes · cover colour	85 000 Ft	340 EUR
1/1 oldal színes · page colour	64 000 Ft	256 EUR
1/1 oldal fekete-fehér · page b&w	32 000 Ft	128 EUR
1/2 oldal színes · page colour	32 000 Ft	128 EUR
1/2 oldal fekete-fehér · page b&w	16 000 Ft	64 EUR
1/4 oldal színes · page colour	16 000 Ft	64 EUR
1/4 oldal fekete-fehér · page b&w	8 000 Ft	32 EUR

Az árak az áfát nem tartalmazzák. · Without VAT.

A hirdetési megrendelő letölthető a folyóirat honlapjáról.
Order-form for advertisement is avaliable on the website of the journal.

WWW.EPITOANYAG.ORG.HU
EN.EPITOANYAG.ORG.HU

Online ISSN: 2064-4477
Print ISSN: 0013-970x
INDEX: 2 52 50 ▪ 73 (2021) 85–130

Analytics of swelling potential on highly expansive (plastic) clayey soils behavior for sustainable admixture stabilization

Kennedy C. ONYELOWE ▪ Department of Civil Engineering, Michael Okpara University of Agriculture, Nigeria ▪ konyelowe@mouau.edu.ng

Michael E. ONYIA ▪ Department of Civil Engineering, Faculty of Engineering, University of Nigeria, Nsukka ▪ michael.onyia@unn.edu.ng

Duc BUI VAN ▪ Research Group of Geotechnical Engineering, Construction Materials and Sustainability, Hanoi University of Mining and Geology, Vietnam ▪ buivanduc@humg.edu.vn

Ali A. FIROOZI ▪ Department of Civil Engineering, Faculty of Engineering and Technology, University of Botswana, Botswana ▪ firoozia@ub.ac.bw

Talal AMHADI ▪ Department of Construction and Civil Engineering, Ecole de Technologie Superieure (ETS), University of Quebec, Canada ▪ talal.amhadi.1@ens.etsmtl.ca

Érkezett: 2020. 04. 25. ▪ Received: 25. 04. 2021. ▪ https://doi.org/10.14382/epitoanyag-jsbcm.2021.13

Abstract

The swelling potential analytics and the ion exchange reaction of highly expansive soils in a soil stabilization process have been reviewed. The importance of these factors in deciding suitable construction materials and chemical additives utilized as alternative or supplementary binders in clayey soil stabilization has been discussed also. The outcome of this study has shown that Al^{3+}, Si^{4+}, and Ca^{2+} are the most suitable exchangeable cations with OH- as the suitable exchangeable anion leading to the formation of C-A-S-H, which is the compound responsible for strengthening. The swelling potential analytics also proposed the expression $w_{sT} = 0.00216 \times \left(\sum_{i=1}^{i=n} I_{P_i}^{2.44}\right)\left(\sum_{i=D_1}^{i=D_n} D_i\right)$ as the total swelling potential with respect to the depth of a foundation material constructed with clayey soil. This study revealed that during the wet season, hydraulically bound foundation materials experience undesirable volume changes with the highest swelling potential expected at the surface within the active (unstable) zone of the foundation. Generally, the treatment of highly expansive soil with very high swelling potential should be concentrated at the surface and reduced along the depth of the foundation matrix. With this proposed guide, the utilization of alternative or supplementary cementing materials as construction materials in the stabilization of clayey soil to improve swelling can be conducted with a more sustainable approach.

Keywords: swelling potential analytics, adsorbed moisture, double diffused layer, pozzolanic reaction

Kulcsszavak: duzzadási potenciál elemzés, nedvesség, kettős diffúz réteg, pozzolán reakció

Kennedy C. ONYELOWE
is a senior lecturer with a PhD in geotechnical engineering. He teaches and conducts research at the MOUAU, & AE-FUNAI, Nigeria and KIU, Uganda. His current research is on artificial intelligence in geoenvironmental engineering and construction materials.

Michael E. ONYIA
is a senior lecturer and published researcher in structural engineering and construction materials. He is a former head of department of civil engineering, UNN, Nigeria.

Duc BUI VAN
is the assistant head of faculty of civil engineering, HUMG, Vietnam, conducts research in geoenvironmental engineering and works as a field engineer.

Ali FIROOZI
is a lecturer and published author at the UoB, Botswana and conducts research in geotechnical engineering and construction materials.

Talal AMHADI
is a PhD scholar at the University of Quebec, Canada and does research in sustainable pavement materials.

1. Introduction

Clayey soils have been considered very important construction materials because of the role they play as foundation materials in earthworks, flexible pavements, compacted clay liners, airfields, backfills, etc. local earthen house builders use clayey soils in their constructions in the countryside [1-3]. This has shown plastic properties that enable the soils clog and bond together in the construction of tach and earthen houses in villages and countryside [4]. This is achieved by mixing clayey soils with moisture sufficient enough to make form clogs and flocs holding the mass together to be used in the local engineering earthworks [5, 6]. This material is manipulated and handled by mixing it with moisture without recourse to the reason behind its clogging behavior. In advanced foundation earthworks, little consideration has been given to the reactions that lead to bonding together of clayey soil particle when mixed with moisture to its optimum content [7]. It is important to note that the behavior of clayey soils when mixed with moisture is of utmost importance to geotechnical engineering practice [7]. More so, its behavior when mixed with an admixture during clayey soils stabilization procedure is more important to the designer. In transport geotechnics, pavement underlay is built with clayey soil and in most cases, the clayey soils are of highly plastic and expansive consistency [8, 9]. These properties make the soils very problematic. Again, when the foundation is exposed to seasonal rise and fall of water table, the clayey soil material responds by undergoing swell and shrink cycle which cause the materials to crack [1, 3, 10, 11]. These cracks may propagate to such undesirable widths that expose the internal structures of the pavement foundation to moisture percolation from runoff [1, 10]. The behavior of hydraulically bound structures during the wet and dry season deserve a clearer understanding at this stage. The moisture content increases and attains maximum condition at the surface of clayey soil mass during the wet season when water tables rise and moisture reaches the foundation by capillary rise [12, 13]. For the maximum moisture at the surface, it

decreases with depth to a value within the unstable zone or the active zone [12]. Beyond this clayey soil zone of activity is the stable or inactive zone. Hydraulically bound structures built within the unstable or active zone prone to swell and shrink cycles due to moisture intake and loss as the case may be are likely to experience undesirable movements according to the seasons and hence suffer collapse [12]. This is the case with most vertical and horizontal structures that experience failures all over the world [1, 12]. These are caused primarily due to differential movement in both axial and lateral directions. The mineral contents and more especially the dominant minerals and exchangeable ions in the clayey soils are responsible for the microstructural and macrostructural behavior and reactions that lead to the failure of foundations [12, 14]. Clayey soils are made of minerals, which are fundamentally responsible for the behaviors observed when mixed with moisture or any additive materials during chemical stabilization [14]. There are three major minerals that may dominate clayey soils, which include kaolinite, illite and montmorillonite as presented in *Table 1*.

Mineral	Liquid limit, w_L (%)	Plastic limit, w_p (%)	Activity, A
Kaolinite	35-100	20-40	0.3-0.5
Illite	60-120	35-60	0.5-1.2
Montmorillonite	100-900	50-100	1.5-7.0
Halloysite 1	50-70	40-60	0.1-0.2
Halloysite 2	40-55	30-45	0.4-0.6
Attapulgite	150-250	100-125	0.4-1.3
Allophane	200-250	120-150	0.4-1.3

Table 1 Values of liquid limit, plastic limit and activity of some clay minerals [14]
1. táblázat Egyes agyagásványok folyási határértéke, képlékeny határértéke és aktivitása [14]

It is important that in earthworks, clayey soils are handled by impregnating the mass with moisture to its optimum content as molding moisture [1, 8]. When this happens, the clayey soils respond by the dispersion of the particles and swelling occurs [2, 11]. During this hydration reaction stage, the minerals in clay are polarized and the dipole ions migrate to either the surface or the edge [12]. The negative ions of the inundated clay minerals are attracted to the surface of the clayey soil and a film of moisture interface is formed, which is called the adsorbed moisture (see *Fig. 1*) [7]. When this happens, the soil experiences swelling caused by the weakening of the van der Waal's forces holding the particles together [7, 12, 14]. Around each clayey particle as they separate from each other and as they lose their interparticle force is formed a diffused double layer (DDL) [6, 9, 12, 15, 16]. This keeps the particles apart and the gap increases as there is further hydration of the clayey soil [7]. Conversely, if dehydration takes place by any means, the diffused double layer reduces and the particles tend to come closer again but the crystalline structure of the clayey soil may be lost due to cracks. This is one the properties of highly expansive soils, which are also called black cotton soils [12]. The swelling cracks in most cases widen to a maximum of 20mm and moisture travel deep through these cracks into the ground [12]. The highly expansive soils swell and shrink in a regular cycle and this brings about severe movements in soil mass and structures built atop are affect by these undesirable behaviors. There is recorded recurring cracking and progressive damage of structures built on these problematic soils [12]. In a polarized clayey soil due to hydration, ions like Al^{3+}, Si^{2+}, Ca^{2+}, Fe^{2+}, O^- and OH^- are observed with Na^+, K^+ and Mg^{2+} depending on the dominant clay mineral in the studied clayey soil. Further, ion exchange reaction takes between the exchangeable ions.

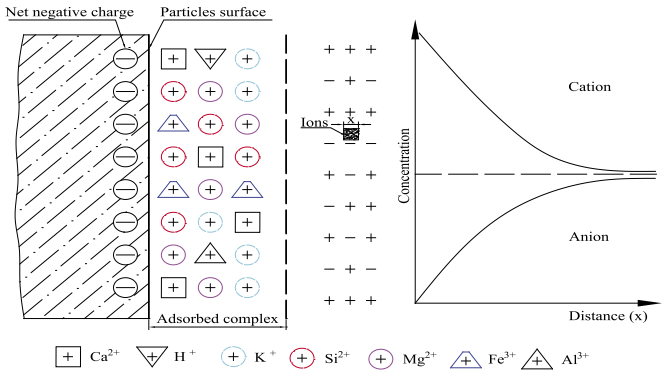

Fig. 1 Release of ions and cations migration and exchange reaction in the adsorbed complex [7, 14]
1. ábra Ionok és kationok felszabadulása és cserereakciója [7,14]

The primary focus of the work is to review the possible exchange reactions that take place during clayey soils stabilization procedure utilizing additives with emphasis on swelling potential analytics [12]. This is important because of the role it plays in the reversal of swell condition of clayey soil, strengthening of highly expansive soils and the achievement of stable and sustainable foundation structures. This aspect of geoenvironmental engineering investigation and more especially soil stabilization and improvement has been neglected by researchers and designers. Without a good understanding and utilizing the knowledge it possesses there will never be any successful stabilization process more so on problematic soils and highly expansive clayey soils would have been useless to earthworks. This review hopes to illuminate this aspect and close the knowledge gap.

2. Discussion of relevant literatures

2.1 Exchangeable ions in soil stabilization

Clay minerals have atomic structures built of two fundamental crystal sheets, which are the tetrahedral or silica sheet and the octahedral or alumina sheet [8]. It is the metallic ions in the crystals as they are stacked differently with different bonding forces that determine the lattice structure of the clay mineral [12, 14]. As soon as clayey soils are hydrated as a result of water percolation in hydraulically bound structures or during a stabilization procedure, hydration reaction takes place and exchangeable ions are released with the ionic composition of the pore water. The exchangeable ions available from clay for kaolinite clay mineral (hydrated) with the chemical formula $(OH)_4{\cdot}Al_4Si_4O_{10}{\cdot}4H_2O$ are Al^{3+}, Si^{4+}, H^+, OH^- and O^-, for montmorillonite clay mineral with chemical formula $(OH)_4{\cdot}Al_4Si_gO_{20}{\cdot}nH_2O$ are Al^{3+}, Si^{4+}, H^+, OH^-, and O^- and for the illite

clay mineral with chemical formula $(OH)_4K_y(Si_{g-y}Al_y)(Al_4{\cdot}Mg_6{\cdot}Fe_4{\cdot}Fe_6)O_{20}$ are K^+, Al^{3+}, Si^{4+}, Mg^{2+}, Fe^{2+}, H^+, OH^- and O^- [8, 12, 14, 17]. The availability of the exchangeable ions can be seen presented in *Figs. 2, 3*, and *4*. However, research results have shown that by Xray Fluorescence (XRF) and Xray Diffraction (XRD), clayey soil chemical oxide composition is composed also of small proportion of oxides of calcium and oxides of sodium in the case of montmorillonite and this is responsible for its highest degree of expansivity compared to the other three clay mineral components [17]. This means that Ca^{2+} and Na^+ are also available as exchangeable ions either during clayey soil hydration or in a case of soil stabilization.

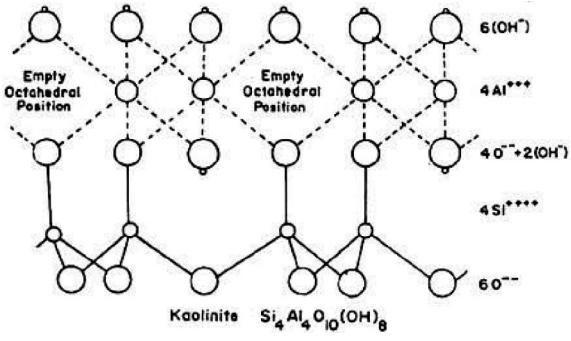

Fig. 2 Structure of kaolinite mineral [8]
2. ábra A kaolinit-ásvány szerkezete [8]

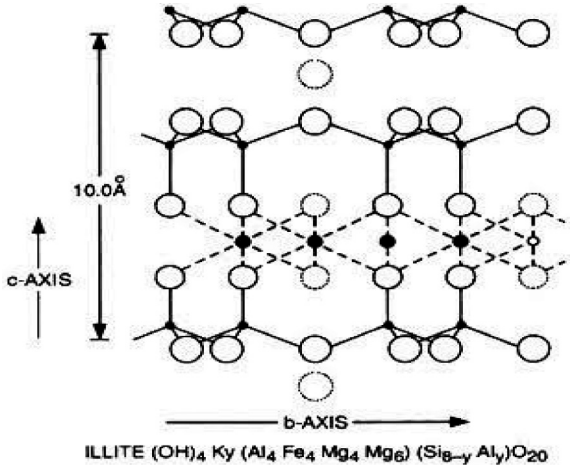

Fig. 3 Structure of illite mineral [8]
3. ábra Az illit ásvány szerkezete [8]

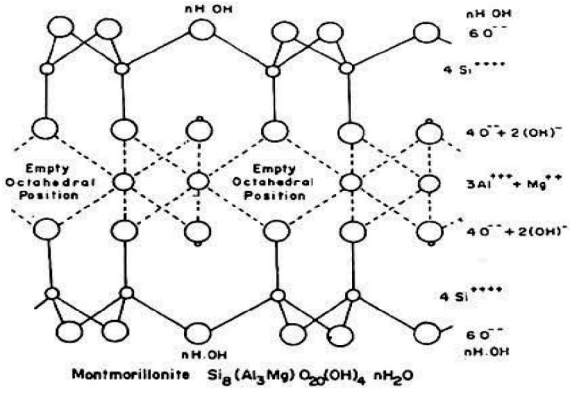

Fig. 4 Structure of montmorillonite mineral [8]
4. ábra A montmorillonit ásvány szerkezete [8]

However, in a clayey soil stabilization procedure, additives are utilized due to the exchangeable ions available, which constitute Ca^{2+}, Al^{3+}, S^{4+}, and Fe^{2+}, which are the cations responsible for the binding properties that ordinary Portland cement and other supplementary and alternative binders possess [18-20] and CO_3^{2-}, which is the anion responsible for carbonation reaction in stabilization operation [7, 21]. Clayey soils of highly expansive consistency are not suitable for earthworks due to their high tendency to swell and shrink due to moisture changes [22-25].

2.2 Hydration, adsorbed moisture and cation exchange reaction in soil stabilization

Hydration is the inundation or the impregnation of soil and more especially clayey soil in this case, with moisture to trigger ionization in aqueous medium [3, 7]. This takes place either through the rise in water table that foundation materials are exposed to moisture ingress or when moisture travels through cracks and percolate into the foundation level [7, 12]. Clayey soils take in moisture and this causes volume changes known as swelling. As moisture is absorbed, a film of surface is formed in the lattice structures of clay to form what is known as absorbed moisture. The adsorbed moisture in clay is responsible for the dipolation of clay composition ions and the availability of exchangeable ions [7, 23, 24]. The dipole ions from clayey soil are separated into cations and the anions. The anions are concentrated at the surface of the clay particles and attract the cations from the dipole ions from additives during the hydration reaction [7]. The cation exchange reaction takes place with respect to the arrangement of the metallic ions in the electrochemical series. In a montmorillonite dominant clayey soil tetrahedral sheet, Al^{3+} from chemical additive exchanges Si^{4+} in clayey soil while either Mg^{2+}, K^+, Fe^{2+}, Li^+ or Zn^+ exchanges Al^{3+} in the octahedral sheet [7, 12]. During the utilization of additives with sufficient calcium-based components in a soil improvement exercise, Ca^{2+} also exchanges other weaker cations in the adsorbed complex. These exchange of cations with those that are stronger in the chemical series leads to the formation of clay flocculants responsible for the formation of calcium aluminate hydrate (C-A-H) and calcium silicate hydrate (C-S-H) or even a composite compound known as calcium aluminate silicate hydrate (C-A-S-H) [1, 7, 10, 26, 27]. These compounds are responsible for the gain in strength in clayey soil by the strengthening of the interparticle bonds. When clayey soils swell, with higher degree of swelling potential on the surface of a clayey soil mass, this can be cured through the impregnation and mixing of the swollen soil with such additives rich in exchangeable ions like Ca^{2+}, Al^{3+} higher in the electrochemical series that can exchange sodium or magnesium ion to reduce the double diffused layer in swollen soils [6].

2.3 Swelling potential analytics and stabilization

The work of H. B. Seed et al. [11] suggested the expression for swelling potential for clayey soils as presented in *Equation 1*;

$$w_S = 0.00216 \times I_p^{2.44} \quad (1)$$

where I_p = plasticity index and w_S = swelling potential.

From the findings of V. N. S. Murthy [12], hydraulically bound foundations built with clayey soils and within the active (unstable) zone experience lattice structure impairments due to moisture intake. The active zone ranges from the clayey soil surface to the depth D_n beyond which the clayey soil belong to the inactive (stable) zone. Volume changes take place within the active zone when foundation materials of clay absorb moisture. During the wet seasons as the water table rises into the active zone, moisture content increases and reaches a maximum at the surface of the compacted mass of clayey soil foundation material [12]. This implies that swelling potential, which is directly proportional to the water intake decreases from maximum at the surface with depth (D_1 [12] to a steady moisture content at the boundary between the active and inactive zones. Consequently, the integral of the swelling potential with respect to the inverse of the depth (x, D) of the foundation matrix is presented in *Equation 2*.

$$\int_i^x w_s = \int_i^x 0.00216 * I_P^{2.44} * \mathrm{dx}^{-1} \quad (2)$$

This operation gives *Equation 3* measured along the points of the depths (D_1, D_2, D_3 ... D_n) of the foundation soil. And from the findings of V. N. S. Murthy [12], *Equation 4* is derived.

$$w_{s(x)} = 0.00216 * I_P^{2.44} * (x_n^{-1})_{D_1}^{D_n}; x^{-1}; D_1, D_2, D_3 \ldots\ldots D_n \quad (3)$$

Where;

$$^1/_{x_1} = D_1,\ ^1/_{x_2} = D_2,\ ^1/_{x_3} = D_3,\ ^1/_{x_4} = D_4,\ ^1/_{x_5} = D_5$$
$$\ldots\ldots\ldots\ldots ^1/_{x_n} = D_n \quad (4)$$

In this case, the point D_1 is measured from the active-inactive zone boundary as x_{max} and this point gives the maximum swelling potential at the surface of the foundation material. This shows that $^1/_{x_1} > {}^1/_{x_2} > {}^1/_{x_3} > {}^1/_{x_4} > {}^1/_{x_5} > {}^1/_{x_n}$ as presented in *Equation 4*. Substituting the depth values of D into *Equations 5, 6, 7*, and *8*, the swelling potential at depths $D_1, D_2, D_3, \ldots\ldots D_n$ are evaluated.

$$w_{s_1} = 0.00216 * I_{P_1}^{2.44} * (D_1) \quad (5)$$

$$w_{s_2} = 0.00216 * I_{P_2}^{2.44} * (D_2) \quad (6)$$

$$w_{s_3} = 0.00216 * I_{P_3}^{2.44} * (D_3) \quad (7)$$

$$w_{s_n} = 0.00216 * I_{P_n}^{2.44} * (D_n) \quad (8)$$

It can also be established that the maximum swelling potential is evaluated using *Equation 5* with the highest depth value measure from the reactive zone boundary of compacted soil. And finally, the total swelling potential is computed with *Equation 9*.

$$w_{s_T} = 0.00216 * \left(\sum_{i=1}^{i=n} I_{P_i}^{2.44}\right)\left(\sum_{i=D_1}^{i=D_n} D_i\right); i; 1, 2, 3\ldots\ldots\ldots\mathrm{n} \quad (9)$$

From the above mathematical analysis, it can be observed that the swelling potential at the surface of the compacted clayey soil mass is maximum due to the highest amount of moisture needed for hydration reaction and further formation of the double diffused layer in the clayey soil particles. This further increase the interparticle distances in the clayey soil mass and consequently reduces the van der Waal's force existing between the particles. This also implies that the van der Waal's forces increase with reduced moisture content along the depth of the foundation clayey soil mass. As the mass of compacted clayey soil is inundated with molding moisture or moisture from capillary rise or runoff ingress, the more the exchangeable ions in clayey soils become available for ion exchange reactions and increased double diffused layer and decreased interparticle forces within the clayey soil mass.

3. Conclusions

In this work, the ion exchange and swelling potential analytics were reviewed based on previous relevant studies. Swelling in highly expansive soils utilized as construction materials in geoenvironmental engineering and transport geotechnics is an important factor in earthworks. A full understanding of the swell-shrink behavior of highly expansive soils as construction materials is an important phase in the design and construction of foundations. In this review, the exchangeable ions available in a clayey soil utilized in construction were studied. Secondly, the behavior of foundations of clayey soil mass at different depths of the foundation were also discussed. It was established that the use of additive binders rich in exchangeable ions high in the electrochemical series is of utmost important. This leads to the formation of strengthening compounds in a soil stabilization protocol. It was also noted from the swelling potential analytics that in a stabilization procedure, the mixing of chemical additives should be more on the surface of the soil mass and reduced along the depth of the mass. This is to accommodate the highest swelling depth of the foundation soil mass.

4. Conflict of interest declaration

The authors declare that they have no known competing financial interests or personal relationships that could have appeared to influence the work reported in this paper.

References

[1] Onyelowe, K. C., Onyia, M. E., Onyelowe, F. D. A., Bui Van, D., Salahudeen, A. B., Eberemu, A. O., Osinubi, K. J., Amadi, A. A., Onukwugha, E., Odumade, A. O., Chigbo, I. C., Saing, Z., Ikpa, C., Amhadi, T., Ugorji, B., Maduabuchi, M., Ibe, K. (2020). Critical state desiccation induced shrinkage of biomass treated compacted soil as pavement foundation Epitőanyag – Journal of Silicate Based and Composite Materials, vol. 72 (2), pp. 40–47.

[2] Soon, N. W. et al. (2013). Improvement in engineering properties of soils through microbial-induced calcite precipitation. KSCE Journal of Civil Engineering, vol. 17, pp. 718-728. https://doi.org/10.1007/s12205-013-0149-8

[3] Hervé Peron, Lyesse Laloui, Tomasz Hueckel & Liang Bo Hu (2009). Desiccation cracking of soils, European Journal of Environmental and Civil Engineering, 13:7-8, 869-888, https://doi.org/10.1080/19648189.2009.9693159

[4] ASTM D4318-17e1 (2017). Standard Test Methods for Liquid Limit, Plastic Limit, and Plasticity Index of Soils, ASTM International, West Conshohocken, PA. https://doi.org/10.1520/D4318-17E01

[5] Shigeki, I. and Toshio, S. (1965). Chemical Reactions Among Clay Minerals' Calcium Carbonate, And Ammonium Chloride, The American Mineralogist, VOL. 50, July_August'.

[6] McBride, M. B. (1997). A critique of diffused double layer models applied to colloid and surface chemistry. Clays and Clay Minerals, vol. 45 (4), pp. 598-608.

[7] Bui Van, D. and Onyelowe, K.C., 2018. Adsorbed complex and laboratory geotechnics of Quarry Dust (QD) stabilized lateritic soils. Environmental Technology and Innovation, Vol. 10, pp. 355-368. https://doi.org/10.1016/j.eti.2018.04.005.

[8] R. E. Grim (1953). Clay mineralogy, chaps. 4, 7, 8, 9, 10, 13. McGraw-Hill Book Company, Inc., London.

[9] Rose, D. A. et al. (1997). A model based on diffuse double layer theory to predict soil salinity. Joint Intl. Conf. on Agric. Engg. & Tech. Exhibition, '97, Dhaka

[10] Onyelowe, K. C., Bui Van, D., Dao-Phuc, L., et al. (2020). Evaluation of index and compaction properties of lateritic soils treated with quarry dust based geopolymer cement for subgrade purpose. Epitőanyag– Journal of Silicate Based and Composite Materials, Vol. 72, No. 1, pp. 12–15. https://doi.org/10.14382/epitoanyag-jsbcm.2020.2
[11] Seed, H. B. et al. (1962). Prediction of swelling potential for compacted clays. Journal of Soil Mechanics and Foundation Division, vol. 88(3), pp. 53-87.
[12] V. N. S. Murthy (2007). Advanced geotechnical engineering; geotechnical engineering series. CBS Publishers and Distributors, New Delhi.
[13] Ambrus, Maria (2019). Mechanikai aktivalas hatasa deponalt pernye alapu geopolimerek nyomoszilardsagara Epitőanyag– Journal of Silicate Based and Composite Materials, Vol. 71, No. 5, pp. 148–152. https://doi.org/10.14382/epitoanyag-jsbcm.2019.26
[14] Das, B. M. and Sobhan, K. (2012). Principles of geotechnical engineering, 8th edition. Cengage Learning, Stamford, USA.
[15] Chen, F. H. (1988). Foundations on Expansive Soils, 2nd Edition, Elsevier Services Publications, New York.
[16] D. L. Rimmeri and D. J. Greenland (1976). Effects of Calcium Carbonate on The Swelling Behavior of a Soil Clay, Journal of Soil Science, 27. 129-39.
[17] Onyelowe, K. C., Aririguzo, J. C. & Ezugwu, C. N. (2019). Sustainable Soils Re-Engineering. Partridge Publishing, Singapore. ISBN 9781543750997
[18] American Standard for Testing and Materials (ASTM) C618 (1978). Specification for Pozzolanas. ASTM International, Philadelphia, USA.
[19] BS 8615-1 (2019). Specification for pozzolanic materials for use with Portland cement. Natural pozzolana and natural calcined pozzolana. British Standard International, London.
[20] ASTM D4829-19 (2019). Standard Test Method for Expansion Index of Soils, ASTM International, West Conshohocken, PA. https://doi.org/10.1520/D4829-19
[21] Haas, S. and Ritter, H. F. (2019). Soil improvement with quicklime-long-time behavior and carbonation. Road Materials and Pavement Design, vol. 20(8), pp. 1941-1951. https://doi.org/10.1080/14680628.2018.1474793
[22] Lewis, D. R. (1988). Ion exchange reactions of clays. Exploration and Prodviction Research Division, Shell Development Co., Houston, Texas. Publication No. 26, Pp. 54-69
[23] Tisdale, S. L. et al. (1975). Soil Fertility and Fertilizers-Chapter 4-Ion Exchange in Soils. 4th Edition, Macmillan Publishing Company, New York.
[24] G. P. Robertson et al. (1999). Standard Soil Methods for Long-Term Ecological Research, Chapter 6: Exchangeable Ion, pH and Cation Exchange Capacity. Oxford University Press, New York.
[25] A. Goraczko and A. Olchawa (2017). The Amounts of Water Adsorbed to the Surface of Clay Minerals at the Plastic Limit. Archives of Hydro-Engineering and Environmental Mechanics, vol. 64 (3–4), pp. 155–162. https://doi.org/10.1515/heem-2017-0010
[26] K. C. Onyelowe, A. B. Salahudeen, A. O. Eberemu, et al. (2020b). Utilization of Solid Waste Derivative Materials in Soft Soils Re-engineering. In book: Recent Thoughts in Geoenvironmental Engineering, Proceedings of the 3rd GeoMEast International Congress and Exhibition, Egypt 2019 on Sustainable Civil Infrastructures – The Official International Congress of the Soil-Structure Interaction Group in Egypt (SSIGE), pp. 49-57. https://doi.org/10.1007/978-3-030-34199-2_3
[27] J. F. Rivera, A. Orobio, R. Mejia de Gutierrez et al. (2020). Clayey soil stabilization using alkali-activated cementitious materials. Materiales de Construccion, vol. 70 (337), pp. 1-12. https://doi.org/10.3989/mc.2020.07519
[28] Amadi, A. A. and Okeiyi, A. (2017). Use of quick and hydrated lime in stabilization of lateritic soil: comparative analysis of laboratory data. International Journal of Geo Engineering, vol. 8(3). https://doi.org/10.1186/s40703-017-0041-3

Ref.:
Onyelowe, Kennedy C. – **Onyia**, Michael E. – **Bui Van**, Duc – **Firoozi**, Ali A. – Amhadi, Talalh: *Analytics of swelling potential on highly expansive (plastic) clayey soils behavior for sustainable admixture stabilization*
Építőanyag – Journal of Silicate Based and Composite Materials, Vol. 73, No. 3 (2021), 86–90. p.
https://doi.org/10.14382/epitoanyag-jsbcm.2021.13

Compressive strength and Scheffe's optimization of mechanical properties of recycled ceramics tile aggregate concrete

Edidiong E. AMBROSE ▪ Department of Civil Engineering, Akwa Ibom State University, Ikot Akpaden, Akwa Ibom State, Nigeria ▪ edidiongambrose@aksu.edu.ng
Fidelis O. OKAFOR ▪ Department of Civil Engineering, University of Nigeria, Nsukka, Nigeria ▪ fidelis.okafor@unn.edu.ng
Michael E. ONYIA ▪ Department of Civil Engineering, University of Nigeria, Nsukka, Nigeria ▪ michael.onyia@unn.edu.ng

Érkezett: 2020. 10. 18. ▪ Received: 18. 10. 2021. ▪ https://doi.org/10.14382/epitoanyag-jsbcm.2021.14

Abstract
Ceramic industry generates a large amount of wastes which are presently not reused in any significant quantity. Reusing these wastes in concrete could solve the ceramic industry waste management problem and also lead to a more sustainable concrete industry. While the use of ceramic wastes as coarse aggregate has been extensively investigated, not much findings are available on its use as fine aggregate and there are presently no models for predicting the properties of ceramic wastes aggregate concretes. This study investigates effect of crushed recycled-ceramic tiles (CRT) fine aggregate content on compressive strength of concrete. Scheffe's second degree polynomial models were also formulated for compressive strength, slump height and cost of CRT concrete. Results show that incorporation of CRT as fine aggregate improves the compressive strength of concrete and this increase is directly proportional to its content. Authors therefore recommend up to 100% replacement of conventional fine aggregate with CRT in concrete production. The formulated models could predict compressive strength, slump and cost of CRT concrete if the mix ratio is known and vice versa. Analysis of variance and normal probability plots of model residuals were used to test adequacy of the models, and the models were found to be adequate at 95% confidence level. With the model equations, sample optimization was carried out to obtain the most economical mix for certain predefined criteria and the results were promising. Several similar optimizations can be carried out using the formulated model equations for any desired criteria of the modeled responses.
Keywords: compressive strength, concrete, optimization, recycled ceramic waste, Scheffe's theory, slump
Kulcsszavak: nyomószilárdság, beton, optimalizálás, újrahasznosított kerámia hulladék, Scheffe elmélet, roskadás

Edidiong E. AMBROSE
Ph.D student at Department of Civil Engineering, University of Nigeria, Nsukka, Nigeria. Lecturer at Akwa Ibom State University, Ikot Akpaden, Akwa Ibom State, Nigeria. Registered Engineer at Council for the Regulation of Engineering in Nigeria (COREN). Member, Nigerian Society of Engineers. Research Interests include: recycled aggregate concrete, durability of cement-based materials, modelling

Fidelis O. OKAFOR
Professor of highway and construction materials at University of Nigeria, Nsukka, Nigeria. Registered Engineer at Council for the Regulation of Engineering in Nigeria (COREN). Member, Nigerian Society of Engineers. Research Interests include: soil, cement and concrete materials.

Michael E. ONYIA
Ph.D (Civil Engineering). Senior Lecturer at the Department of Civil Engineering at the University of Nigeria, Nsukka, Nigeria. Registered Engineer at Council for the Regulation of Engineering in Nigeria (COREN). Member, Nigerian Society of Engineers. Research Interests include: structures, soil, cement and concrete materials.

1. Introduction

Concrete has remained the most versatile and sustainable construction material all over the world. As a result, its demand is ever increasing. It is estimated that over 33 billion tonnes of concrete is consumed annually [1], making it the most widely used construction materials [2], the most consumed manufactured material and the second most consumed material after water [3]. One major advantage of the use of concrete is that its constituents – basically Portland cement, aggregate and water – can almost always be locally sourced. However, the sourcing of these materials is ecologically harmful. For instance, the manufacture of one tonne of Portland cement generates about one tonne of CO_2 into the atmosphere [4, 5, 6], accounting for about 5% of global CO_2 emission [6, 7]. There is also a rapid depletion in the natural reserves of conventional crushed rock aggregate and natural river sand. All these threaten the sustainability of concrete as a construction material.

As a way out, the use of secondary cementitious materials like fly ash, metakaolin and silica fumes as partial replacement for cement in concrete production has become rampant. There have also been attempts to either partially or totally replace the conventional aggregates in concrete production. Materials like recycled aggregate, polystyrene aggregate [8], laterite and quarry dust [9], etc. have been used. A good number of these replacement materials are industrial wastes or by-products. Of recent, there has been a growing number of researches on the use of ceramic wastes as aggregate in concrete production and the results have been promising. Ceramic wastes are industrial waste products from the manufacturing of sanitary wares, earthen wares, ceramic tiles, bricks, electrical insulators, etc. Some of these wastes are as a result of cracks, glazing faults, production error, off-standard products, size discrepancy, production error, etc. [10]. A considerable amount of ceramic wastes is also generated during transportation and distribution while the greatest percentage comes as construction and demolition wastes. These sum up to millions of tonnes of ceramic wastes generated annually and disposed as landfills all over the world [11, 12]. As at present, ceramic waste is not recycled in any significant quantity [10, 11, 12] and it is classified as non-

biodegradable [12, 13]. Hence, its incorporation into concrete production will be a win-win situation to both the construction and ceramics industries. Moreover, ceramic wastes possess qualities expected to improve concrete properties. They are durable and hard with high resistance to physical, chemical and biological degradation [14, 15, 16]. They are pozzolanic with low density and high resistance to abrasion [10, 13].

Investigation on incorporation of ceramic wastes into concrete production is a novel line of research at international level. Most of the researches are on the use of ceramic wastes as aggregate and mostly as coarse aggregate with very few on its use as fine aggregate. Medina et al. [17] carried out extensive studies on strength properties of concrete with partial replacement of conventional coarse aggregate with ceramic sanitary ware waste aggregate and reported that the resulting concrete performs better than conventional concrete in terms of mechanical strengths and that these properties increase as the percentage of ceramic wastes aggregate increases. This result was in line with several other findings on ceramic sanitary ware waste aggregate concrete [18, 19] and those using other ceramic wastes as coarse aggregate [16, 20, 21]. These improved mechanical performances are attributed to the characteristics of ceramic waste aggregate – relatively high strength, irregular shape and rough surface texture – which enhance aggregate/cement paste bonding; and the refined pore system of the resulting concrete [23]. The few researches on use of recycled ceramic wastes as fine aggregate have also reported comparable or improved results. Alves et al. [24] reported that compressive strength does not seem to be significantly affected by incorporation of fine recycled brick aggregate when compared with conventional concrete. This was similar to the result of Aliabdo et al. [25] which showed that compressive strength remains the same or slightly improves as percentage of replacement with recycled bricks aggregate increases. Torkittikul and Chaipanich [14] observed that compressive strength of ceramic waste concrete increased with ceramic waste content and was optimum at 50% replacement; dropping when the ceramic waste content increased beyond 50%. This drop was however linked to workability problem posed by inclusion of ceramic waste aggregate. Comparable compressive strength was also reported by Elci with complete replacement of fine aggregate with recycled floor tile waste [10].

Concrete properties at both fresh and hardened state are – to a great extent – determined by the proportions of the mix constituents. As such concrete mix design is of paramount important to concrete users and concrete mix optimization is of even more importance. The later involves careful selection and proportioning of concrete constituents to achieve the desired concrete properties at optimum point, usually at minimum cost. This was traditionally achieved through trial mixes on a trial and error bases [26, 27]. The traditional method has proved to be inefficient and could be very tedious and complex especially when dealing with concrete with many constituents. The use of statistical experimental design methodology is far more efficient and economical. In this approach, a set of trial batches is employed in any chosen statistically established procedure [27]. These mixes cover a chosen range of proportions for each concrete constituent. Statistical methods usually involve fitting empirical models to experimental data for each performance criterion. The resulting model equations are usually algebraic functions of individual component proportions which may include cement content, water/cement ratio, aggregate content, percentage of cement or aggregate replacement etc. as independent variables, while the required concrete properties like strength, slump, cost etc. are the dependent variables. With these equations, concrete mix optimization can easily be achieved with limited or no trial mix. In general, the process of optimizing a response using a collection of mathematical and statistical techniques for empirical model building is termed response surface methodology (RSM). RSM involves three major steps which are [25]: (1) design of experiment, (2) formulation of model equations, and (3) optimization of the equations under certain given constraints. Design of experiment (DoE) determines points where the desired responses should be evaluated; thereby establishing relationships between a number of independent variables and the responses. It allows multiple input factors to be manipulated simultaneously to determine their combined effects on the desired responses. The two major approaches to design of experiment are factorial method and mixture experiment [26, 27] and one of the first and most popular type of mixture experiment is the simplex-lattice design [28].

There are presently no such mathematical models for ceramic waste aggregate concrete and the need for such is imminent. This study aims to further investigate the feasibility of incorporating recycled ceramic waste tiles as fine aggregate in concrete production by studying the effect of ceramic tile waste aggregate content on compressive strength. Mathematical models are also formulated using Scheffe's simplex lattice theory, for predicting and optimization of compressive strength, slump height and cost of concrete with partial or full replacement of river sand with ceramic tile waste fine aggregates.

1.1 Simplex lattice design

Simplex lattice design is a form of mixture experiment which is a general technique for modelling response and components relationships. Mixture experiment techniques are mainly for cases where the response depends on the mass or volume proportions of individual components and not on their total mass or volume [29 – 32] and this is typical of concrete properties. If q denotes the number of mixture components, X_1, X_2, X_3,…X_q, and the desired response is denoted by y, then for a q-component mixture,

$$y = F(X_1, X_2, X_3, \ldots \ldots \ldots, X_q) \quad (1)$$

For mixture experiments, no component should have a negative value and the sum of the component proportions must be equal to one. Mathematically these can be represented as:

$$X_1 + X_2 + \ldots + X_q = \sum_{i=1}^{q} X_i = 1 \quad (2)$$

$$0 \le X_i \le 1 \quad (3)$$

Since the sum of component proportions (variables) is constrained to unity, it therefore follows that only (q-1) of the variables can be independently chosen. Hence, from *Eq. (2)*,

$$X_q = 1 - \sum_{i=1}^{q-1} X_i \tag{4}$$

1.1.1 Factor space in simplex lattice design

A lattice is an ordered and regular patterned distribution of points. In a *q*-component mixture experiment, the factor space is a regular (*q-1*) simplex and the relationships in *Eqs. (1)* to *(4)* holds [30, 32]. If q = 2, we have the lattice simplex as a straight line, for q = 3, it is an equilateral triangle while for q = 4, the simplex will be a regular tetrahedron with each vertex representing each of the components. As a result of Scheffe's theory, simplex lattice designs are simply referred to as Scheffe's simplex lattice design. Scheffe proposed that each component of the mixture in a mixture design resides on a vertex of a simplex lattice with (*q-1*) factor space such that if the degree of the polynomial to be fitted to the design is denoted by n, then a {*q,n*} simplex lattice for *q*-components consists of uniformly spaced points defined by all the possible combinations of (*n+1*) levels of each component [33].

Properties of concrete depend on the adequate mass or volume proportioning of its constituents and not on its total mass or volume. Therefore, Scheffe's optimization theory can be used to model and optimize concrete properties. Scheffe introduced polynomial regression to model responses. The general form of the polynomial equation of degree n in a *q*-component mixture is given as:

$$\hat{y} = b_0 + \sum_{1\le i\le q} b_i X_i + \sum_{1\le i\le j\le q} b_{ij} X_i X_j + \sum_{1\le i\le j\le k\le q} b_{ijk} X_i X_j X_k + \ldots + \sum b_{i_1 i_2 \ldots i_n} X_{i_1} X_{1_2} X_{i_n} \tag{5}$$

1.1.2 Scheffe's reduced polynomial

The number of terms in *Eq. (5)* is given as C_n^{q+n}. This is also the minimum number of design points required to determine coefficients of the resulting model. However, by substituting *Eq. (2)* into *(5)*, the number of terms in the polynomial can be reduced to:

$$N = C_n^{q+n-1} = \frac{(q+n-1)!}{(q-1)!(n)!} \tag{6}$$

For a 5-compomponent mixture adopted in this work, the reduced second-degree polynomial can be obtained as follows [30 - 32, 34, 35]:

From *Eq. (5)*,

$$\begin{aligned}\hat{y} = {} & b_0 + b_1X_1 + b_2X_2 + b_3X_3 + b_4X_4 + b_5X_5 + b_{12}X_1X_2 + b_{13}X_1X_3 \\ & + b_{14}X_1X_4 + b_{15}X_1X_5 + b_{23}X_2X_3 + b_{24}X_2X_4 + b_{25}X_2X_5 + b_{34}X_3X_4 \\ & + b_{35}X_3X_5 + b_{45}X_4X_5 + b_{11}X_1^2 + b_{22}X_2^2 + b_{33}X_3^2 + b_{44}X_4^2 + b_{55}X_5^2\end{aligned} \tag{7}$$

Recall from *Eq. (2)* that

$$X_1 + X_2 + X_3 + X_4 + X_5 = 1 \tag{8}$$

Multiplying *Eq. (8)* by b_0 gives

$$b_o\left(X_1 + X_2 + X_3 + X_4 + X_5\right) = b_o \tag{9}$$

Multiplying *Eq. (8)* by X_1, X_2, X_3, X_4 and X_5 in succession and rearranging the terms gives:

$$\begin{aligned}X_1^2 &= X_1 - X_1X_2 - X_1X_3 - X_1X_4 - X_1X_5 \\ X_2^2 &= X_2 - X_1X_2 - X_2X_3 - X_2X_4 - X_2X_5 \\ X_3^2 &= X_3 - X_1X_3 - X_2X_3 - X_3X_4 - X_3X_5 \\ X_4^2 &= X_4 - X_1X_4 - X_2X_4 - X_3X_4 - X_4X_5 \\ X_5^2 &= X_4 - X_1X_5 - X_2X_5 - X_3X_5 - X_4X_5\end{aligned} \tag{10}$$

Substituting *Eqs (9)* and *(10)* into *Eq. (7)* and simplifying the terms gives:

$$\begin{aligned}\hat{y} = {} & (b_{12} - b_{11} - b_{22})X_1X_2 + (b_{13} - b_{11} - b_{33})X_1X_3 + (b_{14} - b_{11} - b_{44})X_1X_4 \\ & + (b_{14} - b_{11} - b_{55})X_1X_5 + (b_{23} - b_{22} - b_{33})X_2X_3 + (b_{24} - b_{22} - b_{44})X_2X_4 \\ & + (b_{25} - b_{22} - b_{55})X_2X_5 + (b_{34} - b_{33} - b_{44})X_3X_4 + (b_{35} - b_{33} - b_{55})X_3X_5 \\ & + (b_{45} - b_{44} - b_{55})X_4X_5 + (b_0 + b_1 + b_{11})X_1 + (b_0 + b_2 + b_{22})X_2 \\ & + (b_0 + b_3 + b_{33})X_3 + (b_0 + b_4 + b_{44})X_4 + (b_0 + b_5 + b_{55})X_5\end{aligned} \tag{11}$$

If we denote $\beta_i = b_0 + b_i + b_{ii}$ and $\beta_{ij} = b_{ij} - b_{ii} - b_{jj}$ (12)

Eq. (11) then becomes:

$$\begin{aligned}\hat{y} = {} & \beta_1X_1 + \beta_2X_2 + \beta_3X_3 + \beta_4X_4 + \beta_5X_5 + \beta_{12}X_1X_2 + \beta_{13}X_1X_3 \\ & + \beta_{14}X_1X_4 + \beta_{15}X_1X_5 + \beta_{23}X_2X_3 + \beta_{24}X_2X_4 + \beta_{25}X_2X_5 + \beta_{34}X_3X_4 \\ & + \beta_{35}X_3X_5 + \beta_{45}X_4X_5\end{aligned} \tag{13}$$

Eq. (13) is the reduced second-degree polynomial for a 5-component mixture and the number of terms is 15 according to *Eq. (6)* as against 21. The reduced polynomial is generally referred to as conical polynomial or {*q,n*} polynomial and its general form is given as:

For linear (n = 1); $\hat{y} = \sum_{1\le i\le q} \beta_i X_i$ (14)

For quadratic (n = 2); $\hat{y} = \sum_{1\le i\le q} \beta_i X_i + \sum_{1\le i\le j\le q} \beta_{ij} X_i X_j$ (15)

1.1.3 Interaction of components in Scheffe's factor space

In Scheffe's simplex design, the mixture components are evenly distributed in the simplex. The proportions assumed by each component is n+1 equally spaced level from 0 to 1 based on *Eq. (16)*.

$$X_i = 0, \frac{1}{n}, \frac{2}{n}, \ldots . 1 \tag{16}$$

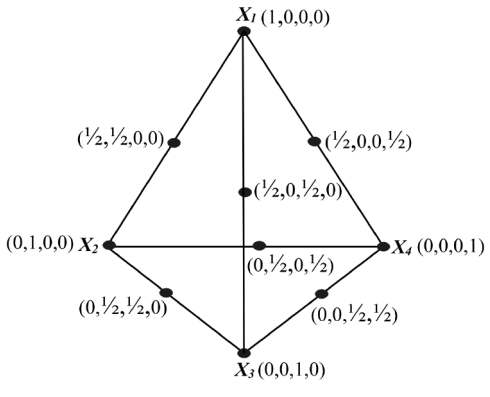

Fig. 1 A {4.2} Scheffe's simplex lattice showing pseudo ratios at design points
1. ábra A {4.2} Scheffe szimplex rács, amely a pszeudó-arányokat mutatja a egyes tervezési pontokon

Thus, for a second-degree polynomial simplex design (n = 2), each component must take the levels: 0, and 1 while for a cubic polynomial (n = 3), the levels are: 0, , and 1. Consider a {4,2}

simplex lattice as in *Fig. 1*. The factor space is a tetrahedron and each component assumes the proportions 0, and 1. There are ten points at the boundaries and vertices of the tetrahedron corresponding to the number of terms in the reduced second-degree polynomial in *Eq. (15)*. At the vertices, the four points defined by (1,0,0,0); (0,1,0,0); (0,0,1,0) and (0,0,0,1) represent single component mixtures while the remaining six points each at the middle of each of the edges represent binary blends of two component mixtures.

1.1.4 Determination of coefficients of Scheffe's polynomial

There is a relationship between design points on Scheffe's lattice simplex and number of terms in the reduced polynomial in *Eqs. (13)*, *(14)* and *(15)*. Thus, the coefficients of the equations can be expressed as functions of expected responses (y_i) at the design and control points of the simplex. The general relationship between the two is given as:

$$\beta_i = y_i \quad \text{and} \quad \beta_{ij} = 4y_{ij} - 2y_i - 2y_j \tag{17}$$

1.2 Augmented simplex lattice design

Simplex lattice design contains design points only at the vertices and edges of the simplex and contains just the necessary design points needed to formulate the model equations. As such, it is a saturated design [32, 35]. It does not give any information about the inside of the simplex. To augment simplex design, it is sometimes necessary to incorporate additional points within the inside of the simplex [26]. These additional points in addition to improving the simplex deign also help in testing the adequacy of the fitted model; hence they are also referred to as check points. According to Anya [26], the common practice is to augment the simplex by selecting design points at the centroid and at midway between the centroid and each of the vertices. Augmented simplex design still maintains the model equation form as that of simplex lattice design. However, estimated model coefficients differ slightly from those obtained using only simplex lattice design points.

2. Materials and methods

Investigation in this study was in two phases. In the first phase (Phase A), compressive strength of concrete with different replacement levels of conventional fine aggregate with Crushed Recycled-ceramic Tiles (CRT) was studied. In the second phase (Phase B), polynomial models were developed using Scheffe's simplex lattice theory for predicting and optimization of compressive strength, slump and cost of concrete incorporating CRT as fine aggregate.

2.1 Materials

Materials used for laboratory experiments in both phases of this work were cement, water, river sand (RS), CRT and granite chippings. Cement and water served as binder, while river sand and CRT served as fine aggregates (FA) and granite chippings was used as Coarse Aggregates (CA). Unicem brand of Portland Limestone cement (Strength class 32.5R) conforming to NIS 444-1 [36] was used. The river sand was obtained from a river sand mining site at Ikot Ekong, Akwa Ibom State while granite chippings used was from a quarry in Akamkpa, Cross River State all in Nigeria. CRT used were floor and wall tiles that had passed through complete manufacturing process but were either cracked or broken during transportation and distribution process. They were obtained from a dealer in Uyo, broken into smaller pieces and crushed into the required size using a mechanical mill. Particle size distributions of fine aggregates and coarse aggregate used are shown in *Table 1* and *Table 2* respectively, while specific gravities and bulk densities of all the aggregates are shown in *Table 3* and chemical composition of cement and CRT are presented in *Table 4*.

Sieve Size (mm)		3.35	1.70	0.85	0.425	0.300	0.212	0.075	Pan
% Passing	Sand	98.00	92.00	74.40	36.80	18.40	6.40	2.00	0.00
	CRT	87.00	60.20	38.80	25.20	20.60	15.40	7.60	0.00

Table 1 Particle size distribution for sand and CRT
1. táblázat A homok **és** *a CRT szemcseméret-eloszlása*

Sieve Size (mm)	28	20	13.2	13	10	8	6.7	pan
% Passing	100	99.6	81.7	80.3	43.6	26.1	7.0	0.0

Table 2 Particle size distribution for CA
2. táblázat A CA szemcseméret-eloszlása

Property	Sand	CRT	CA
Specific gravity	2.61	2.40	2.39
Bulk density (kg/m³)	1635	1373	1386

Table 3 Physical properties of aggregates
3. táblázat Az adalékanyagok fizikai tulajdonságai

Compound	% composition by mass	
	Cement	CRT
Iron Oxide (Fe_2O_3)	2.25	3.07
Aluminum Oxide (Al_2O_3)	4.73	17.50
Silicon dioxide (SiO_2)	19.84	66.13
Calcium Oxide (CaO)	70.32	5.70
Manganese Oxide (MnO)	0.01	0.58
Magnesium Oxide (MgO)	1.47	2.14
Zinc Oxide (ZnO)		0.42
Sulfur trioxide (SO_3)	0.03	-
Sodium Oxide (Na_2O)	0.08	0.09
Potassium Oxide (K_2O)	0.72	1.02
LOI (Loss of Ignition)	1.01	3.30

Table 4 Chemical composition of cement and CRT
4. táblázat A cement **és** *a CRT kémiai* **összetétele**

2.2 Mix proportion for phase A

In this phase, 12 different mixes were used based on the four mix proportions in *Table 5*. The mix proportions in *Table 5*

were designated A, B, C and D respectively. For each of them, the fine aggregate portions were obtained by combining sand and CRT with CRT content ranging from 0 to 100% with a step of 50%. Hence, for each mix proportion, three different mixes were obtained with percentage replacement of sand with CRT of 0%, 50% and 100%.

2.3 Design of experiment for Phase B

In the second phase of this study which involved modelling, number of design components was five and the data would be fitted into Scheffe's second-degree polynomial. Therefore, the mixture experiment was designed using augmented {5, 2} simplex lattice with the aid of a commercial statistical software, Minitab 16 and the design matrix is presented in *Table 6*. There were 21 design points and 27 runs. The 21 design points included 15 design points from *Eq. (6)*, the centroid and five axial points. Six design points (the five vertices and centroid) were replicated and the runs were randomized. From *Eqs (2)* and *(3)*, the lower and upper boundaries for each component were 0 and 1 respectively while the sum of all components for each run equals unity. From the design matrix, the five replicated runs that represent the five mixes at the vertices of the simplex were: Run Orders 10 and 22 (Vertex X_1), 3 and 4 (Vertex X_2), 11 and 18 (Vertex X_3), 6 and 12 (Vertex X_4), then 8 and 13 (Vertex X_5). The results at these vertices would define the bound of the simplex and the resulting models.

Components	A	B	C	D
Cem II 32.5 (kg)	325	406	418.3	553.5
Fine Aggregate (kg) (Sand + CRT)	650	609	627.5	553.5
Coarse Aggregate (kg)	1300	1218	1255	1107
Water (kg)	195	243.5	209	249
w/c	0.6	0.6	0.5	0.45

Table 5 Mix proportions per cubic meter of concrete for phase A
5. táblázat Az A fázis során használt beton keverék **összetétele** *köbméterenként*

2.3.1 Pseudo components and actual components

The relationship between pseudo components and real components is expressed in *Eq. (18)* where $\boldsymbol{Z}$ is a column matrix of real component ratios and $\boldsymbol{X}$ is a column matrix of the pseudo components at each run. $\boldsymbol{A}$ is a square matrix of actual mix (real components) corresponding to the pure blends at the five vertices of the simplex. These mixes were selected by the researchers through experience and a series of trial mixes.

$$Z = AX \tag{18}$$

The mix ratios at the respective vertices that formed the matrix $\boldsymbol{A}$ were as follows:

At Vertex X_1, we have the ratios of water (Z_1), cement (Z_2), sand (Z_3), CRT (Z_4) and CA (Z_5) respectively as: [0.6 : 1 : 0 : 1.5 : 3]. At the other four vertices we have [0.5 : 1 : 1.5 : 0 ; 3], [0.65 : 1 : 2.5 : 0 : 4.5], [0.4 : 1 : 1 : 0 : 2] and [0.45 : 1 : 0 : 1 : 2] respectively. Putting these into a matrix form we have:

$$A = \begin{pmatrix} 0.6 & 0.5 & 0.65 & 0.4 & 0.45 \\ 1 & 1 & 1 & 1 & 1 \\ 0 & 1.5 & 2.5 & 1 & 0 \\ 1.5 & 0 & 0 & 0 & 1 \\ 3 & 3 & 4.5 & 2 & 2 \end{pmatrix}$$

and substituting into *Eq. (18)*, we now have

$$\begin{pmatrix} Z_1 \\ Z_2 \\ Z_3 \\ Z_4 \\ Z_5 \end{pmatrix} = \begin{pmatrix} 0.6 & 0.5 & 0.65 & 0.4 & 0.45 \\ 1 & 1 & 1 & 1 & 1 \\ 0 & 1.5 & 2.5 & 1 & 0 \\ 1.5 & 0 & 0 & 0 & 1 \\ 3 & 3 & 4.5 & 2 & 2 \end{pmatrix} \begin{pmatrix} X_1 \\ X_2 \\ X_3 \\ X_4 \\ X_5 \end{pmatrix} \tag{19}$$

Eq. (19) was used to compute components in real ratios that was used for sample preparation in Phase B. The computation was as follows:

At Run Order 1;

$$\begin{pmatrix} Z_1 \\ Z_2 \\ Z_3 \\ Z_4 \\ Z_5 \end{pmatrix} = \begin{pmatrix} 0.6 & 0.5 & 0.65 & 0.4 & 0.45 \\ 1 & 1 & 1 & 1 & 1 \\ 0 & 1.5 & 2.5 & 1 & 0 \\ 1.5 & 0 & 0 & 0 & 1 \\ 3 & 3 & 4.5 & 2 & 2 \end{pmatrix} \begin{pmatrix} 0.5 \\ 0.5 \\ 0 \\ 0 \\ 0 \end{pmatrix}$$

$Z_1 = 0.55$; $Z_2 = 1$; $Z_3 = 0.75$; $Z_4 = 0.75$; $Z_5 = 3$

At Run Order 2;

$$\begin{pmatrix} Z_1 \\ Z_2 \\ Z_3 \\ Z_4 \\ Z_5 \end{pmatrix} = \begin{pmatrix} 0.6 & 0.5 & 0.65 & 0.4 & 0.45 \\ 1 & 1 & 1 & 1 & 1 \\ 0 & 1.5 & 2.5 & 1 & 0 \\ 1.5 & 0 & 0 & 0 & 1 \\ 3 & 3 & 4.5 & 2 & 2 \end{pmatrix} \begin{pmatrix} 0.5 \\ 0 \\ 0 \\ 0.5 \\ 0 \end{pmatrix}$$

$Z_1 = 0.5$; $Z_2 = 1$; $Z_3 = 0.5$; $Z_4 = 0.75$; $Z_5 = 2.5$.

This procedure was carried out for the 27 run orders and the results are presented in *Table 6* with their corresponding pseudo components.

2.4 Sample preparation and testing

Concrete batching was by weight for both phases of the experiments. For Phase A, the 12 different mixes described in Section 2.2 were batched. For the second phase, a total of 27 mixes were carried out corresponding to the 27 Run Orders in the design matrix in *Table 6*. Mixing, filling of molds, compaction and curing of concrete samples were in accordance with BS EN 12390-2 [37]. For each fresh mix in Phase B, workability was measured immediately after mixing using slump test and in accordance with BS EN 12350-2 [38]. Two slump tests were carried out for each mix. Three 100 mm × 100 mm × 100 mm concrete cube samples were prepared for each mix (in both phases) and cured by immersion in water for 28 days. Compressive strength tests were carried out on the 28th day for each concrete cube sample using a compression testing machine conforming to BS EN 12390-4 [39] and having a test range of 0 – 2000kN. For each test, maximum load at failure was recorded and compressive strength was calculated by diving the failure load by the cross-sectional area of the sample. Three samples were tested for each mix and the average strength is reported in *Fig. 2* and *Table 7*.

Run Order	Pseudo Components					Components in Real Ratios					% Replacement Of sand with CRT
	X_1	X_2	X_3	X_4	X_5	Z_1 Water	Z_2 Cement	Z_3 Sand	Z_4 CRT	Z_5 CA	
1	0.5	0.5	0	0	0	0.55	1	0.75	0.75	3	50.0
2	0.5	0	0	0.5	0	0.5	1	0.5	0.75	2.5	60.0
3	0	1	0	0	0	0.5	1	1.5	0	3	0.0
4	0	1	0	0	0	0.5	1	1.5	0	3	0.0
5	0.5	0	0.5	0	0	0.625	1	1.25	0.75	3.75	37.5
6	0	0	0	1	0	0.4	1	1	0	2	0.0
7	0	0.5	0	0.5	0	0.45	1	1.25	0	2.5	0.0
8	0	0	0	0	1	0.45	1	0	1	2	100.0
9	0.1	0.6	0.1	0.1	0.1	0.51	1	1.25	0.25	2.95	16.7
10	1	0	0	0	0	0.6	1	0	1.5	3	100.0
11	0	0	1	0	0	0.65	1	2.5	0	5	0.0
12	0	0	0	1	0	0.4	1	1	0	2	0.0
13	0	0	0	0	1	0.45	1	0	1	2	100.0
14	0.5	0	0	0	0.5	0.525	1	0	1.25	2.5	100.0
15	0.1	0.1	0.6	0.1	0.1	0.585	1	1.75	0.25	3.7	12.5
16	0.1	0.1	0.1	0.1	0.6	0.485	1	0.5	0.75	2.45	60.0
17	0	0	0.5	0	0.5	0.55	1	1.25	0.5	3.25	28.6
18	0	0	1	0	0	0.65	1	2.5	0	4.5	0.0
19	0.2	0.2	0.2	0.2	0.2	0.52	1	1	0.5	2.9	33.3
20	0.2	0.2	0.2	0.2	0.2	0.52	1	1	0.5	2.9	33.3
21	0	0	0	0.5	0.5	0.415	1	0.5	0.5	2	50.0
22	1	0	0	0	0	0.6	1	0	1.5	3	100.0
23	0.6	0.1	0.1	0.1	0.1	0.56	1	0.5	1	2.95	66.7
24	0.1	0.1	0.1	0.6	0.1	0.46	1	1	0.25	2.45	20.0
25	0	0.5	0.5	0	0	0.575	1	2	0	3.75	0.0
26	0	0.5	0	0	0.5	0.475	1	0.75	0.5	2.5	40.0
27	0	0	0.5	0.5	0	0.525	1	1.75	0	3.25	0.0

Table 6 Design matrix for Phase B showing pseudo and real components
*6. táblázat A B fázis tervezési mátrixa, amely mutatja a pszeudó- **és** valós komponenseket egyaránt*

3. Results and discussion

3.1 Effect of CRT content on compressive strength – Phase A

Result of compressive strength of the four prescribed mixes at their different levels of CRT content is presented in *Fig. 2*. From the result, it is obvious that incorporation of CRT significantly improves compressive strength of the resulting concrete. This is demonstrated in the four different mixes (A, B, C and D). For each of the mixes, samples with 100% CRT content performed best in terms of compressive strength followed by those with 50% CRT content, while samples with no CRT content performed least. This is similar to results of earlier studies with ceramic tiles waste aggregate [10, 11] and those with other ceramic waste aggregates [14, 18], although a few researchers have reported that replacement of conventional fine aggregate with ceramic waste aggregate does not produce any significant improvement in compressive strength of the resulting concrete [24, 25].

3.2 Mathematical modelling – Phase B

3.2.1 Experimental responses for compressive strength

Table 7 presents the average characteristic compressive strength of concrete for the 27 runs. These values define the maximum and minimum obtainable compressive strength response within the factor space of the simplex. The results also confirm that for any given mix, replacing river sand with CRT produces better compressive strength. This could be seen by comparing results at Vertex X_4 (Run Orders 6 and 12) with those at Vertex X_5 (Run Orders 8 and 13). With the same mix ratio of 1:1:2 (cement: fine aggregate: Coarse aggregate), although the latter has a higher water/cement ratio than the former; its compressive strength was far higher than that of the former because CRT was used as 100% fine aggregate in the latter mix.

3.2.2 Experimental responses for slump

Workability of concrete mix for this work was measured in terms of slump height and the average results for each of the 27 runs are presented in *Table 7*. Slump values range from 5 mm to 82.5 mm representing very low to very high slump according to Neville [6]. A close look at the slump values shows that mixes with CRT content have reduced slump heights compared to those without CRT. This has also been the trend in other reported researches [13, 14, 21, 24] and is linked to the high porosity and water absorption of ceramic waste aggregates [13]. The fact that ceramic waste aggregates are usually roughed-textured and angular in shape also results in increased friction which reduces workability.

Run Order	Real Component Ratios Z_1 Water	Z_2 Cement	Z_3 Sand	Z_4 CRT	Z_5 CA	Slump (mm)	$f_{c,28}$ (N/mm^2)	Cost/m^3 (USD)
1	0.55	1	0.75	0.75	3	40.0	33.844	80.343
2	0.5	1	0.5	0.75	2.5	45.0	31.061	82.716
3	0.5	1	1.5	0	3	60.0	28.997	73.146
4	0.5	1	1.5	0	3	60.0	27.375	76.863
5	0.625	1	1.25	0.75	3.75	47.5	23.766	71.816
6	0.4	1	1	0	2	75.0	33.988	93.020
7	0.45	1	1.25	0	2.5	47.5	28.374	84.031
8	0.45	1	0	1	2	17.5	44.635	98.311
9	0.51	1	1.25	0.25	2.95	47.5	27.294	77.835
10	0.6	1	0	1.5	3	5.0	37.064	86.901
11	0.65	1	2.5	0	4.5	15.0	21.795	61.438
12	0.4	1	1	0	2	82.5	36.553	91.269
13	0.45	1	0	1	2	10.0	39.947	98.630
14	0.525	1	0	1.25	2.5	10.0	39.138	90.461
15	0.585	1	1.75	0.25	3.7	22.5	25.427	69.030
16	0.485	1	0.5	0.75	2.45	10.0	34.644	87.770
17	0.55	1	1.25	0.5	3.25	15.0	25.197	74.589
18	0.65	1	2.5	0	4.5	20.0	19.113	60.397
19	0.52	1	1	0.5	2.9	25.0	27.549	78.195
20	0.52	1	1	0.5	2.9	35.0	29.245	78.848
21	0.425	1	0.5	0.5	2	5.0	40.417	96.868
22	0.6	1	0	1.5	3	5.0	33.808	82.051
23	0.56	1	0.5	1	2.95	15.0	30.511	82.880
24	0.46	1	1	0.25	2.45	52.5	31.286	85.390
25	0.575	1	2	0	3.75	10.0	23.872	67.693
26	0.475	1	0.75	0.5	2.5	40.0	33.977	86.024
27	0.525	1	1.75	0	3.25	70.0	26.891	72.030

Table 7 Compressive strength and slump tests results including costs of materials per m^3 of concrete
7. táblázat Nyomószilárdsági **és** *roskadási vizsgálatok eredményei, valamint az anyagköltségek (egy m^3 betonhoz)*

3.2.3 Cost estimate model data

The cost of material required to produce 1m^3 of each of the mixes is also presented in *Table 7*. These values were obtained by adding up the products of the quantities of each constituent in a cubic meter of the mix and their respective unit price. The unit prices of the concrete components at the current rate are given in *Table 8*. These prices are only the cost of materials and exclude cost of labour and equipment for mixing.

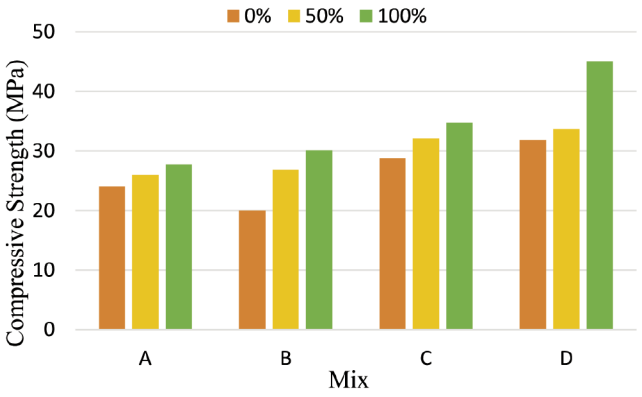

Fig. 2 Compressive strength of mix A, B, C and D at different percentage of CRT content
2. ábra Az A, B, C és D keverék nyomószilárdsága a CRT-tartalom különböző százalékánál

Component	Water	Cement	Sand	CRT	CA
Cost per kg (USD)	0.001	0.120	0.005	0.025	0.016

Table 8 Cost of concrete components per kg
8. táblázat Beton összetevők költsége kilogrammonként

3.2.4 Model formulation and validation

Calibration and validation of Scheffe's augmented simplex lattice models were carried out using the respective experimental data in *Table 7* with the aid of a commercial software, Minitab 16. The models were in pseudo components.

3.2.4.1 Model equation for compressive strength

Scheffe's second degree polynomial was fitted to the compressive strength data in *Table 7* based on *Eq. (13)*. To avoid overfitting the model, backward elimination procedure of stepwise regression was used. As such, insignificant terms in the model were eliminated and the resulting number of terms were less than 15 as it should be based on *Eq. (6)* and *(13)*. *Table 9* shows estimated model coefficients for compressive strength model with the associated statistics at 95% confidence level, while *Table 10* presents results of analysis of variance (ANOVA) and *Fig. 3* is the normal probability plot of the model residuals. From the ANOVA

table, it could be seen that both linear and quadratic sources are significant since each has a p-value less than 0.05. However, it has been a standard practice to select the highest degree model as long as it is significant [26, 27]. Hence, quadratic model being of higher degree was selected. Thus, if the five vertices of the designed {5, 2} simplex lattice are represented in pseudo form as X_1, X_2, X_3, X_4 and X_5 respectively, then compressive strength model equation based on *Eq. (13)* is presented as:

$$f_{c,28} = 35.71X_1 + 27.95X_2 + 20.42X_3 + 35.46X_4 + 42.13X_5 - 17.54X_1X_3 - 20.02X_1X_4 - 15.60X_2X_4 - 24.45X_3X_5 \quad (20)$$

Term	Coef	SE Coef	T	P
X1	35.71	0.9727	*	*
X2	27.95	0.9170	*	*
X3	20.42	0.9739	*	*
X4	35.46	0.9739	*	*
X5	42.13	0.9170	*	*
X1*X3	-17.54	6.6288	-2.65	0.016
X1*X4	-20.02	6.6288	-3.02	0.007
X2*X4	-15.60	6.6371	-2.35	0.030
X3*X5	-24.45	6.6371	-3.68	0.002
	S = 1.55976		R-Sq = 95.62%	
	R-Sq(pred)= 87.31%		R-Sq(adj)= 93.67%	

Legend: Coef = Coefficients of Terms; SE Coef = Standard Error; T = t-test value; P = p-value; S = Variance;

Table 9 Estimated regression coefficients for compressive strength model
9. táblázat Becsült regressziós együtthatók a nyomószilárdság modelljéhez

Validation and test of adequacy:

Normal probability plot in *Fig. 3* shows a close distribution of the model residuals along a reference line. The plot has a p-value of 0.72 (which is greater than 0.05). Hence, the null hypothesis – which states that the data follow a normal distribution – cannot be rejected. This indicates that the residuals of the model follow a normal distribution and justifies the use of ANOVA. The analysis of variance table in *Table 10* shows an insignificant lack-of-fit with a p-value of 0.945 (> 0.05). These and other statistical values in *Table 9*, like r-squared value of 95.62%, adjusted r-squared of 93.67% and predicted r-squared of 87.31% confirm the adequacy of *Eq. (20)* for predicting 28th day compressive strength of recycled ceramics tile waste concrete.

Source	DF	Seq SS	Adj SS	Adj MS	F	P
Regression	8	955.56	955.56	119.445	49.10	0.000
Linear	4	866.05	793.13	198.282	81.50	0.000
Quadratic	4	89.51	89.51	22.378	9.20	0.000
X1*X3	1	16.02	17.03	17.034	7.00	0.016
X1*X4	1	24.29	22.19	22.192	9.12	0.007
X2*X4	1	16.18	13.44	13.443	5.53	0.030
X3*X5	1	33.02	33.02	33.016	13.57	0.002
Residual Error	18	43.79	43.79	2.433		
Lack-of-Fit	12	17.86	17.86	1.488	0.34	0.945
Pure Error	6	25.93	25.93	4.322		
Total	26	999.35				

Legend: DF = Degree of Freedom; Seq SS = Sequential Sum of Squares; F = F-value Adj SS = Adjusted Sum of Squares; Adj MS = Adjusted Mean Squares;

Table 10 Analysis of variance for compressive strength model
10. táblázat Variancia-elemzés a nyomószilárdság modelljéhez

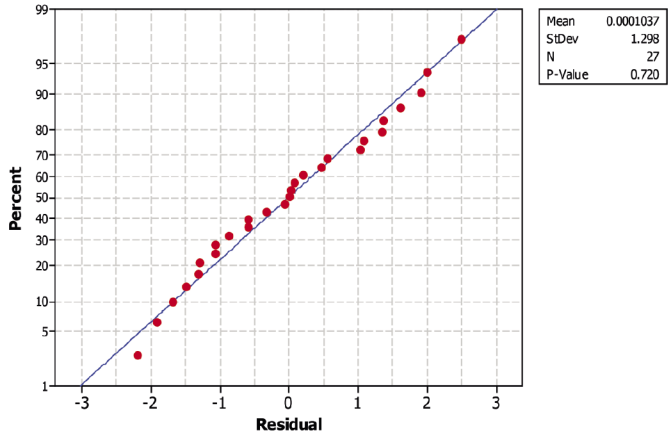

Fig. 3 Normal probability plot for compressive strength model residuals
3. ábra Normál valószínűségi diagram a nyomószilárdsági modell maradékaihoz

3.2.4.2 Model equation for slump and cost

Scheffe's augmented simplex lattice models for slump height and cost, based on *Eq. (13)* were fitted to the respective data in *Table 7*. Cost estimation is usually modelled linearly by summation of cost of concrete components [28] but this was not possible with this work since the independent variables were not concrete components in proportions, rather pseudo components of the simplex. Procedures for model calibration and validation were the same as that of compressive strength model described in *3.2.4.1*. Estimated regression coefficients and analysis of variance results for both models are presented in *Tables 11* to *14* while normal probability plots of model residuals are presented in *Fig. 4* and *Fig. 5*. Using the respective model coefficients from *Tables 11* and *13*, Scheffe's second degree polynomials for slump and cost are presented in *Eq. (21)* and *(22)* respectively.

$$slump = 5.3X_1 + 63.3X_2 + 16.5X_3 + 79.8X_4 + 13.1X_5 + 131.9X_1X_3 - 117.8X_2X_3 - 85.1X_2X_4 + 85.1X_3X_4 - 166.1X_4X_5 \quad (21)$$

$$\cos t = 35168X_1 + 31210X_2 + 25305X_3 + 38584X_4 + 40934X_5 - 9461X_1X_4 - 7926X_3X_4 - 8848X_3X_5 \quad (22)$$

Term	Coef	SE Coef	T	P
X1	5.3	3.207	*	*
X2	63.3	3.402	*	*
X3	16.5	3.603	*	*
X4	79.8	3.603	*	*
X5	13.1	3.207	*	*
X1*X3	131.9	23.223	5.68	0.000
X2*X3	-117.8	23.196	-5.08	0.000
X2*X4	-85.1	23.196	-3.67	0.002
X3*X4	85.1	23.169	3.67	0.002
X4*X5	-166.1	23.223	-7.15	0.000
S = 5.45502			R-Sq = 96.47%	
R-Sq(pred) = 83.17%			R-Sq(adj) = 94.60%	

Table 11 Estimated regression coefficients for slump model
11. táblázat Becsült regressziós együtthatók a roskadás modelljéhez

Source	DF	Seq SS	Adj SS	Adj MS	F	P
Regression	9	13815.4	13815.4	1535.05	51.59 0.000	
Linear	4	9774.6	10581.2	2645.30	88.90	0.000
Quadratic	5	4040.8	4040.8	808.17	27.16	0.000
X1*X3	1	784.8	960.7	960.66	32.28	0.000
X2*X3	1	909.1	768.0	767.98	25.81	0.000
X2*X4	1	373.4	400.2	400.18	13.45	0.002
X3*X4	1	450.8	401.5	401.51	13.49	0.002
X4*X5	1	1522.7	1522.7	1522.68	51.17	0.000
Residual Error	17	505.9	505.9	29.76		
Lack-of-Fit	11	387.1	387.1	35.19	1.78	0.248
Pure Error	6	118.7	118.7	19.79		
Total	26	14321.3				

Table 12 Analysis of variance for slump model
12. táblázat Variancia-elemzés a roskadás modelljéhez

Term	Coef	SE Coef	T	P
X1	35168	315.9	*	*
X2	31210	296.4	*	*
X3	25305	335.2	*	*
X4	38584	335.2	*	*
X5	40934	315.9	*	*
X1*X4	-9461	2283.8	-4.14	0.001
X3*X4	-7926	2281.3	-3.47	0.003
X3*X5	-8848	2283.8	-3.87	0.001
S = 537.693			R-Sq = 98.86%	
R-Sq(pred)= 97.29%			R-Sq(adj)= 98.44%	

Table 13 Estimated regression coefficients for cost model
13. táblázat Becsült regressziós együtthatók a költségmodellhez

Validation and test of adequacy:

Again, normal probability plots in *Fig. 4* and *Fig. 5* both show close distribution of their respective model residuals along a reference line. The plots have p-values of 0.92 and 0.847 (which are both greater than 0.05) respectively. Hence, the null hypothesis cannot be rejected. These indicate that the residuals of both models follow a normal distribution and justifies the use of ANOVA. The analysis of variance tables in *Tables 12* and *14* show insignificant *lack-of-fits* with p-values of 0.248 and 0.987. These and other statistical values in *Tables 12* and *14*, like r-squared values of 96.47% and 98.86%, adjusted r-squared of 94.6% and 98.44% and predicted r-squared of 83.17% and 97.29% confirm the adequacy of *Eqs. (21)* and *(22)*.

Source	DF	Seq SS	Adj SS	Adj MS	F	P
Regression	7	476930824	476930824	68132975	235.66	0.000
Linear	4	464094664	442322554	110580639	382.48	0.000
Quadratic	3	12836160	12836160	4278720	14.80	0.000
X1*X4	1	5241710	4962268	4962268	17.16	0.001
X3*X4	1	3254759	3489671	3489671	12.07	0.003
X3*X5	1	4339691	4339691	4339691	15.01	0.001
Residual Error	19	5493161	5493161	289114		
Lack-of-Fit	13	1845746	1845746	141980	0.23	0.987
Pure Error	6	3647415	3647415	607903		
Total	26	482423985				

Table 14 Analysis of variance for cost model
14. táblázat Varianciaanalízis a költségmodellhez

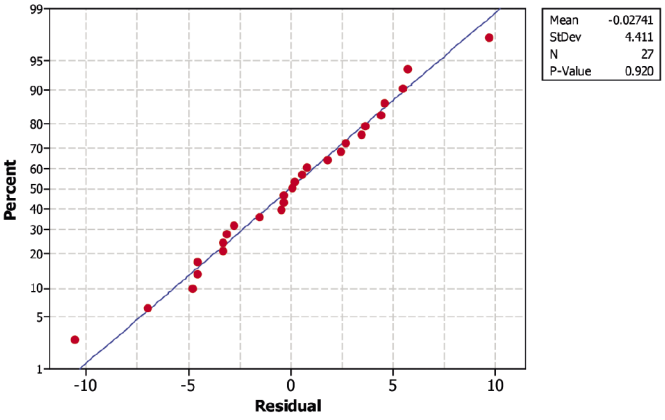

Fig. 4 Normal probability plot for slump model residuals
4. ábra Normál valószínűségi diagram a roskadás modelljének maradékaihoz

3.3 Sample optimization

RSM combines mathematical and statistical methods of experiment design, regression analysis and optimization to provide approaches to mixture optimization. Hence, once the required responses have been modeled, optimization can easily be carried out for any set of desired criteria. In this study, having formulated model equations for compressive strength, slump height and cost estimate, sample optimization of recycled ceramic waste concrete mix was carried out with the aid of Altair Hyperstudy software using three different techniques. The techniques were: Adaptive Response Surface Method (ARSM), Global Response Search Method (GRSM) and Sequential Quadratic Programming (SQP). The main objective of the optimization was to generate the most cost-effective mix designs with compressive strength of at least 35 MPa and minimum slump of 25 mm.

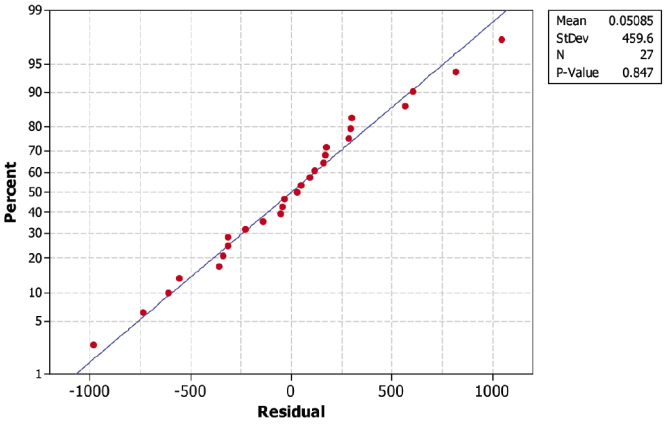

Fig. 5 Normal probability plot for cost model residuals
5. ábra Normál valószínűségi diagram a költségmodell maradékaihoz

3.3.1 Formulation of optimization problem

Design variables for this optimization were the five concrete components in pseudo form denoted as X_1, X_2, X_3, X_4 and X_5 while *Eq. (3)* was used as side constraints for each of the variables. The initial value for the variables was 0.2 representing the centroid of the simplex. Since the objective was to minimize cost, the cost model in *Eq. (22)* was used as objective function. Design constraints were formulated as below based on *Eqs. (2)*, *(20)* and *(21)*:

$$X_1 + X_2 + X_3 + X_4 + X_5 = 1.00$$
$$5.3X_1 + 63.3X_2 + 16.5X_3 + 79.8X_4 + 13.1X_5 + 131.9X_1X_3$$
$$-117.8X_2X_3 - 85.1X_2X_4 + 85.1X_3X_4 - 166.1X_4X_5 \geq 25.00$$
$$35.71X_1 + 27.95X_2 + 20.42X_3 + 35.46X_4 + 42.13X_5$$
$$-17.54X_1X_3 - 20.02X_1X_4 - 15.60X_2X_4 - 24.45X_3X_5 \geq 35.00$$

3.3.2 Optimization results

Optimization results for the three techniques are presented in *Table 15*. Outputs from Hyperstudy were in pseudo components and were therefore transformed to real component ratios using *Eq. (19)*. The three techniques all started their search from the centroid of the simplex using iteration approach. Surprisingly, they arrived at their optimum at different points in the simplex leading to different results. However, GRSM seems to be the most suitable for this optimization because it achieved the most economical mix of \$92.77 per m^3, while still maintaining the required compressive strength and slump height.

3.4 Discussion of results

Results from this work, especially that of Phase A as presented in *Fig. 2*, has confirmed that incorporation of CRT as fine aggregate in concrete increases its compressive strength. This increase is directly proportional to the percentage replacement of sand with CRT. This is not surprising because similar results have been reported elsewhere [10, 11, 14, 18] although some with the use of other ceramic aggregates other than CRT. Torkittikul and Chaipanich had earlier reported 50% as the optimum replacement level and discouraged higher replacement level [14]. However, it should be noted that their decline in compressive strength at replacement level higher than 50% was due to reduced workability associated with the increased ceramic aggregate content. Replacement of conventional fine aggregate with ceramic aggregate can therefore be up to 100% depending on the workability of a mix. Most ceramic aggregates are porous and possess higher water absorption property than sand [10, 13, 14, 24]. This means that during mixing, ceramic aggregates absorb more water than sand, thereby reducing the actual quantity of water used for lubricating the mix constituents. Hence, in designing such mix, provision should be made for this absorbed water.

Using Scheffe's simplex theory, polynomial models have been developed for compressive strength, workability and cost of CRT aggregate concrete. The use of stepwise regression during modelling procedures ensured that all insignificant variables were removed from the model predictors to avoid overfitting. This practice paid off and its benefits are demonstrated in the model statistics shown in *Tables 9 – 14* and *Figs. 3 – 5*. *Tables 9*, *11* and *13* show that only significant model terms at 95% confidence level (terms with p-values less than 0.05) were selected as predictors for each of the formulated models. The high r-squared, adjusted r-squared and predictive r-squared values reflects the high quality of the models. While r-squared and adjusted r-squared values show how well the models fit their respective data, the high predictive r-squared values indicate how well the formulated models can predict new responses outside the design points. The three models show insignificant lack-of-fit as indicated in ANOVA tables in *Tables 10, 12* and *14*.

Maximum predictable response from the compressive strength model was 42.13MPa existing at vertex X_5 of the simplex and corresponding to mix ratio 0f 0.45:1:0:1:2 for water, cement, sand, CRT and CA. On the other hand, the lowest predictable compressive strength was found to be 20.34MPa existing very close to Vertex X_3 and corresponding to mix ratio of 0.64:1:2.35:0.06;4.35. This means that the compressive strength model can be used to predict concrete grades C16/20 to C30/37 according to BS EN 206 [40] and this falls within the range of commonly used concrete grades especially for reinforced concrete.

4. Conclusions

In this study, effect of CRT fine aggregate content on compressive strength of concrete have been studied. From the experimental investigations, incorporation of this recycled waste aggregate increases compressive strength of concrete and the increase is directly proportional to the percentage replacement of sand with CRT. Authors therefore recommends up to 100% replacement of conventional fine aggregate with ceramic aggregate depending on the workability of the mix. Scheffe's second degree polynomial models were also formulated for compressive strength, slump height and cost of concrete incorporating CRT as fine aggregate. Stepwise regression was used during model fitting and selections. The models were validated using analysis of variance and normal probability plots of model residuals and their adequacies were confirmed. Maximum and minimum predictable compressive strengths were 42.13 MPa and 20.34 MPa respectively indicating that the compressive strength model can be used to predict concrete grades C16/20 to C30/37 according to BS EN 206. Optimization was carried out using three optimization techniques (ARSM, GRSM and SQP) to obtain the most economical mix with a compressive strength of at least 35 MPa

Optimization technique	Pseudo components					Real Component Ratios					Response		
	X_1	X_2	X_3	X_4	X_5	Z_1	Z_2	Z_3	Z_4	Z_5	$f_{c,28}$	Slump	Cost
						Water	Cement	Sand	CRT	CA	(MPa)	(mm)	(USD)
ARSM	0.123	0.000	0.037	0.559	0.281	0.448	1.000	0.652	0.466	2.216	35.10	25.83	90.379
GRSM	0.437	0.305	0.000	0.000	0.258	0.531	1.000	0.458	0.914	2.742	35.00	25.00	84.710
SQP	0.000	0.000	0.116	0.549	0.335	0.446	1.000	0.839	0.335	2.290	35.00	25.00	89.598

Table 15 Optimum mix in pseudo and real components and their corresponding responses
15. táblázat A pszeudó- és valós komponensek optimális keveréke és az azokhoz tartozó mechanikai tulajdonságok és költségek

and slump height of at least 25mm. From optimization results, the three techniques arrived at optimum at different points in the simplex leading to different results. However, GRSM proved to be the most suitable technique for this purpose. With the model equations, similar optimization can be carried out for any desired response within the simplex.

Acknowledgement

Authors acknowledge the financial support of Tertiary Education Trust Fund (TETFund) Nigeria for the PhD studies of Edidiong E. Ambrose.

Conflict of interests

Authors declare that there is no conflict of interests in this research work.

References

[1] Ikponmwosa, E. E. – Ehikhuenmen, S. O. (2017): The effect of ceramic waste as coarse aggregate on strength properties of concrete, Nigerian Journal of Technology. Vol. 36, No. 3, pp.691-696. https://dx.doi.org/10.4314/njt.v36i3.5.

[2] Tahar, Z. – Benabed, B. – Kadri, E. H. – Ngo, T. – Bouvet, A. (2020): Rheology and strength of concrete made with recycled concrete aggregate as replacement of natural aggregates, Epitoanyag Journal of Silicate Based and Composite Materials, Vol. 72, No. 2, pp.48-58. https://doi.org/10.14382/epitonyag.jsbcm.2020.8.

[3] Domone, P. – Illston, J. (2010): Construction materials – the nature and behaviour, 4th edn, CRC Press, New York.

[4] Gartner E. (2004): Industrial interesting approaches to low CO_2, Cement and Concrete Research, Vol. 34, No. 9, pp.1489-1498. https://doi.org/10.1016/j.cemconres2004.01.021.

[5] Allahverdi, A. – Mahinroosta, M. – Pilehvar, S. (2017) A temperature-age model for prediction of compressive strength of chemically activated high phosphorus slag content cement. International Journal of Civil Engineering, Vol. 15, No. 5, pp. 839-847. https://doi.org/10.1007/s40999-017-0196-5

[6] Neville, A. M. (2011): Properties of concrete, 5th edn, Pearson Education, London.

[7] Kannan, D. M. – Aboubakr, S. H. – El-Dieb, A. S. – Taha, M. M. (2017): High performance concrete incorporating ceramic wastes powder as large partial replacement of Portland cement. Construction and Building Materials, Vol. 144, pp.35-41. https://doi.org/10.1016/j.conbuildmat.2017.03.115.

[8] Tang, W. C. – Lo, Y. – Nadeem, A. (2008): Mechanical and dryness shrinkage properties of structural-graded polystyrene aggregate concrete, Cement and Concrete Composite, Vol. 30, No. 5, pp.403-409. https://dx.doi.org/10.4314/j.cemconcomp.2008.01.002.

[9] Ambrose, E. E. – Ekpo, D. U. – Umoren, I. M. – Ekwere, U. S. (2018): Compressive strength and workability of laterized quarry sand concrete. Nigerian Journal of Technology, Vol. 36, No. 3, pp.605-610. https://dx.doi.org/10.4314/njtv37i3.7.

[10] Elci, H. (2016): Utilization of crushed floor and wall tile wastes as aggregate in concrete production. Journal of Cleaner Production, Vol. 112 pp.742-752. https://doi.org/10.1016/j.jclepro2015.07.003.

[11] Awoyera, P. O. – Ndambuki, J. M. – Akinmusuru, J. O. – Omole, O. D. (2018): Characterization of ceramic waste aggregate. HBRC Journal, Vol. 14, No. 3, pp.282-287. https://doi.org/10.1016/j.hbrcj.2016.11.003.

[12] Zimbili, O. – Salim, W. – Ndambuki, M. (2014) A review on the usage of ceramic wastes in concrete production, International Journal of Civil, Environmental, Structural, Construction and Architectural Engineering. Vol. 8, No. 1, pp.91-95.

[13] Halicka, A. – Ogrodnik, P. – Zegardlo, B. (2013): Using ceramic sanitary ware waste as concrete aggregate. Construction and Building Materials Vol. 48 pp.295-305. https://doi.org/10.1016/j.conbuildmat.2013.06.063.

[14] Torkittikul, A. – Chaipanich, A. (2010): Utilization of ceramic waste as fine aggregate within Portland cement and fly ash concrete. Cement and Concrete Composite. Vol. 32, pp.440-449. https://doi.org/10.1016/j.cemconcomp.2010.02.004.

[15] Heidari, A. – Tavakoli, D. (2013); A study of the mechanical properties of ground ceramic powder concrete incorporating nano-SiO_2 particles, Construction and Building Materials Vol. 38, pp.255-264. https://doi.org/10.1016/j.conbuildmat.2012.07.110.

[16] Daniyal, M. – Ahmad, S. (2015): Application of waste ceramic tile aggregates in concrete, International Journal of Innovative Research in Science and Engineering Technology, Vol. 4, No. 12, pp.12808-12815. https://doi.org/10.15680/IJIRSET.2015.0412128.

[17] Medina, C. – Rojas, M. I. – Frias, M. (2012): Reuse of sanitary ceramic wastes as coarse aggregate in eco-efficient concretes, Cement and Concrete Composite, Vol. 34, pp.48-54. https://doi.org/10.1016/j.cemconcomp.2011.08.015.

[18] Pacheco-Torgal, F. – Jalali, S. (2010): Reuse of ceramic wastes in concrete, Construction and Building Materials, Vol. 24, pp.832-838. https://doi.org/10.1016/j.conbuildmat.2009.10.023.

[19] Medina, C. – Frias, M. – Rojas, M. I. (2012): Microstructure and properties of recycled concrete using ceramic sanitary ware industry waste as coarse aggregate, Construction and Building Materials, Vol. 31, pp.112-118. https://doi.org/10.1016/j.conbuildmat.2011.12.075.

[20] Shruthi, H. G. – Gowtham, M. E. – Samreen, T. – Syed, R. P. (2016): Reuse of ceramic wastes as aggregate in concrete. International Research Journal of Engineering and Technology, Vol. 3, No. 7, pp.115-119.

[21] Awoyera, P. O. – Akinmusuru, J. O. – Ndumbuki, J. M. (2016): Green concrete production with ceramic wastes and laterite. Construction and Building. Materials, Vol. 117, pp.29-36. https://doi.org/10.1016/j.conbuildmat.2016.04.108.

[22] Adamson, M. – Razmjoo, A. – Poursaee, A. (2015): Durability of concrete incorporating crushed brick as coarse aggregate. Construction and Building Materials, Vol. 94, pp.426-434. https://doi.org/10.1016/j.conbuildmat.2015.07.056.

[23] Zegardlo, B. – Szelag, M. – Ogrodnik, P. (2016): Ultra-high strength concrete made with recycled aggregate from sanitary ceramic wastes – the method of production and the interfacial transition zone. Construction and Building Materials, Vol. 122, pp.736-742. https://doi.org/10.1016/j.conbuildmat.2016.06.112.

[24] Alves, A. V. – Vieira, T. F. – Brito, J. – Correia, J. R. (2014): Mechanical properties of structural concrete with fine recycled ceramic aggregate, Construction and Building Materials, Vol. 64, pp.103-113. https://doi.org/10.1016/j.conbuildmat.2014.04.037.

[25] Aliabdo, A. A. – Abd-Emoatry, A. M. – Hassan, H. H. (2014): Utilization of crushed clay brick in concrete industry. Alexandria Engineering Journal, Vol. 53, No. 1, pp.151-168. https://doi.org/10.1016/j.aej.2013.12.003.

[26] Anya, U. C. (2015): Models for predicting the structural characteristics of sand-quarry dust blocks. Ph.D Dissertation, University of Nigeria.

[27] Simon, M. J. (2003): Concrete mixture optimization using statistical methods: Final Report. Federal Highway Administration, Infrastructure Research and Development, Georgetown Pike McLean, VA, USA.

[28] DeRousseau, M. A. – Kasprzyk, J. R. – Srubar, W. V. (2018): Computational design optimization of concrete mixture: a review, Cement and Concrete Research, Vol. 109, pp.42-53.

[29] Okafor, F. O. – Oguaghamba, O. (2010): Procedures for optimization using scheffe's model, Journal of Engineering Science and Application, Vol. 7, No. 1, pp.36-46.

[30] Osadebe, N. N. – Mbajiorgu, C. C. – Nwakonobi, T. U. (2007): An optimization model development for laterized concrete mix proportioning in building constructions. Nigerian Journal of Technology, Vol. 26, No. 1. Pp.37-45.

[31] Onuamah, P. N. – Osadebe, N. N. (2015): Development of optimized strength model of lateritic hollow block with 4% mound soil inclusion, Nigerian Journal of Technology, Vol. 34, No. 1, pp.1-11. https://doi.org/10.4314/njt.v34i1.1.

[32] Akhnazarova, S. – Kafarov, V. (1982): Experiment Optimization in Chemistry and Chemical Engineering, MIR Publishers, Moscow.

[33] Scheffe, H. (1958): Experiment with mixtures, Journal of Royal Statistics Society, Vol. 20, No. 2, pp.344-360. https://doi.org/10.1111/j.2517-6161.1958.tb00299.x.

[34] Attah, I. C. – Etim, R. K. – George, U. A. – Bassey, O. B. (2020); Optimization of mechanical properties of rice husk ash concrete using Scheffe's theory, SN Applied Sciences, Vol. 2 p.928. https://doi.org/10.1007/s42452-020-2727-y.

[35] Onyelowe, K. – Alaneme, G. – Igboayaka, C. – Orji, F. – Ugwuanyi, H. – Van, D. B. – Van, M. N. (2019): Scheffe optimization of swelling, Califonia bearing ratio, compressive strength, and durability potentials of quarry dust stabilized soft clay soil, Material Science for Energy Technology, Vol. 2, pp.67-77. https://doi.org/10.1016/j.mset.2018.10.005.

[36] NIS 444-1 (2008): Composition, specification and conformity criteria for common cements, Standard Organization of Nigeria, Abuja.

[37] BS EN 12390-2 (2009): Testing hardened concrete – Part 2: making and curing specimens for strength tests. British Standard Institute, London.

[38] BS EN 12350-2 (2009): Testing fresh concrete – part 2: slump test. British Standard Institute, London.

[39] BS EN 12390-4 (2000): Testing hardened concrete – part 4: compressive strength – specification for testing machines. British Standard Institute, London.

[40] BS EN 206 (2013): Concrete – specification, performance, production and conformity. British Standard Institute, London.

Ref.:
Ambrose, Edidiong E. – **Okafor**, Fidelis O.– **Onyia**, Michael E.: *Compressive strength and Scheffe's optimization of mechanical properties of recycled ceramics tile aggregate concrete*
Építőanyag – Journal of Silicate Based and Composite Materials, Vol. 73, No. 3 (2021), 91–102. p.
https://doi.org/10.14382/epitoanyag-jsbcm.2021.14

The influence of foundry wastes on the quality of autoclaved sand-lime materials

Zdzisław PYTEL
is a Doctor in Department of Building Materials Technology, Faculty of Materials Science and Ceramics, AGH University of Science and Technology, Cracow, Poland. His special field is utilization of waste by-products (especially fly ashes) in ceramic building materials made from clays and in the range of cementitious materials in concrete technology. He has worked for many years projects connected with sand-lime bricks production.

Zdzisław PYTEL ▪ AGH University of Science and Technology, Faculty of Materials Science and Ceramics, Department of Building Materials Technology, Poland ▪ pytel@agh.edu.pl

Érkezett: 2021. 10. 18. ▪ Received: 18. 10. 2021. ▪ https://doi.org/10.14382/epitoanyag-jsbcm.2021.15

Abstract

The paper presents the results of research on the possibility of reusing selected types of foundry waste, i.e. used molding and core sands and dust obtained in the process of their regeneration, as alternative or supplementary materials in relation to the quartz sand originally used in manufacturing of sand-lime bricks. In the production technology of sand-lime products, quartz sand is used as aggregate. A rational factor in favor of such a technological solution is the high content of crystalline silica in the waste molding and core sands, in which the mineral matrix is composed of good quality quartz sands.

The research concept covers production of a series of samples of autoclaved silicate materials formed by pressing, from raw material mixtures involving the discussed waste materials. In the laboratory tests conducted for the preparation of autoclaved materials of the sand-lime brick type, apart from traditional raw materials in the form of natural quartz sand and burnt lime, different molding waste and/or core sand materials and post-regenerative dusts were used for composing raw material mixtures. Foundry industry wastes were introduced into the basic raw material based on the gradually increasing substitution of quartz sand, in the amount within the range of 0 - 100% (wt. %).

The assessment of the possibility of using the discussed waste materials in the indicated direction was based on the result of a comparative analysis, covering the main functional characteristics of two types of materials, i.e. reference material, obtained from raw material mixture, containing no waste and series of experimental materials, produced with various quantitative and qualitative contributions of waste materials. The characteristics of the obtained autoclaved materials are also supplemented by the results of the leaching tests, for heavy metal elements and the analysis of selected aspects of the microstructure carried out by the SEM and EDAX method.

The results of the research show that it is possible to use casting waste compounds after their processing, in the production of autoclaved sand-lime products. This processing of wastes is two-stage operation. The purpose of the first stage is to restore the primary graining of quartz sand used to obtain foundry moulds and cores, while the second stage is to remove the organic binder residues that appear on the quartz sand grains in the form of thin layers hindering the reaction with burnt lime.

Keywords: calcium silicate brick, moulding and core waste, organic binder residue, heavy metal leaching

Kulcsszavak: kalcium-szilikát tégla, öntési és maghulladék, szerves kötőanyag maradványok, nehézfémek kioldódása

1. Introduction

Foundry and core molds are in most cases single-use casting molds. In practice, this means that after the process of casting metals or their respective alloys has been completed and the castings are removed from the molds, they are treated as a waste. Thus, they are intended for storage on various types of landfills, with virtually no possibility of their reuse in the foundry process. Considering the fact that the used foundry molds contain a large amount of silica in the form of β-quartz, there are rational premises for their secondary use in non-foundry areas. A good example here can be the building materials industry, and more precisely those manufacturing technologies that require the use of large quantities of quartz sand [1-6]. The assessment of the possibility of reusing quartz sand obtained from the recycling of used foundry molds was analyzed on the example of the autoclaved building materials technology based on natural sand and burnt lime as basic raw materials. In the conducted tests, it was assumed that the silica material obtained as a result of processing of used casting molds [7] will act as aggregate in raw material mixtures intended for obtaining autoclaved materials. Therefore, it will be a partial or complete substitute (replacement) of natural quartz sand, commonly used as aggregate for the production of pressed silicate products. The usefulness of these quartz sands, derived from the recycling of used foundry and core molds, for obtaining this type of products was determined based on the results of comparative analysis. The scope of this analysis included the basic functional characteristics of autoclaved materials obtained with this type of sands (materials with experimental compositions) in relation to the properties of reference materials. On the other hand, in order to confirm or eliminate the potentially negative impact on the natural environment regarding the release of heavy metals from

silicate products obtained with the used of cast foundry sands, which process can take place throughout their entire lifetime, leachability tests were carried out [8-14]. The results obtained during the research are presented in this paper.

2. Materials

During the implementation of this research work, traditional and alternative raw materials were used to obtain silicate product. Industrial raw materials were used as the basic raw materials, while the alternative to quartz sand of natural origin raw material was silica material recycled from the used foundry masses showing different properties, determined mainly by the type of binder used to prepare them. The group of basic raw materials therefore comprised:

- quartz sand of natural origin (symbol QS-LU),
- highly reactive ground burnt lime, non-slaked lime obtained in industrial conditions (symbol LBU-HR),
- distilled water (symbol DW).

On the other hand, the group of alternative silica raw materials used as a partial or complete substitute for natural quartz sand were quartz sands obtained from the recycling of used foundry masses. These masses represented various types of waste foundry or core molds occurring alone or in the form of appropriate compositions. Used foundry sands included in the research program were of the following types:

- casting mass with an organic binder in the form of furan resin (symbol WSK-FU and MP-FU),
- casting mass from Cold Box technology (symbol WSK-CB),
- a mixture of different types of used foundry masses (symbol WSK-M),
- water-glass casting mass (symbol MO-WG),
- alkaline-phenol casting mass (symbol MO-AF),
- regenerative dusts obtained as a result from regeneration of casting mass with furan resin (symbol MP-P).

At the same time, it is worth noting that the abovementioned used foundry sands were derived from the same type of quartz sand from the "Grudzeń Las" mine (symbol QS-GL) used to obtain foundry and core masses.

The raw material mixtures intended for the preparation of individual series of samples were characterized by a constant quantitative composition, while a variable qualitative composition. The constant quantitative composition of these mixtures was ensured by the same shares of aggregate, binder and water in them, which were 83.6%, 8.0% and 8.4% (wt. %) respectively. The given shares of burnt lime and water resulted from the adopted design assumptions regarding the constant of activity "A" and humidity "w" of the raw material mixtures. The variability of the qualitative composition of the raw material mixtures, intended for the preparation of experimental materials, was obtained as a result of gradual (25, 50 and 100 wt. %) substitution of quartz sand QS-LU by the sands obtained from recycling, diversified in terms of properties and source of used foundry masses. In addition, it was assumed that the degree of processing of used casting sands has a significant impact on the quality of the silicate materials obtained. In connection with the above, in the first stage of research, waste casting sands were subjected to an initial processing process, aimed only at restoring the original granulation of the quartz matrix. On the other hand, in the second stage of the study, casting sands were subjected to additional mechanical treatment consisting of a short-term "dry" milling process, carried out to remove the residue of organic binders from the quartz matrix grains surface. It is worth noting that in the second stage of testing, silicate samples were obtained from raw material mixtures, characterized by a constant share of foundry waste, constituting 25% of the mass of natural quartz sand.

Individual series of samples of silicate materials prepared from raw material mixtures of specified compositions were obtained each time in a fixed and repeatable manner. Their activity and humidity were monitored all the time. Required amounts of individual components, resulting from the adopted quantitative composition, were subjected to a two-stage homogenization process; at the beginning without the participation of water, and then with its participation. Distilled water was added in the amount necessary for the total hydration of quicklime and obtaining 6% of the mixture moisture. In order to carry out the lime slaking process, the raw material mixture was placed in a sealed glass vessel and kept for about 1 hour in a laboratory dryer at a temperature of 65 °C. After this period of time, the raw material mixture was cooled to ambient temperature and subjected to final homogenization. From the mass prepared in this way, cylindrical samples with dimensions of diameter and height equal to 25 mm were formed using a fold-out metal mold. Sample formation was carried out using a hydraulic press method of two-sided and two-stage pressing with interstage venting, at pressures of 10 and 20 MPa, respectively. 12 samples were formed in the same way for each mass composition. Then the samples were placed in Teflon crucibles, which in turn were inserted into the chambers of steel pressure cylinders acting as laboratory autoclaves. Stainless-steel cylinders, containing samples and distilled water located in its lower part, were inserted into the heater and subjected to the heating process according to a specific regime. In this way the process of hydrothermal treatment of samples under laboratory conditions was carried out. The conditions used in the sample treatment, reflected the conditions for processing of sand-lime products in industrial autoclaves and were as follows:

- saturated steam pressure - 1.002 MPa
- steam temperature - 180 °C
- total autoclaving time - 9.5 hours

3. Methods

The samples obtained in hydrothermal conditions were tested for the determination of their basic performance characteristics. The tests of physical properties were carried out in accordance with the scope and procedures given in the product standard PN-EN 771-2: 2004 [15] and the standards referred to selected

properties, in particular concerning: compressive strength - PN-EN 772- 1: 2001 [16] and dry density - PN-EN 772-13: 2001 [17]. According to the reference documents provided, the scope of testing of these materials included the following performance parameters:

- compressive strength f_b,
- dry density (in parallel with two methods): $\rho^0_{n,u}$ and $\rho^1_{n,u}$,
- c_w water absorption.

In addition, open porosity P_0 was determined after the obtained materials by hydrostatic weighing [18].

In case of each prepared mixtures intended for obtaining a given series of samples, its molding moisture "w" and activity "A" were monitored [19, 20]. The moisture content was determined by the drying method as the average of two samples. On the other hand, the activity of raw material mixtures was determined by a chemical method consisting of titration a specified amount of mass taken in a wet state with 1M HCl in the presence of a 1% alcohol solution of phenolphthalein. The amount of acid needed to neutralize calcium hydroxide, i.e. the disappearance of the pink color of the suspension, was the basis for calculating the percentage of CaO in the dry form and thus its activity (*Table 1*).

Determination of the leaching level of selected heavy metals in case of silicate samples containing different categories of waste molding and/or core sands was carried out in accordance with the procedure given in the standard PN-EN 12457-2 [21]. The subject of the analysis were eluates prepared in accordance with the guidelines given in this standard, while the determination of the content of selected heavy metals and the interpretation of the obtained test results was made according to the criteria given in the PN-EN ISO 11885 standard [22]. Determination of the content of heavy metal elements in the prepared eluates was performed by the method of atomic emission induction spectrometry (ICP-AES), using the ICP emission spectrometer of the Perkin-Elmer company (model Plasma 400). The measurements included determination of the content of the following elements: chromium, copper, cobalt, molybdenum, selenium, vanadium, zinc, tellurium, lead, cadmium, nickel, tin, antimony, arsenic, boron and barium.

The microstructure examination of the sand-lime materials containing the used casting sands was carried out using the $NOVA_{NANO}$ SEM 200 scanning electron microscope equipped with EDAX microanalyzer, FEI COMPANY.

4. Results

The results concerning the examination of the technological properties of the masses regarding their humidity and activity, as well as the basic functional properties of the sand-lime materials obtained with the use of used casting sands are presented in the *Table 1*.

The results of the microstructure elements examination of selected silicate materials obtained are presented in *Fig. 1*.

The results of the heavy metal leaching tests are presented in *Table 2*.

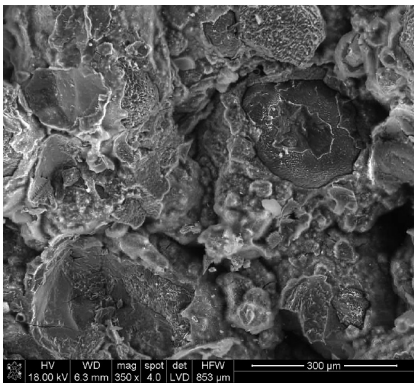

a) PK-LU sample (reference sample of the I stage of the research)

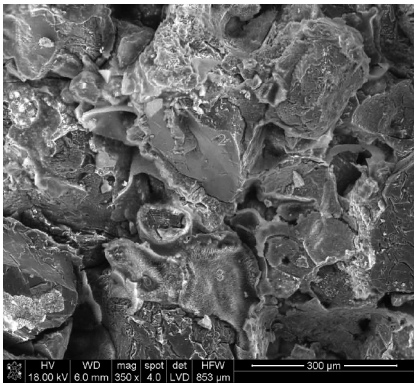

b) Sample WSK-FU_{25} (experimental sample of the I stage of the research)

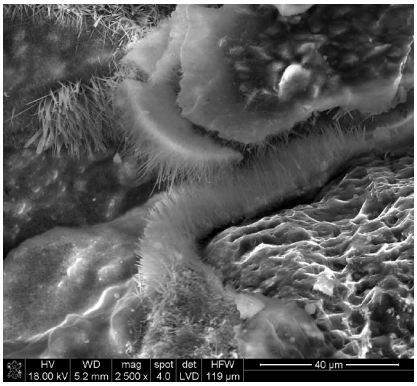

c) m$PK\text{-}LU_{25}$ sample (reference sample of the II stage of the research)

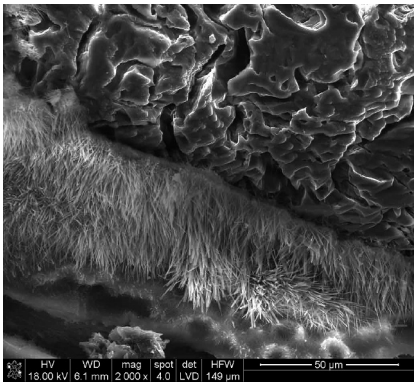

d) mWSK.-FU_{25} sample (experimental sample of the II stage of the research)

Fig. 1 Microstructure of autoclaved sand-lime samples.
1. ábra Autoklávozott homok-mész minták mikrostruktúrája

Mass symbol // Sample symbol	Technological properties of masses		Functional properties of silicate materials samples				
	w, [%]	A, [%]	$\rho^0_{n,u}$, [g/cm³]	$\rho^1_{n,u}$, [g/cm³]	f_b, [MPa]	c_w, [%]	P_o, [%]
I stage of research							
PK-LU	**6.2**	**7.6**	**1.81**	**1.85**	**25.6**	**12.7**	**23.4**
WSK-FU$_{25}$	4.4	7.5	1.76	1.81	23.5	14.0	25.4
WSK-FU$_{50}$	6.4	6.9	1.74	1.78	15.7	15.1	26.8
WSK-FU$_{100}$	4.6	7.6	1.70	1.76	10.3	14.5	25.4
WSK-CB$_{25}$	4.2	7.6	1.77	1.81	23.0	14.6	26.4
WSK-CB$_{50}$	4,6	7.5	1.75	1.79	16.7	15.5	27.8
WSK-CB$_{100}$	4.6	7.5	1.69	1.75	8.3	16.3	28.5
WSK-M$_{25}$	5.7	7.7	1.86	1.85	19.2	13.5	25.0
WSK-M$_{50}$	5.7	7.6	1.80	1.84	19.6	14.3	26.2
WSK-M$_{100}$	5.6	7.3	1.75	1.75	20.2	17.0	29.7
MO-WG$_{25}$	5.5	7.7	1.79	1.82	15.4	13.5	24.7
MO-WG$_{50}$	5.3	8.0	1.76	1.81	11.8	13.4	24.3
MO-WG$_{100}$	4.8	7.3	1.70	1.78	8.0	13.8	24.5
MO-AF$_{25}$	4.1	7.5	1.79	1.83	22.5	14.0	25.8
MO-AF$_{50}$	5.1	7.4	1.77	1.81	15.5	15.4	28.0
MO-AF$_{100}$	6.5	7.4	1.76	1.81	10.5	15.9	28.8
MP-FU$_{25}$	4.7	7.5	1.78	1.82	9.9	15.4	27.9
MP-FU$_{50}$	5.1	7.4	1.76	1.79	4.1	16.9	30.2
MP-FU$_{100}$	6.4	7.4	1.71	1.70	1.1	19.8	33.7
MP-P$_{25}$	6.1	7.4	1,76	1.79	13.7	15.3	27.3
MP-P$_{50}$	6.8	7.0	1.65	1.65	7.2	19.5	32.2
MP-P$_{100}$	6.2	6.6	1.38	1.35	4.9	31.1	42.0
II stage of research							
mPK-LU$_{25}$	**6.2**	**7.5**	**1.82**	**1.85**	**30.7**	**12.4**	**22,9**
mWSK-FU$_{25}$	5.9	7.5	1.81	1.84	30.0	12.7	23,4
mWSK-CB$_{25}$	5.7	6.5	1.79	1.82	28.0	13.5	24,7
mWSK-M$_{25}$	6.2	7.0	1.84	1.85	16.6	13.7	25,4
mMO-WG$_{25}$	6.4	7.4	1.80	1.84	19.3	12.4	22,8
mMO-AF$_{25}$	7.3	7.4	1.82	1.85	27.7	13.1	24,3
mMP-FU$_{25}$	6.3	7.4	1.82	1.85	11.4	14.1	26,2

Table 1 Summary of the results obtained for raw material mixtures and autoclaved materials
1. táblázat A nyersanyag-keverékekkel és autoklávozott anyagokkal kapott eredmények összefoglalása

Analyzed component	Sample designation								Admissible critical leaching levels liquid/solid phase = 10 L/kg for:			Reference data according to
	PK-LU	MO-SW$_{50}$	MO-AF$_{50}$	MP-FU$_{50}$	WSK-CB$_{50}$	WSK-FU$_{50}$	WSK-M$_{50}$	MP-P$_{50}$	Neutral wastes	Other than neutral and hazardous wastes	Hazardous wastes	[14, 22, 25]
	Leaching of the given component mg/kg of dry mass											mg/L
Chromium$_{(total)}$	0.04	0.17	0.08	0.16	0.10	0.09	0.19	0.37	0.5	10	70	0.027
Copper	0.05	0.03	0.02	<0.01	0.09	0.23	<0.01	0.02	2	50	100	0.148
Cobalt	<0.01	<0.01	<0.01	<0.01	<0.01	<0.01	<0.01	<0.01	- (*)	- (*)	- (*)	0.003
Molybdenum	0.24	0.11	0.11	<0.01	0.11	0.09	0.23	0.11	0.5	10	30	- (**)
Selenium	<0.05	<0.05	<0.05	<0.05	<0.05	<0.05	<0.05	<0.05	0.1	0.5	7	- (**)
Vanadium	0.21	<0.01	0.14	<0.01	0.22	0.08	0.21	0.09	-(*)	- (*)	- (*)	- (**)
Zinc	0.10	0.31	0.05	0.38	0.16	0.07	0.09	0.05	4	50	200	0.380
Tellurium	<0.03	<0.03	<0.03	<0.03	<0.03	<0.03	<0.03	<0.03	- (*)	- (*)	- (*)	- (**)
Lead	<0.01	0.21	<0.01	<0.01	<0.01	0.24	0.11	0.35	0.5	10	50	0.063
Cadmium	<0.01	<0.01	<0.01	<0.01	<0.01	<0.01	<0.01	<0.01	0.04	1	5	0.003
Nickel	0.05	0.05	0.06	0.07	0.03	0.10	0.06	0.04	0.4	10	40	0.048
Tin	<0.06	<0.06	<0.06	<0.06	<0.06	<0.06	<0.06	<0.06	- (*)	- (*)	- (*)	- (**)
Antimony	<0.01	<0.01	<0.01	<0.01	<0.01	<0.01	<0.01	<0.01	0.06	0.7	5	- (**)
Arsenic	<0.5	<0.5	<0.5	<0.5	<0.5	<0.5	<0.5	<0.5	0.5	2	25	0.047
Boron	<0.01	<0.01	<0.01	<0.01	<0.01	<0.01	<0.01	<0.01	- (*)	- (*)	- (*)	- (**)
Barium	2.26	3.96	1.94	3.78	1.70	2.02	1.97	2.03	20	100	300	0.707

(*) - no reference data (**) - no data available

Table 2 Leaching of heavy metals from samples containing used molding and core sand
2. táblázat Nehézfémek kimosódása öntvényt és maghomokot tartalmazó mintákból

5. Discussion

Analyzing the obtained test results presented in *Table 1* it should be stated that the numerical values of the tested parameters of the obtained materials are clearly influenced by both the share of used foundry masses in the raw material mixture, expressed by the level of substitution of natural quartz sand, as well as their type and degree of processing. Regardless of the type of foundry waste mass, along with the increase in their share in the raw material mixture, we observe a gradual deterioration of the tested parameters characterizing a given material. However, in relation to the strength parameters, the method of processing of used casting sands has a very beneficial effect. In particular, this applies to the processing method associated with the removal of binder residue from quartz matrix surfaces, especially organic origin, present on them in the form of thin layers. Removing this layer of binder mechanically leads to the activation of the quartz grain surface. As a result, a chemical reaction with the binder is easier, during which the desired mineral phases are formed in quantities that improve the mechanical properties of the obtained materials.

The results of analysis of elements belonging to the heavy metals group in case of silicate material samples obtained in individual series are presented in the *Table 2*. The results were obtained as an average of three determinations. *Table 2*, apart from the results of measurements, also contains the leaching limit values for individual elements given in RMGiP [23] and recommended values [14, 24, 25] for selected types of building materials. These values relate to the criteria and procedures for the admission to deposit in outdoor landfills, three categories of waste, i.e. inert, other than hazardous or neutral and hazardous. The obtained results prove that the level of leachability of the tested elements only slightly, in individual cases, exceeds the leaching limit values for the inert waste category, while these values are definitely lower than the permissible limit values applicable for the other two categories of waste, i.e. other than inert and hazardous and dangerous.

Only selected samples from all prepared series were subjected to microstructure tests. The basic criterion for selecting samples were their final properties. In accordance with the above, the samples with the most favorable parameters, which are equivalents due to the type of casting mass used and its share in the raw material mixture, materials obtained in the first and second stage of research, were assigned for microstructure tests. Samples of reference materials were also analysed for comparative purposes. The most characteristic images of the microstructures of the analyzed samples are shown in *Fig. 1a)* and *1b)* show the images of the reference and experimental materials respectively. Presented figures show microstructure of the samples obtained as part of the first stage of research, with a magnification enabling observation of its individual elements. Therefore, these images show the aggregate grain size and pore distribution. In turn, *Figs 1c)* and *1d)* show images of microstructures of reference and experimental materials respectively, but originating from the second stage of research and covering areas of the surface of sand grains and the products of synthesis formed on this surface under hydrothermal conditions. The basic observation regarding the morphology of these products is that the morphology usually consist of structural elements in the form of needles or fibers, which is a positive phenomenon, but to a much lesser extent in the form of platelets or elongated ribbons.

6. Conclusions

Based on all the preliminary results obtained in this paper, the following conclusions can be made:

1. Used casting sands obtained on the basis of quartz matrix are a potential source of silica raw material, which may be a partial substitute for natural quartz sand used in the production of sand-lime products.
2. The said silica material derived from the recycling of used foundry sands, is obtained as a result of appropriate processing of these sands, aimed primarily at crushing the agglomerates of grains (lumps) and restoring the original granulation, and then to remove the residue of the organic binder used for quartz warp grains preparing fresh molding and core sands.
3. The process of processing used foundry sands consisting in mechanical removal of hardened binder residues from the surface of grains has a very beneficial effect on functional properties, including mainly strength, of sand-lime materials obtained with their participation.
4. Durability, in terms of resistance to low temperatures of sand-lime products containing properly processed spent casting masses, does not deteriorate significantly compared to this type of materials obtained on the basis of traditional raw materials.
5. The presence of used casting sands in raw material mixtures intended for the preparation of sand-lime materials, regardless of their degree of processing, adversely affects the color of these products.
6. There are no visible differences in the microstructure of autoclaved materials obtained with the use of foundry sands, in relation to this type of materials obtained from traditional raw materials.
7. The level of heavy metal leaching from the obtained silicate materials is lower than the recommended values.

Acknowledgement

The article is the result of scientific research financed from the subsidy No. 16.16.160.557 of the Polish Ministry of Science and Education

References

[1] Małolepszy, J. (2004) Materiały budowlane. Podstawy technologii i metody badań, Uczelniane Wydawnictwa Naukowo-Dydaktyczne AGH, Kraków (in Polish).

[2] Praca zbiorowa pod redakcją Dańko, J., Holzer, M. (2009) Możliwości ograniczenia i metody zagospodarowania odpadów z procesów odlewniczych (informator dla odlewni), Wydawnictwo Naukowe "Akapit", Kraków (in Polish).

[3] Praca zbiorowa pod redakcją Dańko, J., Holzer, M. (2010) Metody ograniczenia odpadów z procesów odlewniczych oraz sposoby ich zagospodarowania, Wydawnictwo Naukowe "Akapit", Kraków (in Polish).
[4] Kurdowski, W. (2014) Cement and Concrete Chemistry, Springer-Verlag Publishing.
[5] Neville, A.M. (2011) Properties of Concrete, Fifth Edition.
[6] Stefańczyk B. (2005) Budownictwo ogólne, Tom 1, Materiały i wyroby budowlane, Wydawnictwo Arkady, Warszawa (in Polish).
[7] Pytel, Z., Pichór, W. (2018) Patent nr PL 230095, Sposób wytwarzania materiału budowlanego o właściwościach termoizolacyjnych (English wersion: Method for producing building material with heat-insulating properties).
[8] Miquel, R.E., Ippolito, J.A., Porta, A.A., Noriega, R.B.B., Dungan, R.S. (2013) Use of standarized procedures to evaluate metal leaching from waste foundry sands, Journal of Environmental Quality, 42 (2), pp. 615-620.
[9] Deng, An. (2009) Contaminants in waste foundry sand and its leachate, International Journal of Environmental and Pollution, 38 (4), pp. 425-443.
[10] Dungan, R.S., Dess, N.H. (2008) The characterization of total and leachable metals in foundry molding sands, Journal of Environmental Management, 90 (1), pp. 539-548.
[11] Ji, S., Wan, L., Fan, Z. (2001) The toxic compounds and leaching characteristics of spent foundry sands, Water Air and Soil Pollution, 132 (3-4), pp. 347-364.
[12] Kargulewicz, J., Holtzer, M. (2001) The elution of have metals (Cd, Cu, Pb and Zn) from used molding sands vs conditions of the elution process, Archives of Metallurgy, 46 (1), pp. 33-42 (in Polish).
[13] Siddique R., Kaur G., Rajor A. (2010) Waste foundry sands and its leachate characteristic Resources Conservation and Recycling, 54, pp. 1027-1036.
[14] Zheng, Y. (2012) Preparation, properties, formation mechanism of autoclaved bricks from waste foundry sand, Applied Mechanics and Materials, 174-177, pp. 697-700.
[15] PN-EN 771-2:2004 - Wymagania dotyczące elementów murowych. Część 2: Elementy murowe silikatowe.
[16] PN-EN 772-1:2001/Ap 1 - Metody badań elementów murowych. Część 1: Określenie wytrzymałości na ściskanie.
[17] PN-EN 772-13:2001 - Metody badań elementów murowych. Cześć 13: Określenie gęstości netto i gęstości brutto elementów murowych w stanie suchym (z wyjątkiem kamienia naturalnego).
[18] PN-EN 12390-7:2011 - Badanie betonu--Część 7: Gęstość betonu.
[19] Wolfke, St. (1986) Technologia wyrobów wapienno-piaskowych, Wydawnictwo "Arkady", Warszawa (in Polish).
[20] Dobek, J. (1955) Cegła wapienno-piaskowa. Surowce i proces technologiczny, Wydawnictwo "Budownictwo i Architektura", Warszawa (in Polish).
[21] PN-EN 12457-2:2006 - Charakteryzowanie odpadów. Wymywanie. Badanie zgodności w odniesieniu do wymywania ziarnistych materiałów odpadowych i osadów, cz. 2: Jednostopniowe badanie porcjowe przy stosunku cieczy do fazy stałej 10 l/kg w przypadku materiałów o wielkości cząstek poniżej 4 mm (bez redukcji lub z redukcją wielkości).
[22] PN-EN ISO 11885: 2009 - Jakość wody - Oznaczanie 33 pierwiastków metodą atomowej spektrometrii emisyjnej z plazmą wzbudzaną indukcyjnie.
[23] Rozporządzenie Ministra Gospodarki i Pracy z dnia 7 września 2005 r., Dziennik Ustaw Nr 186, Poz. 1553 (in Polish).
[24] Pytel Z. (2014) Evaluation of potential applications of recycled moulding and core sands to production of ceramic building materials, Ceramics International, 40, pp. 4351-4358.
[25] Alonso-Santurde R., Coz A., Quijorna N., Viguri J.R., Andrés A. (2010) Valorisation of foundry sand in clay bricks at industrial scale, Journal of Industrial Ecology 14 (2), pp. 217-230.

Ref.:
Pytel, Zdzisław: *The influence of foundry wastes on the quality of autoclaved sand-lime materials*
Építőanyag – Journal of Silicate Based and Composite Materials, Vol. 73, No. 3 (2021), 108–108. p.
https://doi.org/10.14382/epitoanyag-jsbcm.2021.15

Wind turbine blades structure based on palm cellulose fibers composite material

Abderraouf GHERISSI ▪ Mechanical Engineering Department, College of Engineering, University of Tabuk, Saudi Arabia ▪ a.gresi@ut.edu.sa
Fahd ALAHMARI ▪ Mechanical Engineering Department, College of Engineering, University of Tabuk, Saudi Arabia ▪ 361007560@stu.ut.edu.sa
Mohamed FADHL ▪ Mechanical Engineering Department, College of Engineering, University of Tabuk, Saudi Arabia ▪ 361000397@stu.ut.edu.sa
Adnan ASIRI ▪ Mechanical Engineering Department, College of Engineering, University of Tabuk, Saudi Arabia ▪ 361000678@stu.ut.edu.sa
Meshal ALHWITI ▪ Mechanical Engineering Department, College of Engineering, University of Tabuk, Saudi Arabia ▪ 361001250@stu.ut.edu.sa
Omar ALAMRI ▪ Mechanical Engineering Department, College of Engineering, University of Tabuk, Saudi Arabia ▪ 341002032@stu.ut.edu.sa
Metab ALANISI ▪ Mechanical Engineering Department, College of Engineering, University of Tabuk, Saudi Arabia ▪ 361000981@stu.ut.edu.sa
Ibrahim NASRI ▪ Mechanical Engineering Department, College of Engineering, University of Tabuk, Saudi Arabia ▪ ibrahimnasri2013@gmail.com

Érkezett: 2020. 11. 01. ▪ Received: 01. 11. 2020. ▪ https://doi.org/10.14382/epitoanyag-jsbcm.2021.16

Abstract
The uses of the cellulosic fibers in the natural fiber reinforced polymer composites (NFC) for constructing a wind turbine blade structure will be evaluated in the present work through experimental study. The blade shape designed according to the local wind characteristics on the Tabuk city in Saudi Arabia. The blade mechanical resistance identifies, according to the different forces applied to wind turbine blades. The palm cellulosic fibers were used as reinforcement. Those fibers were prepared through mechanical and chemical extraction process. The extraction was through mechanical decomposition in thin fibers and chemical extraction method by chloride and alkaline. To evaluate the reinforcement effect on wind turbine blades a horizontal wind turbine was constructed. The palm natural fibers used as reinforcement of blades with resin-epoxy gives an encouraging result in the sense of robustness and efficiency. The uses of NFC based on cellulosic fibers for constructing wind turbine blades can be considered as a potential candidate for the manufacturing of total recycling wind turbine blades from natural fibers.
Keywords: wind energy, wind turbine blades, palm cellulosic fibers, natural fiber composites (NFC)
Kulcsszavak: szélenergia, szélturbina lapátok, pálma cellulózrostok, természetes rost kompozitok (NFC)

Abderraouf GHERISSI
Associate professor of mechanical engineering at the college of engineering at the University of Tabuk in Saudi Arabia

Fahd ALAHMARI
mechanical engineering students at the college of engineering at the University of Tabuk in Saudi Arabia

Mohamed FADHL
mechanical engineering students at the college of engineering at the University of Tabuk in Saudi Arabia

Adnan ASIRI
mechanical engineering students at the college of engineering at the University of Tabuk in Saudi Arabia

Meshal ALHWITI
mechanical engineering students at the college of engineering at the University of Tabuk in Saudi Arabia

Omar ALAMRI
mechanical engineering students at the college of engineering at the University of Tabuk in Saudi Arabia

Metab ALANISI
mechanical engineering students at the college of engineering at the University of Tabuk in Saudi Arabia

Ibrahim NASRI
Assistant professor of mechanical engineering at the college of engineering at the University of Tabuk in Saudi Arabia

1. Introduction

Several countries resort to the use of the renewable energies. The renewable energy power systems, such as solar panels and wind turbines produces fewer emissions than other power sources over their lifetime. In particularly wind turbines, which gives high efficiency in the presence of high wind flow and minimize the uses of fossil fuel and ameliorate the environment protection.

The installation and use of large numbers of wind turbines are one of the keys to increase the production of clean energy in the near future. Then the performances of such a wind turbine can be fulfilled only by using innovative, lightweight and highly durable composite materials such as glass, carbon and Kevlar fibers [1, 2].

The most important part of the wind turbine system, produced from composite material, is the wind turbine blade (WTB). The WTB is subjected to complex solicitations included combined impact, static and random cyclic loading. In order to reduce the different types of forces on WTB, it is recommended to build the wind blades from fiber reinforced polymer composites.

It is apparent that the currently most available solution for fiber reinforced composite is the use of E-glass/epoxy or carbon fiber composite [3]. But in the end life of WTB a recycling problematic will be created [4, 5]. Then the solution for the recycling issue could be fulfilled by the use of recycled composite material . But it is required that this composite has a reinforcement can reach higher fracture and toughness resistance [6]. One of the existing solutions, is to use natural fiber composite (NFC) instead of carbon, Kevlar or glass fibers. The uses of NFC give important resistance to complex wind loading and are environmentally friendly and recyclable.

Blades are the most important composite part and the highest cost component of the wind turbines [7]. A wind turbine blades consists of two faces joined together and stiffened both by one or several integral webs linking the upper and lower parts of the blade shell or by a box spar with shell fairings [8]. For that reason, in this work to evaluate the blade structure made from NFC it is necessary, first, to identify the blade optimum structure and composite laying to withstand the wind solicitations. Secondly extract the cellulose palm fibers and then, construct the blades

by hand lay-up molding. And finally, the experimental test was proposed to be conducted on horizontal wind turbine prototype constructed from three blades made from NFC.

2. Materials and procedures

In order to construct the blades (*Fig. 1*) and test the performance of NFC on horizontal axis wind turbine (HAWT) the blade structure was analyzed numerically and experimentally, see *Fig. 2*.

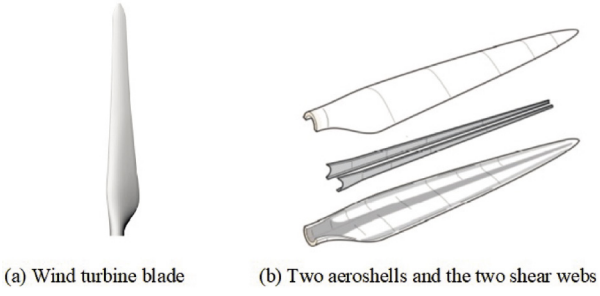

Fig. 1 The two aero-shells and the two shear webs of wind turbine blade [9]
1. ábra A szélturbina lapátjának két burkolata és nyíróöve [9]

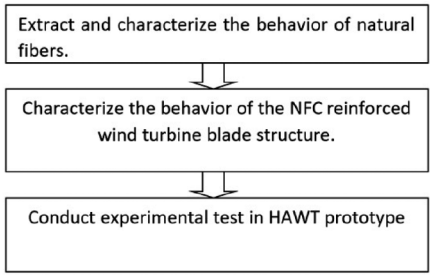

Fig. 2 Construction and evaluation of WTB made from NFC
2. ábra Az NFC-ből készült WTB felépítése és értékelése

3. Characterization of the palm fibers (PF)

The tensile test on palm fibers were conducted in Gant Universal Test Machine WP3, the average curve of the conducted tests is presented in *Fig. 3* [9].

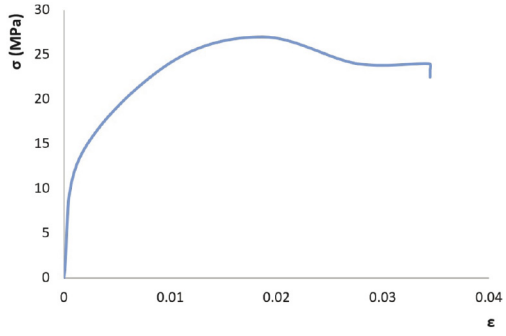

Fig. 3 Tensile test result of the palm fibers (PF) [9]
3. ábra A pálmarostok (PF) szakítóvizsgálati eredménye [9]

According to the *Fig. 1* the ultimate tensile resistance of the PF is about 27 MPa, the maximum tensile strain at break is about 3.44% and the elastic modulus is about 8.96 GPa.

The present mechanical behavior is relatively weak compared with ordinary synthesized fibers usually uses in blade construction such as glass, kevlar and carbon fibers. Then it was necessary to stratify the composite in multi-layers with several fiber directions in order to bring an additional strength resistance to the blades.

4. Principal solicitations in wind turbine blade

The wind turbine blades consist of two faces joined together and stiffened both by one or several integral webs linking the upper and lower parts of the blade shell or by a box spar with shell fairings [7]. The flap wise load on wind turbines is caused by the wind pressure, and the edgewise load is caused by gravitational forces and torque load. *Table 1* gather the solicitation needed to be overcomes during the construction of the blades.

Blade part	Solicitation needed to overcame
The two external faces: The upper part of the blade shell The lower part of the blade shell	Edgewise bending. Cyclic tension-tension loads. Cyclic compression -compression loads
The shear webs	Flap-wise bending
The spar caps	Flap-wise bending
The aero-shells	Elastic buckling
The leading and trailing edge panels	Bending moments associated with the Gravitation loads

Table 1 Common solicitation in wind turbine blades
1. táblázat Gyakori terhelések a szélturbina lapátjaiban

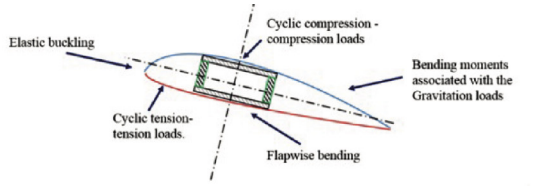

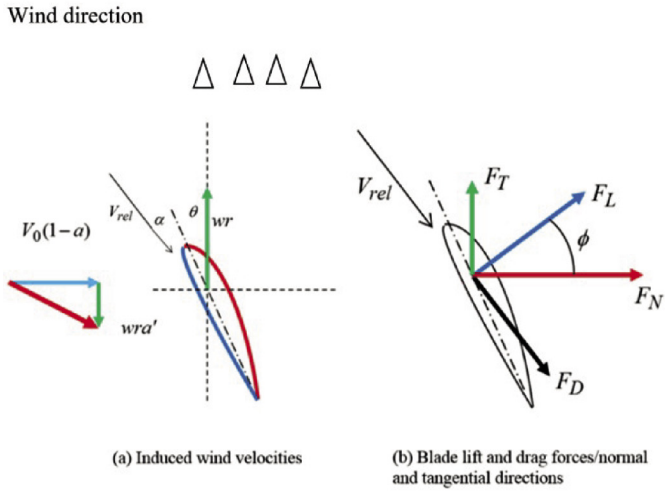

Fig. 4 Representation of the zones of the blade solicitation and the blade induced velocity and forces [10]
4. ábra A penge terhelési zónáinak ábrázolása és a penge által kiváltott sebesség és erők [10]

The modelling of the wind turbine blades structure, starts by the identification of the applicable load case. For this study it was considered two cases of load at normal operation and at extreme wind loading, see *Fig. 4*.

The vortex system induces on a wind turbine composed by an induced axial velocity and an induced tangential velocity component, see *Fig. 4*.

The induced axial velocity is specified as:

$$V_{ia} = a \times V_0 \quad (1)$$

Where:

Vo: is the undisturbed wind speed.

a: the axial induction factor

The induced tangential velocity is in the rotor wake is specified through as

$$V_{it} = 2a'\omega r \quad (2)$$

Where:

a' the tangential induction factor

ω denotes the angular velocity of the rotor

and *r* is the radial distance from the rotational axis.

Since the wind flow does not rotate upstream of the rotor, the tangential induced velocity in the rotor plane is thus approximately $a' \omega r$.

If *a* and *a'* are known, a 2-D equivalent angle of attack could be found based to the work of Martin O. L. Hansen [6] as follow:

The axial velocity specified as shown in *Eq. (3)*

$$V_a = (1- a)\, Vo \quad (3)$$

The rotor velocity specified as shown in *Eq. (4)*

$$V_{rot} = (1+a')\, \omega r \quad (4)$$

The relative wind speed V_{rel} has a flow angle direction ϕ:

$$\phi = \alpha + \theta \quad (5)$$

Where:

θ: The local twist angle of blade

α: The local angle of attack

Based to the *Fig.4*, the angle between wind speed and axial velocity, is the flow angle ϕ determined as shown in *Eq. (6)*:

$$\tan\phi = \frac{(1-a)V_0}{(1+a')\omega r} \quad (6)$$

The lift and drag normal F_N and tangential forces F_T are determined as shown in *Eq. (7)* and *Eq. (8)* respectively:

$$F_N = F_L \cos\phi + F_D \sin\phi \quad (7)$$

$$F_T = F_L \sin\phi - F_D \cos\phi \quad (8)$$

Where:

F_L: The lift force

F_D: The drag force

The normal force coefficient C_N and tangential force coefficient C_T are shown in *Eq. (9)* and *Eq. (10)* respectively:

$$C_N = C_L \cos\phi + C_D \sin\phi \quad (9)$$

$$C_T = C_L \sin\phi - C_D \cos\phi \quad (10)$$

Where:

C_L: The lift coefficient

C_D: The drag coefficient

If the rotor solidity is introduced as σ (see *Eq. (11)*):

$$\sigma(r) = \frac{c(r)B}{2\pi r} \quad (11)$$

Where:

B: Number of blades

C(r): is the local chord

and *r*: is the radial position of the control volume

The uses of the momentum theory to connect the momentum changes in the air flowing through the turbine with the forces acting upon the blades, gives for normal forces as shown in *Eq. (12)*:

$$4\pi r a = \frac{1}{2} B \frac{(1-a)}{\sin^2\phi} c C_N \quad (12)$$

Hence: $$\frac{4\sin^2\phi}{\sigma C_N} a = 1 - a \quad (13)$$

the momentum theory for Tangential forces gives:

$$4\pi r a' = \frac{1}{2} B \frac{(1+a')}{\sin\phi\cos\phi} c C_T \quad (14)$$

Where:

B: the number of blades

c: the local chord

r : the radial position of the control volume

C_N: the normal force coefficient

C_T: the tangential force coefficient

Hence: $$\frac{4\sin\phi\cos\phi}{\sigma C_T} a' = 1 + a' \quad (15)$$

These equations can be rearranged to give the axial and angular induction factors as a function of the flow angle *(Eq. (16)* and *Eq. (17)*).

Axial induction factor: $$a = \frac{1}{\frac{4\sin^2\phi}{\sigma C_N} + 1} \quad (16)$$

Angular induction factor: $$a' = \frac{1}{\frac{4\sin\phi\cos\phi}{\sigma C_T} - 1} \quad (17)$$

The normal force F_N causes a "flapwise" bending moment at the root of the blade as shown in *Eq. (18)*:

$$M_N = \int_{r_{\min}}^{R} F_N (r - r_{\min}) dr \quad (18)$$

Where:

r: the local radius

r_{min}: the local minimum radius

R: the total radius of the rotor

dr: the incremental part of the blade

The tangential force F_T causes a tangential bending moment M_T at the root of the blade shown in *Eq. (19)*:

$$M_T = \int_{r_{\min}}^{R} F_T (r - r_{\min}) dr \quad (19)$$

If neglect the relatively small twist of the blade cross section and assume that these bending moments are aligned with the principal axes of the blade structural cross section.

The maximum tensile stress due to aerodynamic loading is therefore given by *Eq. (20)*:

$$\sigma_{\max,aero} = \frac{M_N}{I_{TT}} \frac{d_o}{2} + \frac{M_T}{I_{NN}} \frac{b}{2} \quad (20)$$

Where:

M_N: flapwise bending moment

M_T: tangential bending moment

I_{TT}: tangential moment of inertia

I_{NN}: moment of inertia about the flapwise

d_0: length of the blade

b: the flapwise length

Consider equilibrium of element of blade, see *Fig. 5* then:

$$\frac{dF_c}{dr} = -m(r)\omega^2 r \tag{21}$$

Where:
m(r) is the mass of the blade per unit length
dFc is the incremental centrifugal force
ω is the angular velocity

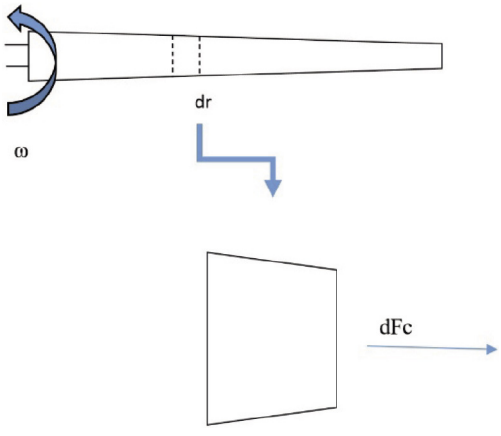

Fig. 5 Element of blade
5. ábra A penge egy eleme

Then, the rotor solidity can be written as:

$$\sigma_c = \frac{F_c(r)}{A(r)} \tag{22}$$

Where, *A(r)* is the local area at the blade element

In the other hand, the bending moment at the blade root due to self-weight loading can dominate the stresses at the blade root. The bending moment is a cyclic load with a frequency of $f = \omega / 2\pi$. The maximum self-weight bending moment occurs when a blade is horizontal, see *Fig. 6*.

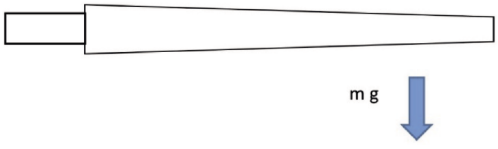

Fig. 6 Blade self-weight
6. ábra Penge önsúlyának figyelembe vétele

The maximum self-weight bending moment could written as shown in *Eq. (23)*, and this is a tangential (edge-wise) bending moment.

$$M_{sw} = \int_{r_{\min}}^{R} m(r)g(r - r_{\min})dr \tag{23}$$

Therefore, the maximum bending stress due to self-weight is given by *Eq. (24)*:

$$\sigma_{\max,sw} = \frac{M_{sw}}{I_{NN}}\frac{b}{2} \tag{24}$$

Finally, the whole Combined Loading could be written as shown in *Eq. (25)*:

$$\sigma_{\max} = \sigma_{\max,aero} + \sigma_c + \sigma_{\max,sw} \tag{25}$$

According to the *Eq. (25)*, it is necessary to conduct a calculation on the combined load of the whole blade structure, in order to fix the dimensions and select the composite structure that could withstand the combined load. For that reason, a FE modelling it was conducted in previous work [8].

5. Construction of the blades and test of the wind turbine

The composite should withstand essentially to the complex loading of the wind. The natural fibers were selected, extracted and treated to prevent any rapid degradation due to existing of water or any other non-desired constituent. A strafed multi-layer layup composite was choosing to withstand combined load, see *Fig. 7*.

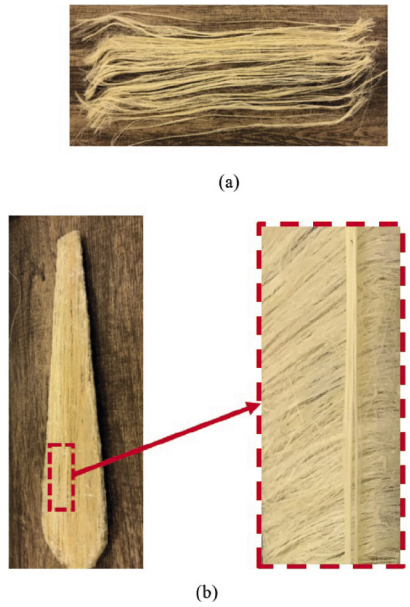

Fig. 7 (a) The extracted Long Palm fibers (b) the construction of the blades from palm natural fibers and resin epoxy
7. ábra (a) A kivont hosszú pálma szálak b) a pengék felépítése természetes pálma szálakból és epoxy gyantából

The wind blade prototype was constructed as shown in *Fig. 8*, with a total length 4400 mm a maximum width 400 mm, the shape was selected with zero airfoil twist angle to prevent any additional vortex and fatigue to the blade structure, see *Fig. 8*.

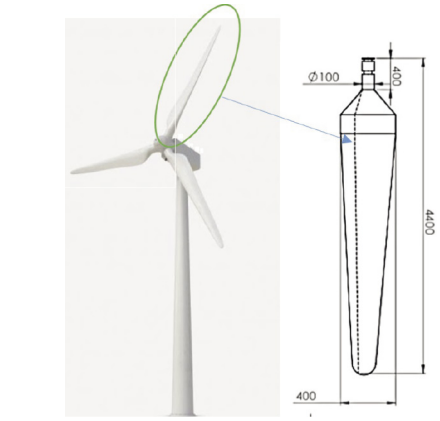

Fig. 8 The blade's dimensions (all dimensions in millimeter)
8. ábra A penge méretei (milliméterben)

6. Results and discussion

All experimental tests were obtained at the month of April 2020, the test were conducted on the wind turbine prototype shown in *Fig. 9*. The test of the wind turbine performance was executed at several wind conditions as shown in the *Table 2*. The maximum wind speed is about 25 km/h and the minimum speed about 5 km/h.

The optimum pitch angle was identifying through the determination of the wind direction and the maximum experimental rotational speed of the rotor. The actual measured power was calculated as an input mechanical power without generation of electricity.

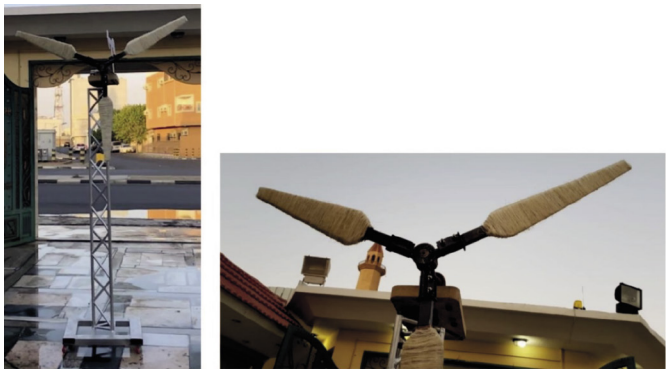

Fig. 9 The wind turbine prototype
9. ábra A szélturbina prototípusa

Date	Wind Speed [km/h]	N [rpm]	Torque [N.m]	Input Power [Watt]	Optimum Pitch Angle [Degree]
7-Apr	14	10	9.8	10	15
8-Apr	7	5	9.8	5.1	5
9-Apr	22	14	9.8	14	22
10-Apr	14	10	9.8	10	15
11-Apr	18	12	9.8	12	20
12-Apr	15	10	9.8	10	15
13-Apr	25	18	9.8	18	24

Table 2 Test of the wind turbine at several wind conditions
2. táblázat A szélturbina vizsgálata többféle szélviszony mellett

The change in power versus the rotation speed of the wind turbine is shown in the *Fig. 10*.

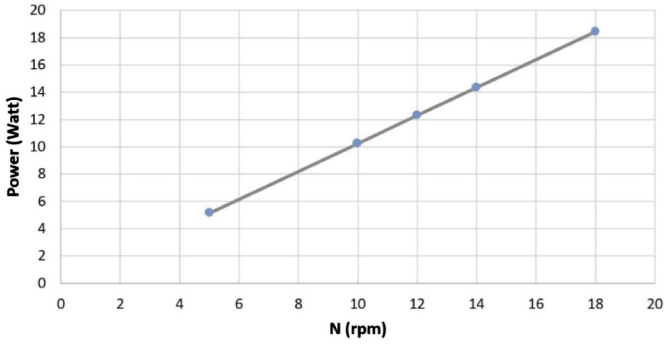

Fig. 10 The change of power according to the rotation speed of the wind turbine.
10. ábra A teljesítményváltozás a szélturbina forgási sebessége szerint.

The change in power versus the wind speed is shown in the *Fig. 11*.

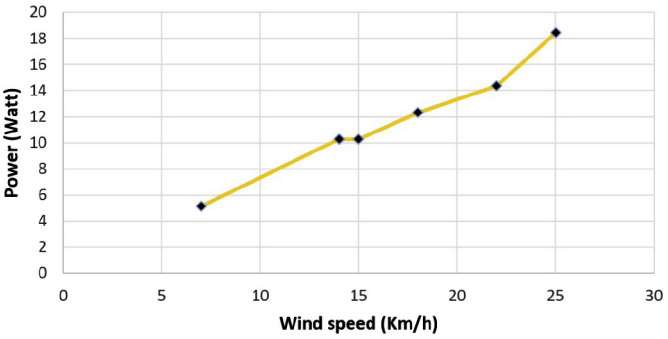

Fig. 11 The change of power versus the wind speed
11. ábra A teljesítményváltozás a szélsebesség függvényében

The influence of wind speed vs the rotation speed of the wind turbine is shown in the *Fig. 12*.

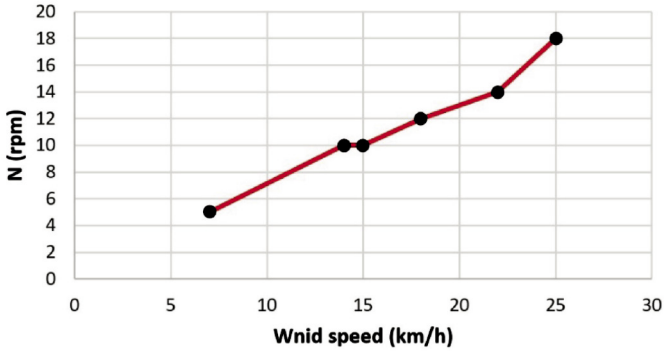

Fig. 12 The change in wind turbine rotation speed versus the wind speed
12. ábra A szélturbina forgási sebességének változása a szélsebességhez viszonyítva

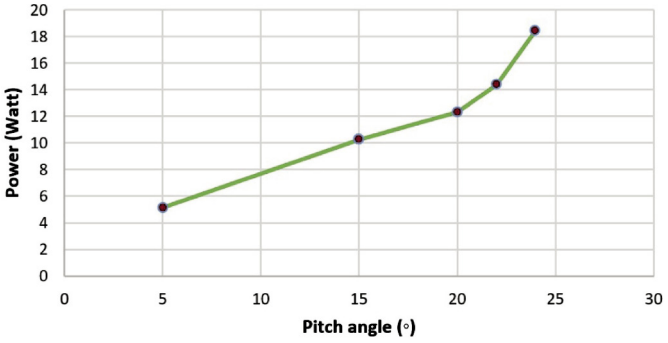

Fig.13 The change in power according to the blade pitch angle
13. ábra A teljesítményváltozás a penge dőlésszöge szerint

The variation of pitch angle could increase the input power of the wind turbine, see *Fig. 13*.

The observed tests and results shows that the power increases linearly with the rotation speed and wind speed, the power could reach 18 Watt. As well as, the change of the blade pitch angle influence positively the input power of the wind turbine.

Also it was observed that, at slow wind speed v= 7 km/h the wind turbine gives a power about 5 Watt, due to light weight of wind blades. The blade structure was tests at several wind conditions and the structure is remaining stable and the composite withstand climatic severe conditions without any damage.

7. Conclusions

Small wind turbine applications are now becoming a solution for producing alternative energy. Actually, as the cost of small wind turbines drops through mass production and technical developments, and as the fee of electrical energy rises, mounting small wind turbines in windy sites will become progressively sustainable. However, the end life of wind turbine and wind turbine blades will challenge the society to a huge waste volume of no recycling material. Then, in the present investigation, the solution was to use natural palm fibers (PF) instead of glass fiber, Kevlar and carbon fiber.

The experimental tests and results on wind turbine made from PF, indicates that the power increases linearly with the rotation speed and wind speed, the power could reach 18 Watt. As well as, the change of the blade pitch angle influence positively the input power of the wind turbine.

Also, it was observed that, at slow wind speed v= 7 km/h the wind turbine gives power about 5 Watt, due to the light weight of wind blades, which represent a great advantage compared with the heavy classic wind turbines. The blade structure was tested at several wind conditions and the structure is remaining stable and the composite withstand climatic severe conditions without any damage. The palm natural fibers used as reinforcement of blades with resin, epoxy gives an encouraging result in the sense of robustness and efficiency.

The palm fibers have proved an excellent mechanical properties and are available free of charge in the Tabuk region in Saudi Arabia. Also near to Tabuk city a significant high continues wind speed, especially in the Neom region, where the wind speed could provide high input power to the wind turbines. The uses of NFC based on cellulosic fibers for constructing wind turbine blades can be considered as a potential candidate for the manufacturing of total recycling wind turbine blades from natural fibers.

Funding

This research was funded by [Deanship of scientific Research at The University of Tabuk, Saudi Arabia] grant number [s-1440-0180]

Acknowledgments

The author acknowledge the financial support provided by the Deanship of Scientific Research (DSR) at University of Tabuk, Tabuk, Saudi Arabia, under grant No. s-1440-0180.

Conflicts of Interest

The authors declare no conflict of interest.

References

[1] Boyano, A.; Lopez-Guede, J.M.; Torre-Tojal, L.; Fernandez-Gamiz, U.; Zulueta, E.; Mujika, F. Delamination Fracture Behavior of Unidirectional Carbon Reinforced Composites Applied to Wind Turbine Blades. Materials 2021, 14, 593. https://doi.org/10.3390/ma14030593

[2] Souad A. M. AlBat'hi 1, a, Yose Fachmi Buys 1, Muhammad Hazwan Hadzari 1 Maizatulnisa Othman, A Light Material for Wind Turbine Blades, Advanced Materials Research Vol 1115 ,2015, pp 308-313; https://doi.org/10.4028/www.scientific.net/AMR.1115.308

[3] K. L. Pickering, M.G. Aruan Efendy, T.M. Le, A review of recent developments in natural fibre composites and their mechanical performance, Composites: Part A 83, 2016, 98–112; https://doi.org/10.1016/j.compositesa.2015.08.038

[4] Beauson J., Brøndsted P., Wind Turbine Blades: An End of Life Perspective. In: Ostachowicz W., McGugan M., Schröder-Hinrichs JU., Luczak M. (eds) MARE-WINT. Springer, Cham.,2016 https://doi.org/10.1007/978-3-319-39095-6_23

[5] Constantinos S. Psomopoulos , Konstantinos Kalkanis, Stavros Kaminaris, George Ch. Ioannidis and Pavlos Pachos A Review of the Potential for the Recovery of Wind Turbine Blade Waste Materials Recycling 2019, 4, 7; https://doi.org/10.3390/recycling4010007

[6] Leon Mishnaevsky Jr., Kim Branner, Helga Nørgaard Petersen, Justine Beauson, Malcolm McGugan and Bent F. Sørensen, Materials for Wind Turbine Blades: An Overview, Materials 2017, 10, 1285; https://doi.org/10.3390/ma10111285

[7] Brøndsted P, Nijssen R. (Eds.) Advances in Wind Turbine Blade Design and Materials; Woodhead Publishing, Oxford, UK, 2013; ISBN 978-0-85709-426-1

[8] Martin O. L. Hansen, Aerodynamics of Wind Turbines, 2nd ed. Earthscan 2008; ISBN 9781844074389

[9] Abderraouf GHERISSI, Faris SHUREDYA, Emad ALATAWI, Abdulrahman ALBALAWI, Bareq ALBALAWI, Sustainable Investigation On Thermoforming Of Cellulose Fibers Composites, Technical University Of Cluj-Napoca Acta Technica Napocensis Series: Applied Mathematics, Mechanics, and Engineering Vol. 62, Issue IV, November, 2019, p583-588; ISSN 2393–2988

[10] Abderraouf GHERISSI, A Study of Wind Turbine Blade Structure Based on Cellulose Fibers Composite Material, International Conference on Green Energy & Environmental Engineering, Proceedings of Engineering and Technology – PET, 2018, Vol 38, P80 – P85; ISSN 2356-5608

Ref.:
Gherissi, Abderraouf – **Alahmari**, Fahd – **Fadhl**, Mohamed – **Asiri**, Adnan – **Alhwiti**, Meshal – **Alamri**, Omar – **Alanisi**, Metab – **Nasri**, Ibrahim: *Wind turbine blades structure based on palm cellulose fibers composite material*
Építőanyag – Journal of Silicate Based and Composite Materials, Vol. 73, No. 3 (2021), 109–114. p.
https://doi.org/10.14382/epitoanyag-jsbcm.2021.16

Laboratory study of the effect of saturation degree on quality of fair-faced concrete surfaces

Kitti AJTAYNÉ KÁROLYFI
is assistant lecturer and PhD student at the Department of Structural and Geotechnical Engineering, Széchenyi István University. Area of scientific interest: concrete technology, fair-faced concrete, digital image processing.

Ferenc PAPP
is DSc professor at the Department of Structural and Geotechnical Engineering, Széchenyi István University. Area of scientific interest: design and analysis of steel structures, CAD/CAM systems, overall imperfection method, free-form structures.

Kitti AJTAYNÉ KÁROLYFI ▪ Department of Structural and Geotechnical Engineering, Széchenyi István University, Hungary ▪ karolyfi.kitti@sze.hu
Ferenc PAPP ▪ Department of Structural and Geotechnical Engineering, Széchenyi István University, Hungary ▪ pappfe@sze.hu

Érkezett: 2021. 03. 26. ▪ Received: 26. 03. 2021. ▪ https://doi.org/10.14382/epitoanyag-jsbcm.2021.17

Abstract
The concrete composition is one of the most significant factor influencing the quality of the fair-faced concrete surfaces. Practical experiences showed, that in case of architectural concrete slightly oversaturated concrete mixtures result in higher quality surfaces. In this work the surface quality of fair-faced concrete samples was examined depending on the saturation degree of the cement paste and the dimensions of the mould. The main evaluation aspects were the surface void ratio, the discoloration, the honeycomb and bleeding. The surface void ratio was obtained by using digital image processing techniques, while the other surface irregularities were examined using manual methods. The concrete samples were classified according to the Austrian and German guidelines. The effect of saturation degree on the mechanical properties of the concrete was also studied. Results show that the increase in saturation degree of cement paste improves significantly the surface quality, while the dimensions of the mould have a reduced, but also a positive effect. In the meantime, there is a decrease in the mechanical properties of the concrete.
Keywords: fair-faced concrete, surface quality, saturation degree, surface void ratio
Kulcsszavak: látszóbeton, péptelítettség, felületi minőség, felületi pórustartalom

1. Introduction

Fair-faced concrete surfaces have become even more popular in today's architecture due it's advantageous mechanical properties and high surface quality [1]. The final appearance of the surface is strongly influenced by the used concrete composition. Practical experiences show, that the saturation degree of the cement paste is a key factor in improving the surface quality. Regarding the saturation degree three conditions of the fresh concrete can be identified: the mixture is undersaturated if there is less cement paste than the void content of the aggregate (*Fig. 1 a*); the mixture become saturated if the cement paste fills the gaps between the particles (*Fig. 1 b*); if there is more cement paste than the void content the particles are distancing from each other and the mixture becomes oversaturated (*Fig. 1 c*). In the case of fair-faced concrete surfaces a slightly oversaturated condition is recommended according to the practical experience [2]. However, it can be assumed, that the ideal saturation degree of cement paste depends on the dimensions of the structural element and the required surface quality.

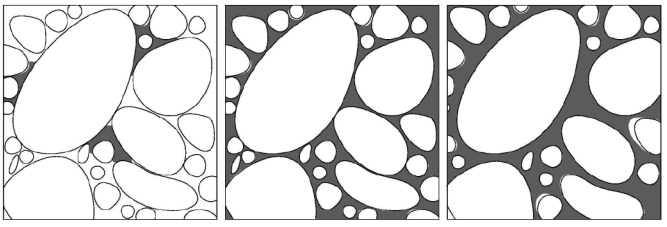

Fig. 1 a) Undersaturated, b) saturated and c) oversaturated conditions of concrete mix
1. ábra a) Telítetlen, b) telített és c) túltelített betonkeverék

The saturation degree affects on the mechanical properties of hardened concrete as well. In principle, the void content of saturated or oversaturated mixtures is zero, while the undersatured mixtured have air content in some degree, therefore the hardened concrete will have lower compressive strength. However, if the water-cement ratio is greater than 0.38, the porosity of the oversaturated mixture is increasing which results in decrease in the compressive strength as well [3,4].

2. Materials and methods

During the experiments a total number of 12 fair-faced cast-in-place concrete wall samples were made by using 3 moulds of different sizes (*Fig. 2*) and 4 types of concrete mixtures. Furthermore, 6 cube and 3 beam specimens were also casted from each concrete compositions in order to examine the mechanical properties of the hardened concrete.

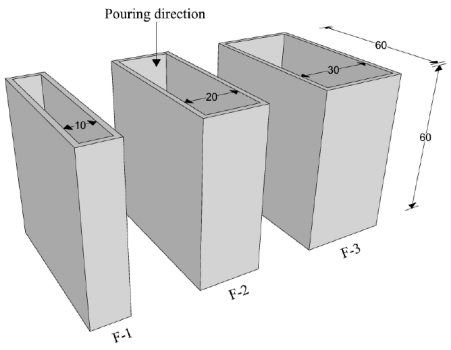

Fig. 2 Dimensions and marking of the moulds
3. ábra Az alkalmazott zsaluzatok mérete és jelölése

2.1 Materials

Quartz sand and gravel was applied as aggregate originated from a quarry pond in Hungary. The rounded fine and coarse fractions were divided with sieving method into components of the following sizes: 0.063, 0.125, 0.25, 0.5, 1, 2, 4, 8, 16, 32 mm. The components were mixed according to the particle size distribution of the standard limit curve 'C' [5]. The relative density and the bulk density of the aggregate sample was measured and the packing density was calculated, from which the precise value of the cement paste demand could be defined [6].

The facing material was 3-ply formwork sheet with 120 g/m² phenolic resin coating on both sides. Mineral oil based, mould release agent was applied in order to prevent adherence between the concrete and the mould and provide a smooth concrete surface.

Four concrete compositions were mixed with increasing amount of cement and water beside a constant water-cement ratio of 0.50 (*Table 1*). CEM II/A-S portland slag cement was used for the mixes. Superplasticizer was applied in order to assure similar characteristics of fresh concrete by reaching the F4 consistency class according to the flow table test [7]. The moulds were filled with fresh concrete in 3 layers by using internal vibration. Each samples were kept in moulds for 3 days.

No.	Cement [kg/m³]	Water [l/m³]	Aggregate [kg/m³]	Saturation degree [l/m³]
1.	330	165	1893.38	+76.45
2.	360	180	1828.35	+101.13
3.	390	195	1763.33	+125.81
4.	420	210	1698.30	+150.48

Table 1. Concrete compositions
1. táblázat Alkalmazott betonösszetételek

2.2 Evaluation methods

The evaluation of the surface quality is a complex problem due to the versatility of fair-faced concrete and the lack of regulation in several countries. In Hungary, the MSZ EN 24803 [8] standard can be used for assessment, which deals with the requirements for the appearance of building structural elements, not expressly the fair-faced concrete. In Austria, the ÖNORM B2211 [9] standard and the fair-faced concrete guideline [10] is the basis of evaluation, while in Germany only the guideline [11] can be used. These specifications usually define four concrete classes with tolerances for the different evaluation criteria. These aspects are examined manually, therefore some criteria, such as discoloration can be evaluated only subjectively. A few research was intended to develop automatic evaluation methods by using digital image processing techniques and reported promising results [12,13].

In this study the surface quality of the samples was examined on two sides with the dimensions of 60×60 cm. The main evaluation aspects were the surface void ratio, the discoloration, the honeycomb and bleeding. In the case of the surface void ratio a newly developed method was applied for the evaluation based on digital image processing techniques. The algorithm was created by using Python software, which method requires one photo of the examined surface. The basis of the method is fitting a third order polynomial to the previously created image containing the selected regions which are free from surface defects. The detection of surface void ratio is made based on the difference between the original and the fitted image using contour finding methods. The algorithm was tested on reference surfaces and it was concluded that it overestimates the results of the manual method with a maximal of 5%, however the time needed for the process is a fraction of it [14]. The mechanical properties of the hardened concrete were examined by measuring the compressive strength, the flexural strength and the water penetration at 28 days.

3. Results

3.1 Surface quality

3.1.1 Surface void ratio

The surface void ratio was evaluated on reference surfaces with a size of 50×50 cm cutted out from the photo of each samples. Three intervals of the pores' diameter were examined:

a. between 0.01 and 15 mm;
b. between 1 and 15 mm according to the Hungarian standard and Austrian guideline;
c. between 2 and 15 mm according to the German guideline.

The surface void ratio decreases significantly while the saturation degree and the width of the formwork increases. Results show a considerable difference between the values of the three diameter intervals (*Fig. 3*). In the case of the 4. mixture the surface void ratio decreases by 20-48% if the minimal pore diameter was changed from 0.01 to 1 mm due to the large number of smaller pores of these surfaces. In general, these values halve by increasing the minimal diameter from 1 to 2 mm.

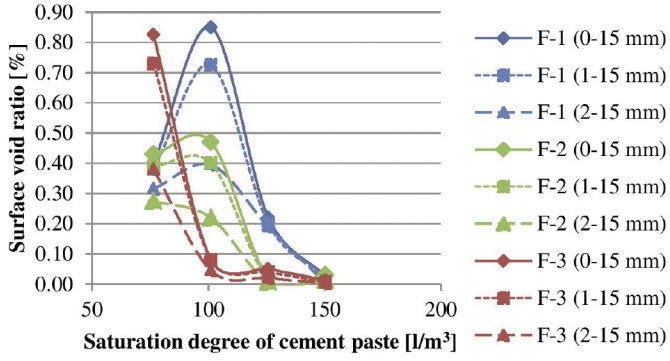

Fig. 3 Surface void ratio of the samples according to the three diameter intervals
3. ábra Felületi pórustartalom a vizsgált pórusátmérő-intervallumok szerint

The results of the examination can be seen in *Table 2* in detail by using the diameter interval between 0.01 and 15 mm. The increase in saturation degree results in a decrease of the average quantity of the pores by 91.8%, the expected value of the diameter by 29.5%, the variance by 77%, the standard deviation by 53% and the surface void ratio by 96.4%. The increase in the width of the mould has a reduced effect on surface quality with a decrease in the pore quantity by 21% and the surface void ratio by 35.1%. The distribution of the pores was also examined by their diameter with a precision of 0.5 mm. The skewness and the kurtosis of the distribution is positive in all cases, which

means that the pores with smaller diameter (d≤2mm) are in greater proportion and the distribution has a peak around these values. Furthermore, the increase in saturation degree results in a growth of the skewness by 27.7% and the kurtosis by 68.1%, while there is no significant change in these values with increasing width of the mould.

Aspect		Concrete composition				Mould		
		1.	2.	3.	4.	1.	2.	3.
Average quantity of pores	[pc]	680	696	107	56	453	343	358
Average expected value	[mm]	1.76	1.52	1.37	1.24	1.50	1.43	1.48
Average value of variance	[mm]	1.87	0.99	1.41	0.43	1.74	0.98	0.80
Average of standard deviation	[mm]	1.32	0.98	1.10	0.62	1.21	0.95	0.86
Average of surface void ratio	[%]	0.55	0.47	0.10	0.02	0.37	0.24	0.24
Skewness of the distribution	[-]	2.78	2.99	3.49	3.55	3.32	2.98	3.32
Kurtosis of the distribution	[-]	7.56	8.36	11.98	12.71	11.01	8.35	11.10

Table 2. Main results of the surface void examination (diameter interval: 0.01-15 mm)
2. táblázat A felületi pórustartalom vizsgálat főbb eredményei (pórusátmérő-intervallum: 0,01-15 mm)

3.1.2 Discoloration

The increase in saturation degree of the cement paste improves significantly the quality of the surfaces under in regard to the discoloration constant mould dimension, and vice versa (*Fig. 4*). The samples made of the 4. concrete composition reached the highest quality class according to the German and Austrian guideline. The Hungarian standard uses a previously accepted reference surface to evaluate the colour tone of the examined element, therefore this is not relevant here.

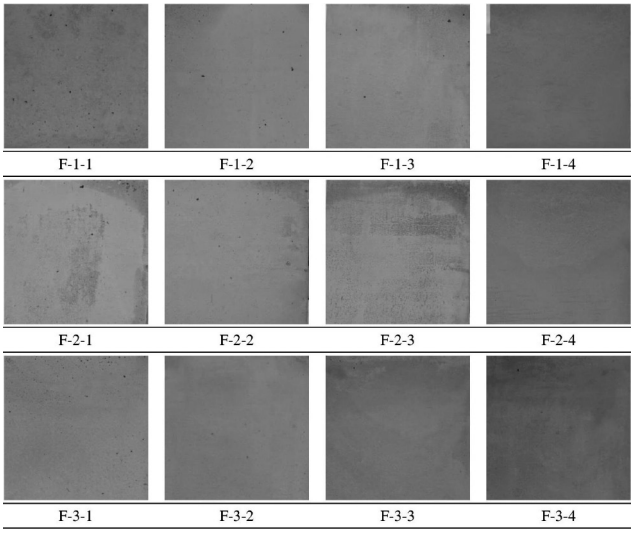

Fig. 4 Surfaces of the samples ordered by the applied mould (F-1-F4) and concrete composition (1-4)
4. ábra A próbatestek felületei az alkalmazott zsaluzat (F-1-F-4) és betonösszetétel (1-4) szerint

3.1.3 Honeycomb and bleeding

Different levels of honeycomb and bleeding occurred on the samples near to the edges. These irregularities can be avoided by the use of proper sealing in the joints of the sheets. The affected area is decreasing with increasing saturation degree of the cement paste and the best result was shown on the samples made by the F-3 mould (*Fig. 5*).

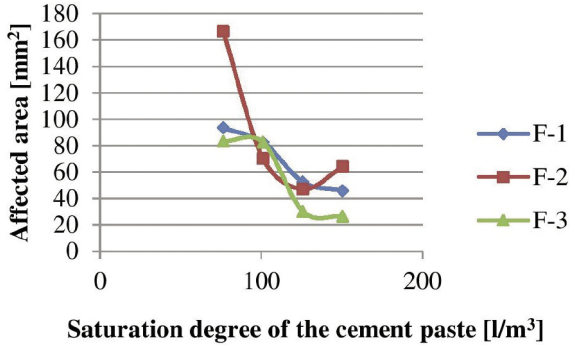

Fig. 5 Extent of area affected by honeycomb and bleeding depending on the saturation degree
5. ábra Vérzéssel és fészkességgel érintett felületek nagysága a péptelítettség függvényében

3.2 Mechanical properties

The mean value of the measured compressive strength can be seen in *Fig. 6* compared to the literature [3]. In general, the compressive strength is higher by using water-cement ratio of 0.50, however it decreases by a total of 12.9% with increasing cement paste content of the mixture.

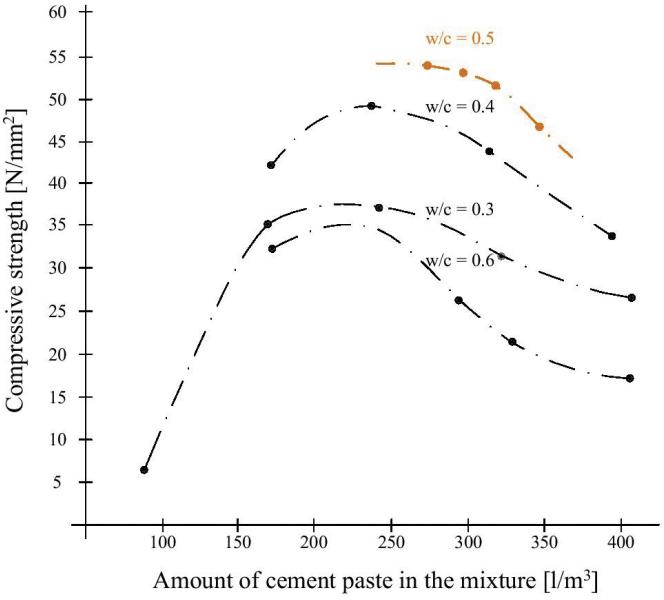

Fig. 6 Compressive strength of concrete depending on cement paste content, (new data coloured) D_{max}=32 mm [2]
6. ábra A beton nyomószilárdsága a péptartalom függvényében (saját adat színesen) D_{max}=32 mm [2]

Similar trend can be observed with the flexural strength of concrete, which has a total decrease of 9% (*Fig. 7*). The increasing saturation degree of the cement paste has also a negative impact on the water penetration (*Fig. 8*).

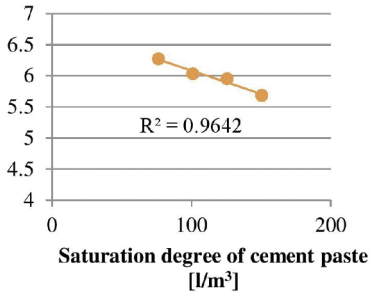

Fig. 7 Flexural strength of concrete depending on the saturation degree of cement paste
7. ábra A beton hajlító-húzó szilárdsága a péptelítettség függvényében

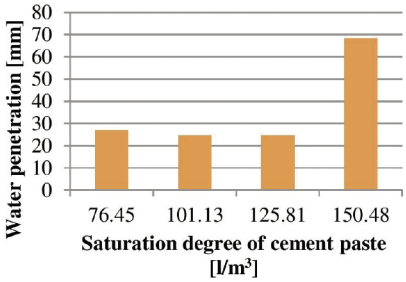

Fig. 8 Results of the water penetration test depending on the saturation degree of cement paste
8. ábra A vízbehatolás mértéke a péptelítettség függvényében

4. Conclusions

Based on the laboratory investigations it can be concluded, that both of the saturation degree and of the moulds' dimensions affect the surface quality of the fair-faced concrete elements. With increasing saturation degree of the cement paste the extent of surface void ratio, discoloration, honeycomb and bleeding is decreasing significantly.

Sample	Class according to the German guideline	Class according to the Austrian guideline
F-1-1	SB1	SB1
F-1-2	SB2	SB2
F-1-3	SB4	SB3
F-1-4	SB4	SB3
F-2-1	SB1	SB2
F-2-2	SB3	SB2
F-2-3	SB1	SB2
F-2-4	SB4	SB3
F-3-1	SB2	SB1
F-3-2	SB4	SB2
F-3-3	SB4	SB3
F-3-4	SB4	SB3

Table 3 Classification of the samples according to the applied guidelines
3. táblázat A felületek osztályba sorolása az alkalmazott irányelvek szerint

The samples made by the fourth, highly oversaturated mixture reached the highest quality class according to the applied regulations (*Table 3*). In the meantime, the mechanical properties of the concrete decreased, which should be considered especially in the case of load-bearing elements. The increase of dimensions of the mould has a reduced, but also a positive effect on the surface quality in accordance with the evaluated aspects. Based on the results authors recommend to use higher saturation degrees (125-150 l/m³) in the case of slender concrete structures and high or special surface quality with consideration of the changes in mechanical properties.

Acknowledgements

This article was elaborated in the framework of the project GINOP-2.2.1-15-2016-00030.

References

[1] Kapu L. (2014) Látszóbeton – Látványbeton, TERC Kft, Budapest, 304 p.
[2] Fenyvesi O., Simon T., Nemes R., Stocker Gy. (2017) Jártunkban-keltünkben, avagy egy Magyarországon eddig nem alkalmazott látszóbeton fajta, Beton, XXV. (II) http://www.betonujsag.hu/lapszamok/cikk/1940/jartunkban-keltuenkben-avagy-egy-magyarorszagon-eddig-nem-alkalmazott-latszobeton-fajta
[3] Nehme S.G. (2004) A beton porozitása, PhD értekezés, Budapest University of Technology and Economics
[4] Ujhelyi J.(1980) A beton levegőtartalmának hatása, Magyar Építőipar, 8, pp. 469-481.
[5] MSZ EN 12620 (2006) Aggregates for concrete
[6] Ajtayné K. K., Harrach D., Papp F. (2020) Investigation of the effect of formwork shape on packing density of aggregates, Pollack Periodica: An International Journal for Engineering and Information Sciences, 15 (3) pp. 124-135.
[7] MSZ EN 12350-5 (2009) Testing fresh concrete. Part 5: Flow table test
[8] MSZ EN 24803-6-3:2010 (2010) Épületszerkezetek megjelenési módjának előírásai, Monolit beton- és vasbeton szerkezetek. A helyi alakhűség és a felületi állapot követelményei, Magyar Szabványügyi Testület
[9] ÖNORM B2211 (1998) Beton-, Stahlbeton- und Spannbetonarbeiten – Werkvertragsnorm, 9 p.
[10] Österreichischen Vereinigung für Beton- und Bautechnik (ÖVBB) Richtlinie (2002) Sichtbeton – Geschalte Betonflächen
[11] Deutscher Beton- und Bautechnik Verein e.V, Bundesverband der Deutschen Zementindustrie (2004) Merkblatt Sichtbeton, 52 p.
[12] Stanke G. (2003) Schlussbericht zum Verbundprojekt Baustellenphotogrammetrie - Photogrammetrisches Verfahren als objektorientiertes Ingenieursystem zur Produktionssicherung in der Bauwirtschaft - Teilvorhaben: Sichtbetonalayse, TU Dresden, Rollei Fototechnik, Dywidag, Gesellschaft zur Förderung angewandter Informatik e.V. (GFaI), Berlin, 36 p.
[13] Gesellschaft zur Förderung angewandter Informatik e.V. (GFaI), Bundesministerium für Wirtschaft und Technologie (2003) Schlussbericht Sichtbeton II./15940 B - Bildgeschützte Bewertungsverfahren für Sichtbetonoberflächen 42 p.
[14] Ajtayné K. K., Horváth A., Papp F. (2020) A new assesment methodology for fair-faced concrete surfaces based on digital image processing, Proceedings of the 13th International PhD Symposium in Civil Engineering, Paris, France, pp. 288-295.

Ref.:
Ajtayné Károlyfi, Kitti – **Papp**, Ferenc: *Laboratory study of the effect of saturation degree on quality of fair-faced concrete surfaces*
Építőanyag – Journal of Silicate Based and Composite Materials, Vol. 73, No. 3 (2021), 115–118. p.
https://doi.org/10.14382/epitoanyag-jsbcm.2021.17

Effect of different supplementary cementitious materials and superplasticizers on rheological behavior of eco-friendly mortars

Salim SAFIDDINE ▪ Materials and Environmental Laboratory (LME), University of Yahia Fares, Algeria ▪ safiddine.salim@univ-medea.dz
Hamza SOUALHI ▪ Civil Engineering Research Laboratory (LRGC), University of Amar Telidji, Algeria ▪ h.soualhi@lagh-univ.dz
Benchaa BENABED ▪ Civil Engineering Research Laboratory (LRGC), University of Amar Telidji, Algeria ▪ b.benchaa@lagh-univ.dz
Akram Salah Eddine BELAIDI ▪ Civil Engineering Research Laboratory (LRGC), University of Amar Telidji, Algeria ▪ s.belaidi@lagh-univ.dz
El-Hadj KADRI ▪ Laboratory L2MGC, University of Cergy-Pontoise, F9500, France ▪ el-hadj.kadri@u-cergy.fr
Érkezett: 2021. 05. 03. ▪ Received: 03. 05. 2021. ▪ https://doi.org/10.14382/epitoanyag-jsbcm.2021.18

Abstract
The drive towards using eco-friendly binders with increasing proportion of supplementary cementitious materials (SCMs) will lead to the development of more complex mixtures. However, the availability of fly ash (FA) would not cover future needs due to restrictions on the combustion of coal in power plants. Accordingly, the addition of limestone filler (LF) has an inherent advantage throughout the world of its availability in large deposits. The first main aim of this study was to determine the effect of high-volume LF used as Portland cement replacement with up to 60% on the rheological properties of cement mortar compared to the FA and the slag (BFS). Unlike FA and BFS, an increase in LF replacement reduced the rheological properties of the mortar. The relationship obtained between relative solid concentration and rheological properties of mortar with different SCMs was reasonable. The second aim of this study was to determine the rheological behavior of the mortar with different superplasticizer (SP) admixtures. Three SP types were utilized, ether-polycarboxylic modified (SP1), phosphonate modified (SP2) and new generation of polycarboxylate (SP3), with various dosages. The results show that, SP2 reduced the rheological properties better than SP1 and SP3 with dosages of less than 1%.
Keywords: eco-friendly mortars, rheological behavior, limestone filler, fly ash, slag, superplasticizer
Kulcsszavak: környezetbarát habarcsok, reológiai viselkedés, mészkő töltőanyag, pernye, salak, folyósító

Salim SAFIDDINE
Associate Professor at the Department of Civil Engineering, University of Medea, Algeria. His research interests include rheology and durability of eco-friendly concrete.

Hamza SOUALHI
Assistant Professor at the Department of Civil Engineering, University of Laghouat, Algeria. His research interests include rheology, tribology and durability of concrete.

Benchaa BENABED
Professor at the Department of Civil Engineering, University of Laghouat, Algeria. His research interests include self-compacting concrete, rheology and durability of concrete.

Akram Salah Eddine BELAIDI
Professor at the Department of Civil Engineering, University of Laghouat, Algeria. His research interests include self-compacting concrete, rheology and durability of cement-based materials.

El-Hadj KADRI
Professor at Laboratory of Mechanics and Materials of Civil Engineering, University of Cergy-Pontoise, France. His research interests include rheology and strength of high-strength concrete and self-compacting concrete.

1. Introduction

Just after the power sector, the cement industry is one of the biggest contributors to greenhouse gases emissions and anthropogenic carbon dioxide in the world [1]. One of the most effective ways to minimize environmental damage associated with cement production is to increase the wider exploit of supplementary cementitious materials (SCMs) in cement composition. In some countries, the amount of fly ash (FA) is expected to be significantly affected in the future due to recent limits on coal combustion. As a result, there is an urgent need for the development of new SCMs, that are comparable or superior to FA and finely blast furnace slag (BFS) [2–4]. Accordingly, the use of limestone filler (LF) has a benefit of its availability in large quantity. Recent studies [5–7] show that it is possible to replace up to 50% by mass of cement with LF without reduction or with a slight decrease in mechanical strength. According to John et al. [6], this can be achieved if the effect of dilution is offset by a decrease in the amount of water used. Nevertheless, this is not a simple task as the rheological behavior of the mixture becomes more and more difficult to control with a low water-binder (W/B) ratio.

Many authors have investigated the use of SCMs for the production of low-impact environmental cement-based materials (grout, mortar or concrete). They have studied their effects on rheology, mechanical properties, durability, thermal conductivity and microstructure analysis of cement suspensions [8–30] as a result of nonlinear behaviour of concrete carbonation and uncertainties of environmental factors affecting the progress of carbonation. In reality, the performance of a developed predictive model lies on its ability to accurately generalise (simulate. The fact that equivalent performance can be reached, combined with a significantly enhanced sustainability and in some cases improved long-term durability, is driving the development of Portland cement-SCM blends towards an increase in substitution levels [2]. Likewise, the use of SCMs with different morphology and grain-size distribution can improve rheological properties and packing of solid particles [31]. This improvement in workability is most frequently associated with the less chemical activity and the smooth surface of SCMs grains compared to ordinary Portland cement (OPC). The most commonly used model in the rheology of cement suspensions is that of Bingham [32–34]elasticity and plasticity and with the\nappearance of new materials and the complex behaviour of concrete\npumpability, since the field of civil engineering is interested in the\nstudy of concrete flow. This work will examine how the use of catodique\nray tube (CRT.

A low yield stress and a moderate viscosity can be achieved by increasing the paste volume, to replace some part of the OPC with one or more SCMs, for a given W/B ratio [29]. The increased paste volume due to the difference in specific density of SCMs (less than 2.5 g/cm^3) and that of cement (3.0-3.2 g/cm^3) [35]. However, the evolution of rheological properties as a function of the partial substitution of cement by SCMs, in the literature, seems to be contradictory in some cases. This is due to the use of SCMs with different physical properties, chemical compositions, activity and filling effect [35–39]consistency, flowability, and predict stability, pumpability, shootability, pressure of formwork, multi-layer casting. This paper presents a critical review on the rheological properties of fresh concrete in recent publications. The applicable rheological models for the flow of concrete are revealed. The effects of constituents of fresh concrete, including cement, supplementary cementitious materials (fly ash, ground blast furnace slag, and silica fume. Furthermore, even if the addition is considered chemically inert, it can have major physical effects like the effects of improved surface area and particle packing [40] heat evolution, microstructure, and setting time. The properties of hardened mortar and concrete made with limestone portland cement are examined and compared to those made with non-limestone portland cements–including compressive and flexural strength, volume stability, durability (permeability, carbonation, freeze/thaw resistance, sulfate and chloride resistance, and alkali-silica reaction. On the other hand, it is important to know how different types of superplasticizer (SP) affect the rheological properties of cement-based materials. Since the nature of admixture used plays an important role in the rheology. It is usually reported that, the dispersion of cement particles, caused by SP, due to the electrostatic repulsion associated with zeta potential measurements. However, in reality this is not necessarily the case, it would seem that, at least for the acrylic polymer-based admixtures, the polymer adsorption itself is responsible for dispersing large agglomerates of cement particles into smaller ones resulting in a remarkable increase in the fluidity of cement mixes. It may be related more to a steric hindrance effect, i.e. repulsive particle-particle interactions [41,42].

For this purpose, the current study focuses on the rheological behavior of cement mortar containing various amounts of FA, LF and BFS as a partial replacement of cement. Thereafter, the effect of LF and tow SCMs used on laboratory tested rheological properties of cement mortar is compared. The aim of this study is also to compare the effects of the use of different types of SP admixtures (polymer and organic admixtures based). In view of the above, the rheological behavior of cement mortars with different content of LF, FA and BFS (0, 10, 20, 30, 40, 50 and 60%) is studied. As well as with different dosages (0, 0.2, 0.4, 0.6 and 0.8%) of three types of SP admixture.

2. Experimental program

2.1 Materials

All mortar mixtures were prepared using an OPC (CEM I 52.5). The SCMs used are fly ash (FA), finely blast furnace slag (BFS), and whitened limestone filler produced by direct grinding of limestone (LF). *Table 1* presents the chemical composition and physical properties of the cement and mineral additions used. The particles size distribution of these materials, which was obtained using a laser scattering technique, is given in *Fig. 1*. From the curves, the particles size distribution of LF is large compared to that of cement, FA and BFS, which is small. Fine aggregate with a maximum size of 4 mm was used, with specific gravity of 2.5 according to Standard EN 1097-6 [43], and fineness modulus is 1.88. Three types of superplasticizer (SP) were used in this study (*Table 2*). The first one is high water reducer (SP1) based on ether-polycarboxylic modified, with a specific gravity of 1.05, a solid content of 20%, and a pH of 7.0. The second one is based on phosphonate modified (SP2). It has a specific gravity, a solid content, and pH of 1.06, 30%, and 4, respectively. The third one is high water reducer (SP3) from new generation of polycarboxylate with a specific gravity of 1.07, a solid content of 30%, and pH of 6.5.

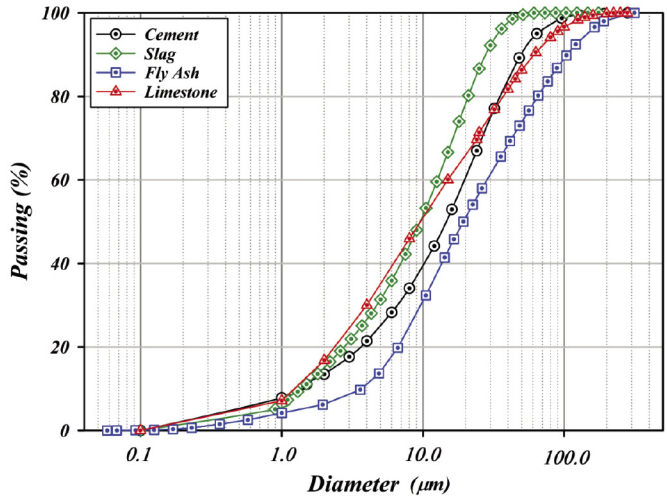

Fig. 1 Particle size distributions of cement and SCMs used
1. ábra A felhasznált cement kiegészítő anyagok és cement szemcse eloszlása

Fig. 2 presents the scanning electron microscopy (SEM) images of OPC, FA, LF and BFS obtained with a microscope at 15.00 kV. The morphological characteristics of these powders are clearly shown in this figure. LF presents smaller particles with angular shape and rough surface (*Fig. 2d*). Both OPC and BFS present more regular particles with smooth surface (*Fig. 2a* and *2c*). However, FA exhibits spherical shape with slightly larger particles sizes and a smoother surface (*Fig. 2d*).

2.2 Mix proportioning

In this work, four series of cement mortars were produced:

- Series A, B and C have of 10 to 60% per step of 10% of OPC weight replaced by FA, BFS and LF respectively, with a control cement mortar without SCMs for the three series. This replacement level was adopted in order to have a high volume of SCM in the cement mortar. A polycarbonate-based SP was used just to maintain the stability of the mixes;
- Series D of SP has of 0.2 to 0.8%, per step of 0.2%, with a control cement mortar without admixture. This dose level was adopted in order to have an ordinary cement mortar. A total, 32 cement mortar samples were made for testing.

Note that, the water to binder ratio (cement plus SCM) is

equal to 0.37 for the SCMs series and 0.40 for admixtures series. The details of the mixing proportions are presented in *Table 3*.

Element (%)	OPC	FA	BFS	LF
S_iO_2	20.23	50.00	35.90	0.30
Al_2O_3	04.29	29.00	11.20	–
Fe_2O_3	02.35	08.50	00.30	–
T_iO_2	00.25	01.00	00.70	–
MnO	00.02	00.50	00.40	–
CaO	63.67	03.00	42.30	–
MgO	03.88	03.00	08.00	–
SO_3	02.80	00.60	00.20	–
K_2O	00.69	00.60	–	–
Na_2O	00.14	00.60	00.70	00.01
P_2O_5	00.31	00.25	–	–
Cl	00.02	00.04	00.01	00.001
SO_4	–	–	–	00.011
CaO_3	–	–	–	98.80
LOI	01.63	04.50	–	–
Activity coefficient	01.00	00.60	00.90	00.25
Specific density	03.13	02.19	02.91	02.70
Fineness Blaine (cm²/g)	4470	3930	5000	4690
Compactness	00.54	00.49	00.58	00.62
D_{10} (μm)	01.50	03.60	01.40	01.50
D_{50} (μm)	15.00	19.30	10.00	10.00
D_{90} (μm)	48.00	104.00	28.00	63.00

Table 1 Chemical analysis and physical properties of cementitious materials used
1. táblázat A felhasznált anyagok kémiai összetétele és fizikai tulajdonságai

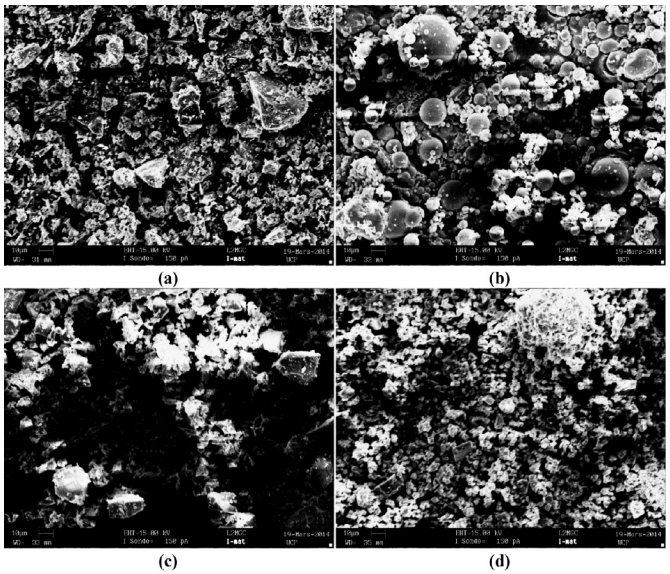

Fig. 2 SEM images of the materials: (a) OPC, (b) FA, (c) BFS and (d) LF (x2000)
2. ábra A vizsgált anyagok pásztázó elektronmikroszkóppal készült képei: (a) OPC, (b) FA, (c) BFS és (d) LF (x2000)

2.3 Mixing procedure

A mixer according to European Standard EN 196-1 [44] at stage I (62.5 rpm) was used to prepare the all fresh cement mortars. The mixing process was kept constant in order to ensure the same homogeneity and uniformity for all mixtures. For the mixes containing SCMs, these additions were previously hand-mixed with the OPC and the necessary water containing SP during 2 min, before adding fine aggregates and mixing for 1 min. The mixing procedure continues for 5 min. Then, the mixture was kept settling for 2 min before remixing for 1 min.

Id	Trade name	Main characteristic	Composition	Manufacturer
SP1	Glenium SKY 537	SP and high rate water-reducing	Modified polycarboxylic ethers	BASF
SP2	CHRYSO Fluid Optima 100	New generation SP	Modified phosphonate	CHRYSO
SP3	Glenium ACE 456	SP and high rate water-reducing	New generation of polycarboxylates	BASF

Table 2 Properties and composition of admixtures (SP) used
2. táblázat A felhasznált adalékszerek (SP) tulajdonságai és összetétele

2.4 Test methods

The workability properties of mortars tested were determined immediately after mixing. Before starting the rheological test, the slump flow test according to standard EN 12350-2 [45] is performed as an empirical test.

The rheological test was conducted using a rheometer developed by Soualhi et al. [46]. It is a rotational rheometer model where four-bladed vane geometry rotates with axial symmetry at a variable speed. The agitator characteristics are: rotational speed from 4 to 540 rpm (± 1 rpm) and maximum torque of 740 Ncm (±0.1 Ncm). It is operated by a computer using software (watch & control). *Fig. 3* presents the dimensions of the vane and the container.

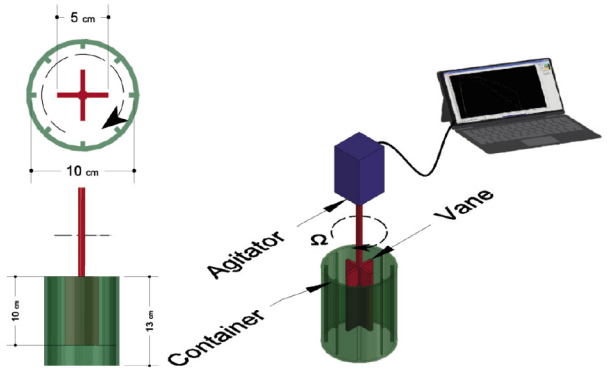

Fig. 3 Rheometer and position of the vane in cement mortar container
3. ábra Reométer és a lapát elhelyezése a cementhabarcs tartályában

The principle is to rotate at different speeds a vane in a cylindrical sample of fresh cement mortar and measuring the torques applied to maintain rotation. A rheological test is performed by imposing a decreasing rotational speed to the vane interrupted by a stabilization stage in order to perform the measurements (*Fig. 4*).

Mix	V_{paste} (m^3)	W/B	C (kg)	W (kg)	Add (%)	Add (kg)	SP (%)	Slump* (cm)	Sand (kg)	
Limestone	Control	0.426	0.37	616.6	227.4	0.0	0.0	1.4	5.0	1377
	M LF1	0.429		555.0		10.0	61.7		9.0	
	M LF2	0.432		493.3		20.0	123.3		22.5	
	M LF3	0.435		431.6		30.0	185.0		26.0	
	M LF4	0.438		370.0		40.0	246.6		28.5	
	M LF5	0.441		308.3		50.0	308.3		34.0	
	M LF6	0.444		246.6		60.0	370.0		38.0	
Fly ash	Control	0.426	0.37	616.6	227.4	0.0	0.0	1.4	5.0	1377
	M FA1	0.435		555.0		10.0	61.7		7.0	
	M FA2	0.443		493.3		20.0	123.3		9.5	
	M FA3	0.451		431.6		30.0	185.0		11.5	
	M FA4	0.459		370.0		40.0	246.6		22.5	
	M FA5	0.468		308.3		50.0	308.3		24.0	
	M FA6	0.476		246.6		60.0	370.0		29.5	
Slag	Control	0.426	0.37	616.6	227.4	0.0	0.0	1.4	5.0	1377
	M S1	0.428		555.0		10.0	61.7		7.5	
	M S2	0.429		493.3		20.0	123.3		9.5	
	M S3	0.430		431.6		30.0	185.0		11.5	
	M S4	0.432		370.0		40.0	246.6		22.5	
	M S5	0.433		308.3		50.0	308.3		24.0	
	M S6	0.434		246.6		60.0	370.0		29.5	
SP 1	M 0	0.397	0.4	550	220	0	0	0	6.5	1566.7
	M SKY 02							0.2	9.5	
	M SKY 04							0.4	11.5	
	M SKY 06							0.6	13.5	
	M SKY 08							0.8	14.5	
SP 2	M 0	0.397	0.4	550	220	0	0	0	6.5	1566.7
	M OPT 02							0.2	12.0	
	M OPT 04							0.4	15.0	
	M OPT 06							0.6	15.0	
	M OPT 08							0.8	15.0	
SP 3	M 0	0.397	0.4	550	220	0	0	0	6.5	1566.7
	M ACE 02							0.2	10.0	
	M ACE 04							0.4	12.0	
	M ACE 06							0.6	13.0	
	M ACE 08							0.8	13.5	

**: for a slump greater than 15cm, the flow diameter is measured using the mini-slump test.*

Table 3 Mix proportions for 1 m^3 of cement mortar
3. táblázat 1 m^3 habarcs összetétele

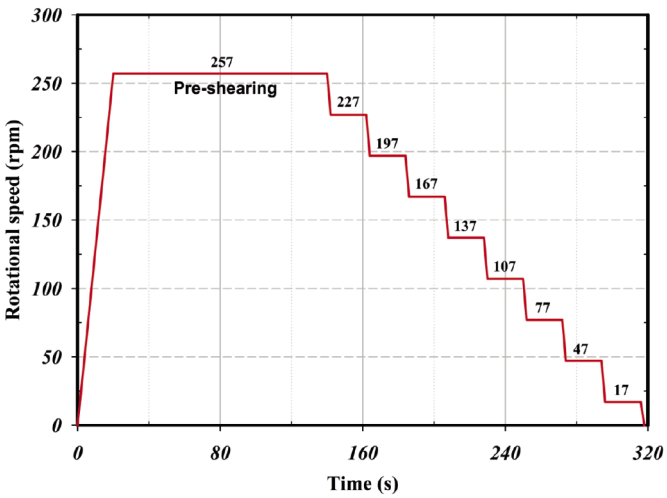

Fig. 4 The profile of the imposed rotational speed
4. ábra A forgási sebesség profilja

The results of the rheometer test are in the form of a linear function relating the torque and the rotational speed according the *Eq. (1)*:

$$M = M_0 + k.\Omega \quad (1)$$

Where: M (Nm) total torque applied to the concrete, M_0 (Nm) torque at the origin, k (Nms) coefficient of proportionality, and Ω (rpm) speed of rotation of the vane.

In order to develop the rheological parameters from measurements, a procedure was used to convert the vane torque and rotational velocity data into shear stress versus shear rate relationships. The method used considered the locally sheared material as a Bingham fluid *(Eq. (2))* and determined the characteristic shear rate from Couette analogy [47].

$$\tau = \tau_0 + \mu\dot{\gamma} \quad (2)$$

Where: τ is the shear stress applied to the material; τ_0 the yield stress (minimum stress necessary for flow to occur: interaction of the linear curve with the shear stress axis); μ the plastic

viscosity (slope of the linear curve given by the plot of shear stress versus shear rate) and $\dot{\gamma}$ is the shear rate.

The shear rate is expressed by *Eqs. (3)* and *(4)*:

$$\dot{\gamma} = \dot{\gamma}_1 = 2M\frac{\partial\Omega}{\partial M}\ if\ \tau_c \le \tau_0 \le \tau_b \quad (3)$$

$$\dot{\gamma} = \dot{\gamma}_2 = 2\frac{M\frac{\partial\Omega}{\partial M}}{\left(1-\frac{R_b^2}{R_c^2}\right)} - \frac{\Omega - M\frac{\partial\Omega}{\partial M}}{ln\left(\frac{R_b}{R_c}\right)}\ if\ \tau_c > \tau_0 \quad (4)$$

Then, the characteristic shear rate is defined as:

$$\dot{\gamma} = \max(\dot{\gamma}_1; \dot{\gamma}_2) \quad (5)$$

The derivative dΩ/dM in *Eqs. (3)* and *(4)* can be approximated by *Eq. (6)*:

$$\frac{\partial\Omega_j}{\partial M_j} \cong \frac{\Omega_{j+1}-\Omega_j}{M_{j+1}-M_j}\ ; j = \overline{1,n} \quad (6)$$

The shear rate corresponding to the rotation speed Ω_j (i = j) can be calculated by *Eq. (7)*:

$$\dot{\gamma}_i = \max\left(\dot{\gamma}_{1j}; \dot{\gamma}_{2j}\right) where\ i = j\ and\ j = \overline{1,n} \quad (7)$$

Once the shear rate has been estimated by *Eq. (7)*, it is deemed to correspond to the following wall shear stress *(Eq. (8))*:

$$\tau_i = \frac{1}{2}\left(\tau_j + \tau_{j+1}\right) avec : \tau_{jouj+1} = \frac{M_{j\,ou\,j+1}}{2\pi h R_b^2}\ ; i = j\ et\ j = \overline{1,n} \quad (8)$$

Also, M_j and M_{j+1} are calculated by *Eq. (9)*:

$$M_i = M_{t,i} - M_{v,i} \quad (9)$$

Where: *i* is the indication of speed level, $M_{t,i}$ the average of total measured torque for each level when the container is filled with cement mortar, and $M_{v,i}$ the average of measured torques for each level when the container is empty (without cement mortar).

Eqs. (7) and *(8)* allow drawing the shear stress curves τ(Pa) according to the shear rate $\dot{\gamma}$ (1/s) and estimating then the rheological parameters τ_0 and μ.

However, the maximum solid concentration of the powder (Φ^*_{paste}) (OPC + SCM) is measured with test water demand [48]. Whereas, the solid volume of paste (Φ) is calculated using *Eq. (10)*:

$$\emptyset = \frac{V_C + V_{SCM}}{V_C + V_{SCM} + V_W + V_{SP}} \quad (10)$$

Where: V_C, V_{SCM}, V_W, V_{SP} are respectively the volumes of cement, SCM, water and SP.

3. Results and discussion

3.1 Rheological properties of limestone fillers based mortar

The rheological properties of SCM based mortar, under the same conditions, were followed in order to understand its behavior at fresh state. The effect of partial cement replacement by LF on the rheological properties and relative solid concentration of cement mortar is shown in *Fig. 5* and *Table 4*. The *Fig. 5.a* shows that the incorporation of LF reduces the yield stress and the plastic viscosity of cement mortar in an approximately linear way. However, it can be seen that, the rheological properties are not influenced when using 10 to 30% of LF in mixtures. Then, both properties decrease more for up to 60% of LF. These results are in agreement with those reported in previous studies [19,25]. It should be noted that, this research work does not disclose contradictory results with those reported in the study conducted by Safiddine [27]. In the present work, the LF used was a powder produced by direct grinding of limestone and its addition was made by replacement of the cement. While, the authors in reference [27], have used a quarry waste limestone powder and have incorporated LF as a replacement of crushed sand, where the specific surface of the sand is much smaller than that of LF. Even, these results are in good agreement with those found by Felekoglu [38,39]. It should be noted that, the physical effect, such as particle size distribution and compactness, is clear on the obtained results of rheological properties of mixtures made with LF. Apparently, in this situation, the effect of the morphology of the LF particles on the rheology of the cement mortar is more dominant than the effect of their specific surface. In fact, since the cement mortar contains a SP admixture, it is very important to keep in mind that, once the SP admixture is adsorbed on the surfaces of the particles, the water requirement is no longer a function of the surface to be wet, but of the interparticles space to be filled. According to Panesar and Zhang [3] partly because of the limited availability of SCMs in some geographic regions. This study provides a comprehensive review based on published literature on the properties of cement-based materials (paste, mortar and concrete, LF has physical effect on the behavior of cement by modification the particles size distribution, and leads to the dilution of the paste. The modification of particle size distribution can improve the rheology of concrete, whereas the dilution may have potentially an adverse effect on the fresh and rheological properties of the material. In addition, the ease of grinding of LF compared to the clinker acquires it a large particle size distribution, as shown in *Fig. 1*. As a result, replacing cement with LF improves particle size distribution of the resulting binder. This allows the LF particles (with average size D_{50} = 10μm) to occupy the space between the coarser cement (with average size D_{50} = 15μm) and sand particles. This results in the release of an amount of water, which is trapped in this space, making it accessible as a supplementary inner lubricant. This leads to increase in the release water and improves the workability of the mortar.

In other words, the quantity of water released reduces the water demand for the same slump, which decreases the plastic viscosity and the yield stress of the cement mortar.

Mix	Limestone (%)	V_{Paste} (m³)	Φ_{Paste}	Φ^*_{Paste}	Φ/Φ^*_{Paste}	μ (Pa.s)	τ_0 (Pa)
Control	0.0	0.426	0.458	0.539	0.850	10.8	33.8
MLF1	10.0	0.429	0.462	0.542	0.853	7.6	24.1
MLF2	20.0	0.432	0.465	0.545	0.853	7.6	23.8
MLF3	30.0	0.435	0.469	0.551	0.852	8.3	26.1
MLF4	40.0	0.438	0.472	0.559	0.845	6.0	22.4
MLF5	50.0	0.441	0.476	0.568	0.837	5.6	21.8
MLF6	60.0	0.444	0.479	0.568	0.844	4.4	16.0

Table 4 Rheological parameters of limestone fillers based mortar
4. táblázat A mészkő kitöltőanyag alapú habarcs reológiai paraméterei

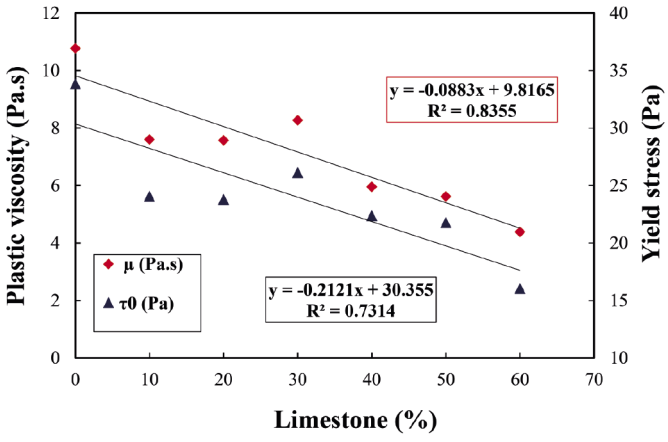

(a)

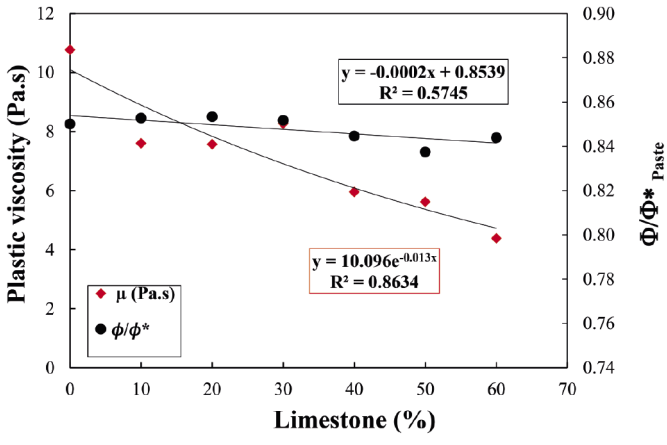

(b)

Fig. 5 Evolution of (a) rheological properties and (b) relative solid concentration with plastic viscosity of limestone fillers based mortar
5. ábra A (a) reológiai tulajdonságok és (b) relatív szilárd koncentráció alakulása a mészkő kitöltőanyag alapú habarcs viszkozitásának függvényében

Fig. 5.b and *Table 4* show the influence of LF content in cement on the viscosity and the relative solid concentration of the cement paste (without sand). From *Fig. 5* it is revealed that, the influence of the Lf on the viscosity and compactness of mortar is quite logical, although it can be poorly explained. Since the decrease in the ϕ/ϕ^* ratio is due to the increase in ϕ^* and not to the decrease in ϕ. According to *Table 4,* these last two parameters increase simultaneously with the increase of the LF, due to the higher compactness of LF compared to that of cement as seen in *Table 1*. Therefore, decreasing this ratio could mean that the distance between particles is increasing, which increases their mobility by reducing friction and reduces the rheological parameters of the cement mortar. This argues well for the interpretation given previously regarding the effect of LF on the rheology of the cement mortar.

According to Hawkins et al. [40] heat evolution, microstructure, and setting time. The properties of hardened mortar and concrete made with limestone portland cement are examined and compared to those made with non-limestone portland cements–including compressive and flexural strength, volume stability, durability (permeability, carbonation, freeze/thaw resistance, sulfate and chloride resistance, and alkali-silica reaction, the influence of LF on rheology could be more pronounced, if the hydration reaction is delayed by the low reactivity of LF (coefficient of reactivity 0.25) compared to cement. However, the chemical effect of LF is far from being present here, because the tests were carried out in the first 30 minutes, i.e.: before the start of setting of the cement.

3.2 Rheological properties of fly ash based mortar

The evolution of the yield stress and plastic viscosity of FA based mortars is shown in *Fig. 6*. From *Fig. 6a*, it is shown that, the yield stress increases exponentially with an increase in FA replacement level. Likewise, the plastic viscosity increases linearly with an increase in percentage of FA. According to Koehler and Fowler [49], there are two conflicting mechanisms that influence the workability of concrete with FA. As the FA particles are much smaller than the cement particles, for which they replace them, the area to be wetted is increased. Hence, the workability is reduced. However, the spherical shape of the FA particles produces a bearing that allows larger particles to flow more easily and improves the workability of the mixture. The spherical shape of the FA particles has the smallest specific surface area compared to other SCMs used (*Table 1*). This does not lead to a reduction in the rheological properties of the cement mortar, contrary to what is expected. The use of FA is generally recognized to reduce the yield stress, but has varying effects on plastic viscosity [49]. However, there are also some researchers, [4,13,29]the mixture's rheological parameters should be adjusted to achieve a given profile of yield stress and plastic viscosity. Supplementary cementitious materials (SCM, who have found that FA increases the rheological properties of concrete.

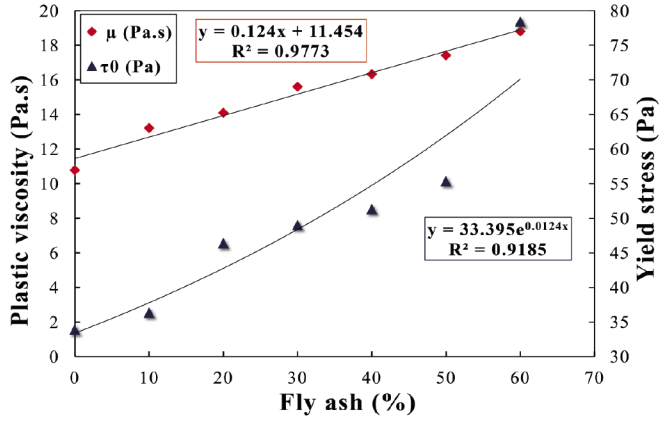

(a)

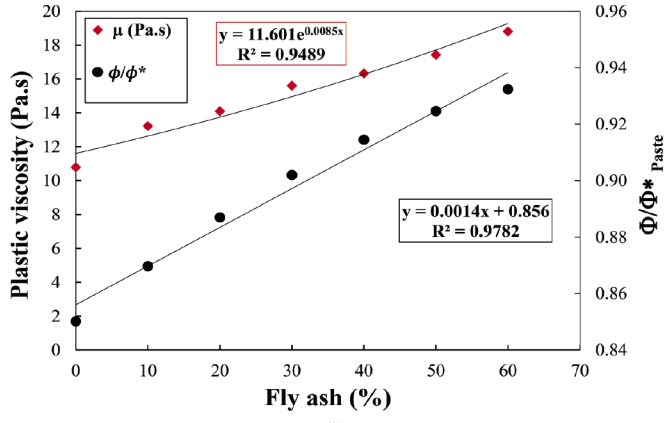

(b)

Fig. 6 Evolution of (a) rheological properties and (b) relative solid concentration with plastic viscosity of flay ash based mortar.
6. ábra A (a) reológiai tulajdonságok és (b) relatív szilárd koncentráció alakulása a pernye alapú habarcs viszkozitásának függvényében

In this study, the rheological behavior of the FA based mortar could be explained in physical manner using the evolution of ϕ/ϕ^* ratio, as shown in *Fig. 6.b* and *Table 5*. The density of FA (2190 kg/m³), which is slightly lower than that of cement (3130 kg/m³), increases the solid volume of the paste by a rate of about 43%, with the same mass replaced. This is expressed in the increase in ϕ (*Table 5*) and ϕ/ϕ^* ratio of cement mortar. According to Roussel [50], as the fraction of solid volume increases, the viscosity of cement-based materials increases exponentially until it reaches infinity, while the fraction of solid volume approaches to a maximum value. This is exactly what happened with the increase in the rate of cement replacement with FA. The evolution in viscosity is due to the decrease in interparticle distance, which contributes to a significant increase in the interparticle hydrodynamic forces.

Mix	Fly ash (%)	V_{Paste} (m³)	Φ_{Paste}	Φ^*_{Paste}	Φ/Φ^*_{Paste}	μ (Pa.s)	τ_0 (Pa)
M T	0.0	0.426	0.458	0.539	0.850	10.8	33.8
MFA1	10.0	0.435	0.468	0.538	0.870	13.2	36.3
MFA2	20.0	0.443	0.478	0.539	0.887	14.1	46.4
MFA3	30.0	0.451	0.487	0.540	0.902	15.6	49.0
MFA4	40.0	0.459	0.496	0.543	0.914	16.3	51.3
MFA5	50.0	0.468	0.505	0.546	0.925	17.4	55.3
MFA6	60.0	0.476	0.514	0.551	0.932	18.8	78.4

Table 5 Rheological parameters of fly ash based mortar
5. táblázat A pernye alapú habarcs reológiai paraméterei

3.3 Rheological properties of slag based mortar

Fig. 7 and *Table 6* show the evolution of the rheological behavior of the cement mortar through the measurement of the plastic viscosity and the yield stress and they give the variation of ϕ/ϕ^* ratio up to 60% replacement of cement by BFS. From *Fig. 7.a*, it is noted that, the yield stress increases for mass replacement of the BFS up to 40%, and decreases for 50% and 60% of BFS. However, it remains higher compared to that of the control cement mortar without BFS. Furthermore, the plastic viscosity increases in an approximately linear way with an increase in mass replacement of BFS in the cement mortar as shown in *Fig. 7.b*. These results are in agreement with some previous studies [13,30]. The same interpretation could be given as with FA, except that in the case of BFS this result was expected, with shape, size, specific surface, particle size distribution and density of BFS. The use of BFS in general improves workability and its effect on yield stress is variable, while increases plastic viscosity [49]. Indeed, this is what is noted from *Table 3*, the slump increases as well as the plastic viscosity and the yield stress. This is may be due to an increase in viscosity, which means that the viscosity has an impact on the yield stress [51].

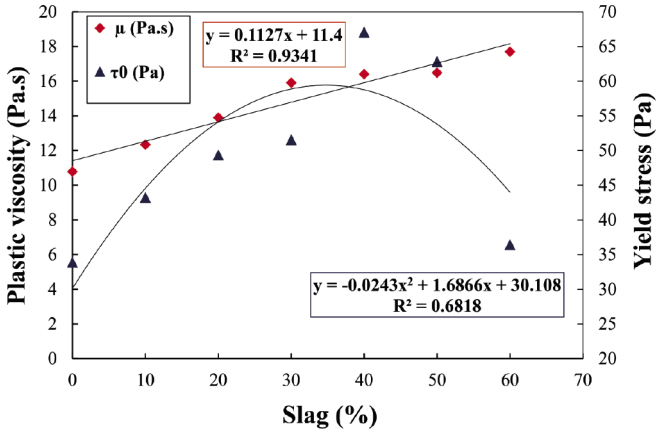

(a)

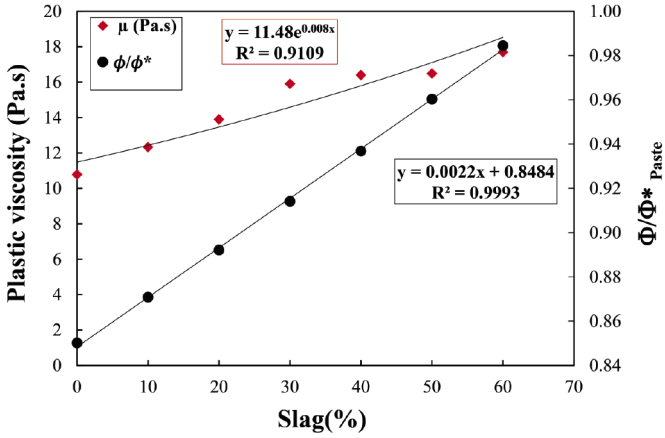

(b)

Fig. 7 Evolution of (a) rheological properties and (b) relative solid concentration with plastic viscosity of slag based mortar
7. ábra A (a) reológiai tulajdonságok és (b) relatív szilárd koncentráció alakulása a salak alapú habarcs viszkozitásának függvényében

Mix	Slag (%)	V_{Paste} (m³)	Φ_{Paste}	Φ^*_{Paste}	Φ/Φ^*_{Paste}	μ (Pa.s)	τ_0 (Pa)
M T	0.0	0.426	0.458	0.539	0.850	10.8	33.8
M S1	10.0	0.428	0.460	0.528	0.871	12.3	43.19
M S2	20.0	0.429	0.461	0.517	0.892	13.9	49.33
M S3	30.0	0.430	0.463	0.506	0.914	15.9	51.5
M S4	40.0	0.432	0.465	0.496	0.937	16.4	67.0
M S5	50.0	0.433	0.466	0.485	0.960	16.5	62.8
M S6	60.0	0.434	0.468	0.475	0.984	17.7	36.4

Table 6 Rheological parameters of slag based mortar
6. táblázat A salak alapú habarcs reológiai paraméterei

3.4 Comparison of rheological behavior of SCM based mortars

Fig. 8 shows the rheological behavior of cement mortars with 20, 40 and 60% of different SCMs used as cement replacement. At high content of SCM (60%), it is clear that, LF reduces the rheological properties. In contrast, the BFS and the FA increase the rheological properties, in particular the plastic viscosity. However, according to *Figs. 5.a*, *6.a* and *7.a*, it can be seen that, the evolution of the yield stress varies from one SCM to another under the same dosage conditions. Indeed, the evolution of the plastic viscosity is almost superimposed for the FA and the BFS by increasing this parameter. On the contrary,

the variation of the plastic viscosity takes on another meaning with the LF, which improves this parameter. For this reason, it is very important to combine the effect of LF with other SCMs, to produce ternary cement (OPC-LF-BFS or OPC-LF-FA), in order to improve the rheology of the cement mortar and reduce the release of CO_2 in one hand. Also, to fill the gap induced by the decrease in the amount of FA in the near future, due to recent limits on coal combustion in power plants to reduce air pollution. Since, in practice, it is usually important to have a certain viscosity in order to prevent segregation and improve the quality of the cement-based materials thus obtained. This is particularly important with the evolution of admixtures use and long-distance pumping.

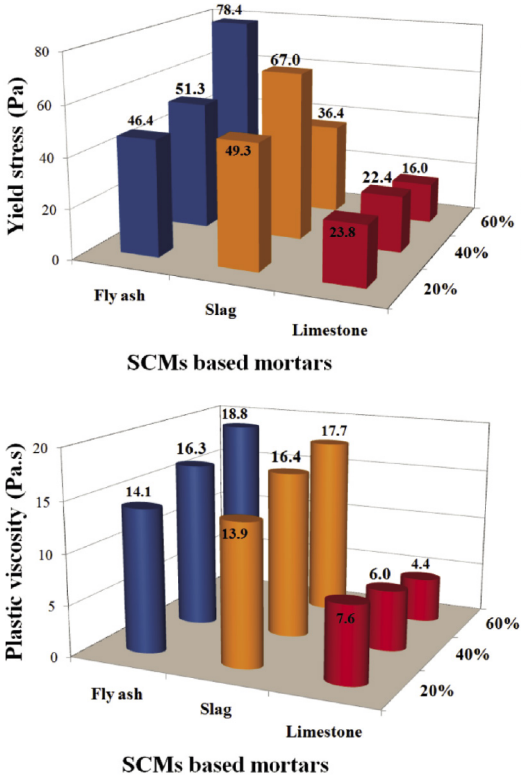

Fig. 8 Comparison of (a) the yield stress and (b) the plastic viscosity of cement mortar with 20, 40 and 60% of SCMs content
8. ábra A cementhabarcs (a) folyási feszültségének és (b) viszkozitásának összehasonlítása 20, 40 és 60% cement kiegészítő anyag tartalom esetén

3.5 Relationship between the plastic viscosity of cement mortar and the relative solid concentration

In this study as shown in *Fig. 9*, the measured values of plastic viscosity were plotted against the measured values of relative solid concentration of nineteen fresh cement mortars with different SCMs (six mixes for each SCM in addition to the control mortar). According to Roussel [50], the relative solid concentration of fresh paste (ϕ/ϕ_{Paste}^*) is the ratio of the solid volume of powder (ϕ) (i.e. the ratio of the total volume of the powder to the total sample volume of cement mortar) and another critical parameter namely (ϕ_{Paste}^*); i.e. the maximum solid concentration of powder, which is the maximum volume fraction that can be reached with the grains. Usually, when the solid fraction approaches to ϕ^*, the concentrated regime is established and the viscosity tends to infinity.

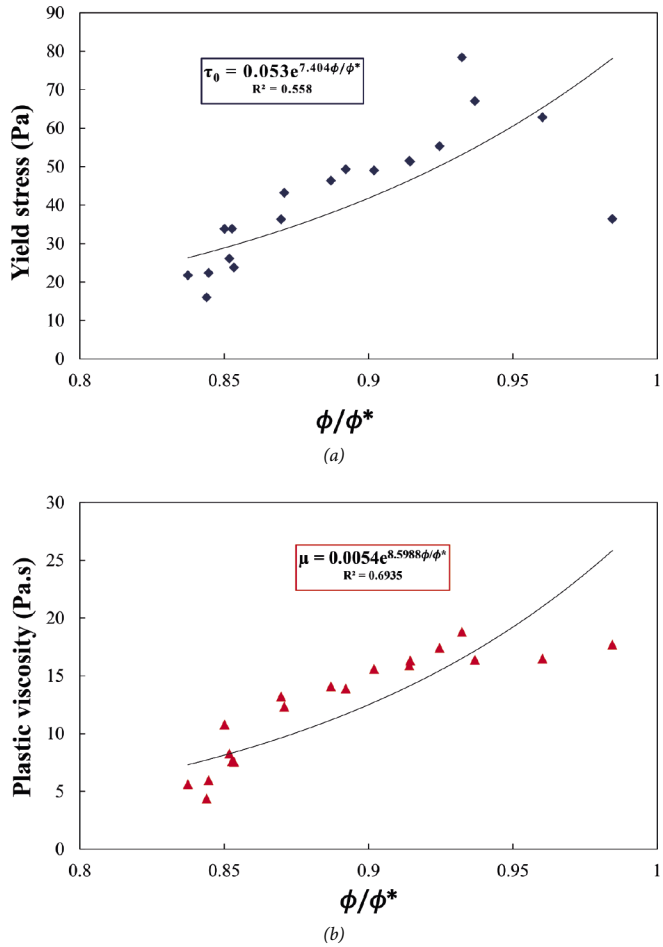

Fig. 9 Relationship between relative solid concentration (a) the yield stress; (b) the plastic viscosity of SCMs based mortar
9. ábra A cement kiegészítő anyag alapú habarcs relatív szilárd koncentrációjának kapcsolata (a) a folyási feszültséggel; b) viszkozitással

Fig. 9.a indicates the good relationship between the relative solid concentration and the yield stress. Similarly, *Fig. 9.b* shows a reasonable relationship between the relative solid concentration and the plastic viscosity. It is concluded that, the trend of yield stress is similar to that of plastic viscosity for all mixtures with the different SCMs used. The increase in relative solid concentration increased the rheological properties regardless the SCM used. Similar results have been reported by previous studies on rheological behavior of concrete.

3.6 Influence of superplasticizer admixture type and dosage

As shown in *Fig. 10* that, the rheological behavior of cement mortar each type of admixture is affected differently by each type of admixture. At least for dosages of less than 1%, the SP based on modified phosphonate (SP2) has better efficiency than the admixtures based on polycarboxylates (SP1 and SP3), which results in reducing the rheological properties of the cement mortar. However, its effectiveness decreases as the dosage increases, unlike SP1 and SP3, which reduces the rheological properties, in particular the plastic viscosity.

It is reported that, the phosphonates are organophosphorus compounds containing C-PO(OH)$_2$ or C-PO(OR)$_2$ groups (where R=alkyl, aryl), while the polycarboxylates are linear polymers. According to Criado et al. [52], organic admixtures

based on both hydrophilic and hydrophobic group. The electrical charge resulting from the adsorption of these compounds on the surface of cement particles induces the repulsive forces that increase fluidity of the paste. However, the lateral chains in admixtures based on polycarboxylates generate steric repulsion among the cement grains, causing deflocculation and dispersion of the particles, which in turn improves workability by releasing the water trapped in the flocs, which results in decreasing the slump of the cement mortars (*Table 3*).

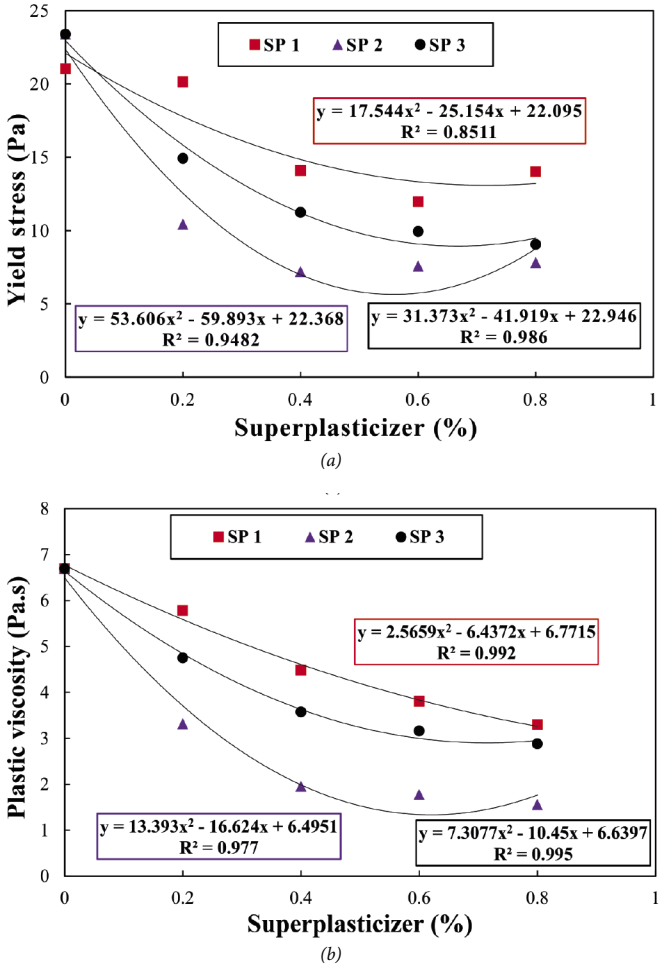

Fig. 10 Influence of SP admixtures on: (a) the yield stress and (b) the plastic viscosity
10. ábra Az SP adalékszerek hatása a: (a) a folyási feszültségre és (b) a viszkozitásra

The results show that, the dosage of 0.2% for SP2 results in a similar effect to the dosage of 0.6% for SP3 and better than the dosage of 0.8% for SP1. However, beyond 0.4%, SP2 has become steadily less efficient compared to SP1 and SP3. This is may be due of the steric effect of polycarboxylates, which has become more and more dominant as the dosage increases.

4. Conclusions

The rheology of cement mortars containing three SCMs (LF, FA, BFS) and three different SP admixture types is compared based on an evolution of the plastic viscosity and the yield stress of the control mix without SCMs and SP, respectively. The following conclusions can be drawn from this research work:

- Increasing the amount of LF from 0 to 60% reduced the yield stress and the plastic viscosity of cement mortar by 52% and 59%, respectively.
- The cement mortar containing FA or BFS exhibited higher yield stress and plastic viscosity compared to those of the control mortar. In addition, with the use of 60% of FA, the yield stress and the plastic viscosity increased by 132 % and 75% respectively.
- At a replacement level up to 40% of BFS, the yield stress of cement mortar increased with a rate of 98%. However, for a replacement level of 50 to 60%, the yield stress is decreased. When using 60% of BFS, an improvement rate of about 8% and 64% for the yield stress and the plastic viscosity is recorded, respectively
- Cement mortar incorporating FA has similar behavior in increasing the plastic viscosity compared to that of cement mortar containing BFS.
- In addition, the obtained results confirm the compatibility of the incorporation of SP with LF. This makes the use of the high-volume eco-friendly binder in mortars and concretes very promising in terms of improving workability or reducing the W/B ratio for a given slump.
- For dosage less than 1% of SP, the SP2 based on phosphonate reduced the rheological properties better compared to the SP based on polycarboxylate (SP1 and SP3).
- Dosage of 0.2% of SP2 had an equivalent effect to that when using dosage of 0.8% of SP1 and 0.6% of SP3, in terms of reducing the rheological properties of the cement mortar.
- In the same way, the steric effect of polycarboxylates became more and more dominant as the dosage of SP increases.

This study provides a reference for use of FA, BFS and LF to develop green building materials with the desired rheological properties. Overall, LF can be used to produce the low rheological properties cement mortar. While, FA and BFS can be used for the production of high rheological properties cement mortar. This helps to reduce the high cement consumption in the production of cement-based materials and contributes to environmental sustainability and resource savings.

In this regard, it is recommended that, this study to be accompanied by scientific investigations on combining LF with the BFS and the FA, with a high percentage of the LF, in order to have the sufficient rheological properties for different applications and different types of concrete, in particular self-compacting concrete. Moreover, future research is recommended in order to study the synergistic effect of these additions on the rheology of ternary and quaternary cementitious blends-based materials.

Acknowledgements

The authors gratefully acknowledge the Directorate-General of Scientific Research and Technological Development of Algeria (DGRSDT) for its valuable support.

References

[1] J. Ofosu-Adarkwa, N. Xie, S.A. Javed, Forecasting CO2 emissions of China's cement industry using a hybrid Verhulst-GM(1,N) model and emissions' technical conversion, Renew. Sustain. Energy Rev. 130 (2020) 109945. https://doi.org/10.1016/j.rser.2020.109945.

[2] J. Skibsted, R. Snellings, Reactivity of supplementary cementitious materials (SCMs) in cement blends, Cem. Concr. Res. 124 (2019) 105799. https://doi.org/10.1016/j.cemconres.2019.105799.

[3] D.K. Panesar, R. Zhang, Performance comparison of cement replacing materials in concrete: Limestone fillers and supplementary cementing materials – A review, Constr. Build. Mater. 251 (2020) 118866. https://doi.org/10.1016/j.conbuildmat.2020.118866.

[4] E. Ghafari, S. Ghahari, D. Feys, K. Khayat, A. Baig, R. Ferron, Admixture compatibility with natural supplementary cementitious materials, Cem. Concr. Compos. 112 (2020) 103683. https://doi.org/10.1016/j.cemconcomp.2020.103683.

[5] S.H. Kang, Y. Jeong, K.H. Tan, J. Moon, High-volume use of limestone in ultra-high performance fiber-reinforced concrete for reducing cement content and autogenous shrinkage, Constr. Build. Mater. 213 (2019) 292–305. https://doi.org/10.1016/j.conbuildmat.2019.04.091.

[6] V.M. John, B.L. Damineli, M. Quattrone, R.G. Pileggi, Fillers in cementitious materials — Experience, recent advances and future potential, Cem. Concr. Res. 114 (2018) 65–78. https://doi.org/10.1016/j.cemconres.2017.09.013.

[7] A.M. Rashad, W.M. Morsi, S.A. Khafaga, Effect of limestone powder on mechanical strength, durability and drying shrinkage of alkali-activated slag pastes, Innov. Infrastruct. Solut. 6 (2021) 1–12. https://doi.org/10.1007/s41062-021-00496-y.

[8] P. Turgut, A. Ogretmen, Optimum limestone powder amount in mortars with over silica fume, Epa. - J. Silic. Based Compos. Mater. 71 (2019) 58–64. https://doi.org/10.14382/epitoanyag-jsbcm.2019.11.

[9] I.D. Uwanuakwa, Deep Learning Modelling and Generalisation of Carbonation Depth in Fly Ash Blended Concrete, Arab. J. Sci. Eng. (2020). https://doi.org/10.1007/s13369-020-05093-2.

[10] A.K.H. Kwan, Y. Li, Effects of fly ash microsphere on rheology, adhesiveness and strength of mortar, Constr. Build. Mater. 42 (2013) 137–145. https://doi.org/10.1016/j.conbuildmat.2013.01.015.

[11] A.Y. K. H. Khayat and M. Sayed, K.H. Khayat, A. Yahia, M. Sayed, Effect of Supplementary Cementitious Materials on Rheological Properties, Bleeding, and Strength of Structural Grout, ACI Mater. J. 105 (2008). https://doi.org/10.14359/20200.

[12] J. Assaad, K.H. Khayat, Assessment of Thixotropy of Self-Consolidating Concrete and Concrete-Equivalent-Mortar - Effect of Binder Composition and Content, ACI Mater. J. 101 (2004) 400–408. https://doi.org/10.14359/13426.

[13] I. Mehdipour, A. Kumar, K.H. Khayat, Rheology, hydration, and strength evolution of interground limestone cement containing PCE dispersant and high volume supplementary cementitious materials, Mater. Des. 127 (2017) 54–66. https://doi.org/10.1016/j.matdes.2017.04.061.

[14] L.A. Qureshi, B. Ali, A. Ali, Combined effects of supplementary cementitious materials (silica fume, GGBS, fly ash and rice husk ash) and steel fiber on the hardened properties of recycled aggregate concrete, Constr. Build. Mater. 263 (2020) 120636. https://doi.org/10.1016/j.conbuildmat.2020.120636.

[15] P. Narasimha Reddy, B.V. Kavyateja, Durability performance of high strength concrete incorporating supplementary cementitious materials, Mater. Today Proc. 33 (2020) 66–72. https://doi.org/10.1016/j.matpr.2020.03.149.

[16] A. Elahi, P.A.M. Basheer, S. V. Nanukuttan, Q.U.Z. Khan, Mechanical and durability properties of high performance concretes containing supplementary cementitious materials, Constr. Build. Mater. 24 (2010) 292–299. https://doi.org/10.1016/j.conbuildmat.2009.08.045.

[17] S. Tsimas, A. Moutsatsou-Tsima, High-calcium fly ash as the fourth constituent in concrete: Problems, solutions and perspectives, Cem. Concr. Compos. 27 (2005) 231–237. https://doi.org/10.1016/j.cemconcomp.2004.02.012.

[18] Y. Du, W. Yang, Y. Ge, S. Wang, P. Liu, Thermal conductivity of cement paste containing waste glass powder, metakaolin and limestone filler as supplementary cementitious material, J. Clean. Prod. (2020) 125018. https://doi.org/10.1016/j.jclepro.2020.125018.

[19] J. Wang, J. Xie, Y. Wang, Y. Liu, Y. Ding, Rheological properties, compressive strength, hydration products and microstructure of seawater-mixed cement pastes, Cem. Concr. Compos. 114 (2020) 103770. https://doi.org/10.1016/j.cemconcomp.2020.103770.

[20] Z. Yingliang, Q. Jingping, M.A. Zhengyu, G. Zhenbang, L. Hui, Effect of superfine blast furnace slags on the binary cement containing high-volume fly ash, Powder Technol. 375 (2020) 539–548. https://doi.org/10.1016/j.powtec.2020.07.094.

[21] S. Cheng, Z. Shui, T. Sun, R. Yu, G. Zhang, Durability and microstructure of coral sand concrete incorporating supplementary cementitious materials, Constr. Build. Mater. 171 (2018) 44–53. https://doi.org/10.1016/j.conbuildmat.2018.03.082.

[22] J.Y. Petit, E. Wirquin, K.H. Khayat, Effect of temperature on the rheology of flowable mortars, Cem. Concr. Compos. 32 (2010) 43–53. https://doi.org/10.1016/j.cemconcomp.2009.10.003.

[23] J.J. Chen, B.H. Li, P.L. Ng, A.K.H. Kwan, Adding granite polishing waste as sand replacement to improve packing density, rheology, strength and impermeability of mortar, Powder Technol. 364 (2020) 404–415. https://doi.org/10.1016/j.powtec.2020.02.012.

[24] D. Youness, A. Mechaymech, R. Al Wardany, Flow assessment and development towards sustainable self-consolidating concrete using blended basalt and limestone-cement systems, J. Clean. Prod. (2020) 124582. https://doi.org/10.1016/j.jclepro.2020.124582.

[25] Z. Zhang, J. Xiao, K. Han, J. Wang, X. Hu, Study on the structural build-up of cement-ground limestone pastes and its micro-mechanism, Constr. Build. Mater. 263 (2020) 120656. https://doi.org/10.1016/j.conbuildmat.2020.120656.

[26] D. Jiao, C. Shi, Q. Yuan, Time-dependent rheological behavior of cementitious paste under continuous shear mixing, Constr. Build. Mater. 226 (2019) 591–600. https://doi.org/10.1016/j.conbuildmat.2019.07.316.

[27] S. Safiddine, F. Debieb, E.H. Kadri, B. Menadi, H. Soualhi, Effect of Crushed Sand and Limestone Crushed Sand Dust on the Rheology of Cement Mortar, Appl. Rheol. 27 (2017) 1–9. https://doi.org/10.3933/APPLRHEOL-27-14490.

[28] H. Soualhi, E.H. Kadri, A. Bouvet, T.T. Ngo, F. Cussigh, A.S.E. Belaidi, New model to estimate plastic viscosity of eco-friendly and conventional concrete, Constr. Build. Mater. 135 (2017) 323–334. https://doi.org/10.1016/j.conbuildmat.2017.01.009.

[29] R. Saleh Ahari, T. Kemal Erdem, K. Ramyar, Effect of various supplementary cementitious materials on rheological properties of self-consolidating concrete, Constr. Build. Mater. 75 (2015) 89–98. https://doi.org/10.1016/j.conbuildmat.2014.11.014.

[30] H. Soualhi, E.H. Kadri, T.T. Ngo, A. Bouvet, F. Cussigh, B. Benabed, Rheology of ordinary and low-impact environmental concretes, J. Adhes. Sci. Technol. 29 (2015) 2160–2175. https://doi.org/10.1080/01694243.2015.1059641.

[31] M. Sonebi, M. Lachemi, K.M.A. Hossain, Optimisation of rheological parameters and mechanical properties of superplasticised cement grouts containing metakaolin and viscosity modifying admixture, Constr. Build. Mater. 38 (2013) 126–138. https://doi.org/10.1016/j.conbuildmat.2012.07.102.

[32] Y. Ouldkhaoua, B. Benabed, R. Abousnina, H. El-Kadri, Rheological properties of blended metakaolin self-compacting concrete containing recycled CRT funnel glass aggregate, Epa. - J. Silic. Based Compos. Mater. 71 (2019) 154–161. https://doi.org/10.14382/epitoanyag-jsbcm.2019.27.

[33] C. Özel, K.T. Yücel, Effect of Cement Content, Fibers, Chemical Admixtures and Aggregate Shape on Rheological Parameters of Pumping Concrete, Arab. J. Sci. Eng. 38 (2013) 1059–1074. https://doi.org/10.1007/s13369-012-0345-8.

[34] H. Jiang, M. Fall, E. Yilmaz, Y. Li, L. Yang, Effect of mineral admixtures on flow properties of fresh cemented paste backfill: Assessment of time dependency and thixotropy, Powder Technol. 372 (2020) 258–266. https://doi.org/10.1016/j.powtec.2020.06.009.

[35] Z. Giergiczny, Fly ash and slag, Cem. Concr. Res. 124 (2019). https://doi.org/10.1016/j.cemconres.2019.105826.

[36] D. Jiao, C. Shi, Q. Yuan, X. An, Y. Liu, H. Li, Effect of constituents on rheological properties of fresh concrete-A review, Cem. Concr. Compos. 83 (2017) 146–159. https://doi.org/10.1016/j.cemconcomp.2017.07.016.
[37] M. Nehdi, Why some carbonate fillers cause rapid increases of viscosity in dispersed cement-based materials, Cem. Concr. Res. 30 (2000) 1663–1669. https://doi.org/10.1016/S0008-8846(00)00353-7.
[38] B. Felekoğlu, K. Tosun, B. Baradan, A. Altun, B. Uyulgan, The effect of fly ash and limestone fillers on the viscosity and compressive strength of self-compacting repair mortars, Cem. Concr. Res. 36 (2006) 1719–1726. https://doi.org/https://doi.org/10.1016/j.cemconres.2006.04.002.
[39] B. Felekoglu, Utilisation of high volumes of limestone quarry wastes in concrete industry (self-compacting concrete case), Resour. Conserv. Recycl. 51 (2007) 770–791. https://doi.org/10.1016/j.resconrec.2006.12.004.
[40] P. Hawkins, P. Tennis, R. Detwiler, The Use of Limestone in Portland Cement : A State-of-the-Art Review, n.d.
[41] B. Łaźniewska-Piekarczyk, The influence of selected new generation admixtures on the workability, air-voids parameters and frost-resistance of self compacting concrete, Constr. Build. Mater. 31 (2012) 310–319. https://doi.org/10.1016/j.conbuildmat.2011.12.107.
[42] D. Leonavičius, I. Pundienė, J. Pranckevičienė, M. Kligys, Selection of superplasticisers for improving the rheological and mechanical properties of cement paste with CNTs, Constr. Build. Mater. 253 (2020) 119182. https://doi.org/10.1016/j.conbuildmat.2020.119182.
[43] European Standard EN 1097-6:2000, Tests for mechanical and physical properties of aggregates - Part 6: Determination of particle density and water absorption, Brussels Eur. Comm. Stand. (2000).
[44] European Standard EN 196-1:2005, Methods of testing cement - Part 1: Determination of strength, Brussels Eur. Comm. Stand. (2005).
[45] European Standard EN 12350-2:2009, Testing fresh concrete Slump-test, Brussels Eur. Comm. Stand. (2009).
[46] H. Soualhi, E.H. Kadri, T.T. Ngo, A. Bouvet, F. Cussigh, S. Kenai, A vane rheometer for fresh mortar: Development and validation, Appl. Rheol. 24 (2014) 1–7. https://doi.org/10.3933/ApplRheol-24-22594.
[47] J. Jeong, E. Chuta, H. Ramézani, S. Guillot, Rheological properties for fresh cement paste from colloidal suspension to the three-element Kelvin–Voigt model, Rheol. Acta. 59 (2020) 47–61. https://doi.org/10.1007/s00397-019-01171-x.
[48] T. Sedran, F. De Larrard, L. Le Guen, Determination of the compaction of cements and mineral admixtures using the vicat needle, Bull. Des Lab. Des Ponts Chaussees. (2007) 155–163.
[49] E.P. Koehler, D.W. Fowler, Development of a Portable Rheometer for Fresh Portland Cement Concrete, ICAR REP. (2004) 103–105.
[50] N. Roussel, Understanding the Rheology of Concrete, Woodhead Publishing, 2012. https://doi.org/10.1533/9780857095282.index.
[51] O.H. Wallevik, J.E. Wallevik, Rheology as a tool in concrete science: The use of rheographs and workability boxes, Cem. Concr. Res. 41 (2011) 1279–1288. https://doi.org/10.1016/j.cemconres.2011.01.009.
[52] M. Criado, A. Palomo, A. Fernández-Jiménez, P.F.G. Banfill, Alkali activated fly ash: Effect of admixtures on paste rheology, Rheol. Acta. 48 (2009) 447–455. https://doi.org/10.1007/s00397-008-0345-5.

Ref.:
Safiddine, Salim – **Soualhi**, Hamza – **Benabed**, Benchaa – **Belaidi**, Akram Salah Eddine – **Kadri**, El-Hadj: *Effect of different supplementary cementitious materials and superplasticizers on rheological behavior of eco-friendly mortars*
Építőanyag – Journal of Silicate Based and Composite Materials, Vol. 73, No. 3 (2021), 119–129. p.
https://doi.org/10.14382/epitoanyag-jsbcm.2021.18

GUIDELINE FOR AUTHORS

The manuscript must contain the followings: title; author's name, workplace, e-mail address; abstract, keywords; main text; acknowledgement (optional)**; references; figures, photos with notes; tables with notes; short biography** (information on the scientific works of the authors).

The full manuscript should not be more than 6 pages including figures, photos and tables. Settings of the word document are: 3 cm margin up and down, 2,5 cm margin left and right. Paper size: A4. Letter size 10 pt, type: Times New Roman. Lines: simple, justified.

TITLE, AUTHOR

The title of the article should be short and objective.

Under the title the name of the author(s), workplace, e-mail address.

If the text originally was a presentation or poster at a conference, it should be marked.

ABSTRACT, KEYWORDS

The abstract is a short summary of the manuscript, about a half page size. The author should give keywords to the text, which are the most important elements of the article.

MAIN TEXT

Contains: materials and experimental procedure (or something similar), results and discussion (or something similar), conclusions.

REFERENCES

References are marked with numbers, e.g. [6], and a bibliography is made by the reference's order. References should be provided together with the DOI if available.

Examples:

Journals:

[6] Mohamed, K. R. – El-Rashidy, Z. M. – Salama, A. A.: In vitro properties of nano-hydroxyapatite/chitosan biocomposites. *Ceramics International.* 37(8), December 2011, pp. 3265–3271, http://doi.org/10.1016/j.ceramint.2011.05.121

Books:

[6] Mehta, P. K. – Monteiro, P. J. M.: Concrete. Microstructure, properties, and materials. *McGraw-Hill*, 2006, 659 p.

FIGURES, TABLES

All drawings, diagrams and photos are figures. The **text should contain references to all figures and tables**. This shows the place of the figure in the text. Please send all the figures in attached files, and not as a part of the text. **All figures and tables should have a title**.

Authors are asked to submit color figures by submission. Black and white figures are suggested to be avoided, however, acceptable.

The figures should be: tiff, jpg or eps files, 300 dpi at least, photos are 600 dpi at least.

BIOGRAPHY

Max. 500 character size professional biography of the author(s).

CHECKING

The editing board checks the articles and informs the authors about suggested modifications. Since the author is responsible for the content of the article, the author is not liable to accept them.

CONTACT

Please send the manuscript in electronic format to the following e-mail address: femgomze@uni-miskolc.hu and epitoanyag@szte.org.hu or by post: Scientific Society of the Silicate Industry, Budapest, Bécsi út 122–124., H-1034, HUNGARY

We kindly ask the authors to give their e-mail address and phone number on behalf of the quick conciliation.

Építőanyag – *Journal of Silicate Based and Composite Materials*, Quarterly peer-reviewed periodical of the Hungarian Scientific Society of the Silicate Industry, SZTE.
http://epitoanyag.org.hu